THE GEOLOGICAL SOCIETY OF AMERICA®

Paleomagnetism of the Chuar Group and evaluation of the late Tonian Laurentian apparent polar wander path with implications for the makeup and breakup of Rodinia

Athena Eyster[1,†], Benjamin P. Weiss[1], Karl Karlstrom[2], and Francis A. Macdonald[3]

[1]*Department of Earth, Atmospheric and Planetary Sciences, Massachusetts Institute of Technology, 77 Massachusetts Avenue, Cambridge, Massachusetts 02139, USA*

[2]*Department of Earth and Planetary Sciences, University of New Mexico, Albuquerque, New Mexico 871311, USA*

[3]*Department of Earth Science, University of California–Santa Barbara, Santa Barbara, California 93106, USA*

ABSTRACT

Paleogeographic models commonly assume that the supercontinent Rodinia was long-lived, with a static geometry involving Mesoproterozoic links that developed during assembly and persisted until Neoproterozoic rifting. However, Rodinian paleogeography and dynamics of continental separation around its centerpiece, Laurentia, remain poorly constrained. On the western Laurentian margin, geological and geochronological data suggest that breakup did not occur until after 720 Ma. Thus, late Tonian (ca. 780–720 Ma) paleomagnetic data are critical for reconstructing paleogeography prior to dispersal and assessing the proposed stasis of Rodinia. Here, we report new paleomagnetic data from the late Tonian Chuar Group in the Grand Canyon, Arizona. We combined this new data set with reanalyzed existing data to obtain a new paleopole preserved in hematite, the reliability of which is supported by six of the seven (Q1–Q6) Van der Voo reliability quality criteria. In addition, we identified pervasive mid- to high-temperature overprints. This new paleomagnetic pole was incorporated with recent high-precision geochronological data and existing paleomagnetic data to present a new late Tonian Laurentian apparent polar wander path (APWP). Having examined the paleomagnetic data of other cratons, global reconstructions for 775 Ma, 751 Ma, and 716 Ma are presented. These reconstructions are consistent with Australia located near the present southern margin of Laurentia. However, a stringent analysis of the global data set does not support a good match between any major craton and the rifted conjugate margin to western Laurentia. Breakup on the western Laurentian margin may have involved rifting of a continental fragment or a craton with uncertainties in its late Tonian geochronologic and paleomagnetic constraints. Our revised Laurentian APWP will allow for more robust tests of paleogeography and evaluation of the proposed supercontinent Rodinia.

INTRODUCTION

Identification of the supercontinent Pangea and the associated concept of changing surface continental configurations have dramatically altered our understanding of Earth dynamics. Currently, there are detailed reconstructions of plate speeds and configurations over the past 200 m.y., spanning the tenure of Pangea (e.g., Seton et al., 2012; Morra et al., 2013; Zahirovic et al., 2015; Müller et al., 2016). Paleogeographic reconstructions of earlier eras are less certain. Although it has been suggested that supercontinent amalgamation and breakup were cyclic continuing back into the Proterozoic, the supercontinent cycle is still being constrained prior to the formation of Pangea (Li et al., 2008; Zhong et al., 2007; Murphy et al., 2009; Evans, 2009, 2013; Nance et al., 2014). Nonetheless, continental configurations associated with the putative supercontinent cycle have been associated with climate and evolutionary change on geologic time scales. In particular, the breakup of the Proterozoic supercontinent Rodinia has been implicated as a causal factor in the initiation of snowball Earth (Li et al., 2004; Goddéris et al., 2003) and a second rise of oxygen (e.g., Knoll et al., 1986; Shields-Zhou et al., 2012). To fully investigate proposed connections between supercontinents within the Earth system, the timing and configuration of each potential supercontinent must be accurately reconstructed.

Rodinia was initially hypothesized based on evidence for extensive Mesoproterozoic (Grenville in age) orogenic events combined with identification of Neoproterozoic rift and passive-margin sequences (e.g., Hoffman, 1991; Moores, 1991). Subsequently, multiple configurations have been proposed for the long-lived supercontinent that endured from ca. 1100 to 750 Ma (Sears and Price, 1978; Moores, 1991; Hoffman, 1991; Dalziel, 1991; Sears and Price, 2003; Pisarevsky et al., 2003; Cawood, 2005; Li et al., 2008; Evans, 2009; Merdith et al., 2017). These models, despite their differences, generally regard Laurentia as forming the core of Rodinia, as Laurentia was subsequently surrounded by Cambrian passive margins suggested to have developed during the supercontinent's breakup in the late Neoproterozoic (Bond and Kominz, 1984; Bond et al., 1985; Hoffman, 1991). In proposing Rodinian paleogeography, it may be tempting to assume there are overlooked errors either in paleomagnetic uncertainties, reliability, or ages, in order to support a long-lived supercontinent. Alternatively, it may not be reasonable to expect a long-lasting stable supercontinent configuration with static geometry from amalgamation to disintegration. It is worthwhile to consider possible changes during the proposed tenure of the supercontinent and focus on geometric constraints at specific times. This approach may result in clarification of Rodinia's changing geometry during its lifetime or even revision of its lifetime or existence. Here, we chose to focus on Rodinia near the end of its life prior to geological constraints for initial rifting.

†aeyster@mit.edu

GSA Bulletin; https://doi.org/10.1130/B32012.1; 10 figures; 3 tables; Data Repository item 2019239.

Different published reconstructions, based primarily on paleomagnetic data, depict various crustal blocks rifting from the western (Cordilleran) margin of Laurentia by 750 Ma (Sears and Price, 1978; Hoffman, 1991; Sears and Price, 2003; Pisarevsky et al., 2003; Meert and Torsvik, 2003; Cawood, 2005; Li et al., 2008; Evans, 2009; Merdith et al., 2017). This age of Laurentian rifting depicted in paleogeographic models is at odds with age constraints recorded by North American Neoproterozoic strata. The rift history of the North American Cordillera is recorded in the Windermere Supergroup (Fig. 1A; Ross, 1991; Link et al., 1993), which is commonly divided into three main stratigraphic ensembles: (1) narrow, ca. 780–720 Ma fault-bounded extensional basins that accommodated the Chuar, Uinta Mountains, Pahrump, Coates Lake, and Mount Harper groups (ChUMP basins; Dehler et al., 2001, 2010, 2017; Macdonald et al., 2013; Strauss et al., 2014, 2015; Smith et al., 2016); (2) Cryogenian siliciclastic and volcanic successions interbedded with glacial diamictites that have been interpreted as representing rift basins (Stewart, 1972; Eisbacher, 1985; Jefferson and Parrish, 1989); and (3) Ediacaran successions of carbonate and siliciclastic strata, composed largely of turbidites, which are widely interpreted to be related to subsidence and the initiation of passive-margin sedimentation (Stewart, 1972; Ross, 1991; Jefferson and Parrish, 1989), or a later rift (Colpron et al., 2002; Macdonald et al., 2013).

Although evidence for ca. 775 Ma volcanism is present in the form of sills, dikes, and basalts associated with the Gunbarrel event (Harlan et al., 2003; Milton et al., 2017), these volcanic rocks are widely distributed, but not voluminous, with outcrops in the Wyoming Province, the Mackenzie Mountains in the northern Cordillera, and the Canadian Shield (Fig. 1). Furthermore, the ChUMP basins are largely intracratonic and lack volcanic rocks (Dehler et al., 2001, 2017). At the same time, to the north, there is evidence for transpressional faulting (e.g., Eisbacher, 1981; Thorkelson et al., 2005) and fault-influenced deposition of carbonate platforms (Strauss et al., 2014). Abundant volcanism did not occur until ca. 720 Ma, with the eruption of the Franklin large igneous province centered in northern Canada. Cryogenian volcanic rocks with rift-related geochemical signatures are also found farther south in the Canadian Cordillera, Washington, Idaho, and Death Valley (Miller, 1985; Miller, 1994; Keeley et al., 2013; Lund et al., 2010). This volcanism has been dated at ca. 717 Ma in the Yukon (Macdonald et al., 2010), ca. 696–690 Ma in northern British Columbia (Eyster et al., 2018), and ca. 697–667 Ma in Idaho (Keeley et al., 2013; Lund et al., 2010; Condon and Bowring, 2011; Fanning and Link, 2004). However, subsidence analysis of Neoproterozoic and Cambrian strata (Bond and Kominz, 1984; Armin and Mayer, 1983) shows that the rift-drift transition and development of the passive margin did not occur until the Precambrian-Cambrian boundary (now 539 Ma; Linnemann et al., 2019). This also coincides with the position of the breakup unconformity in the southwestern United States

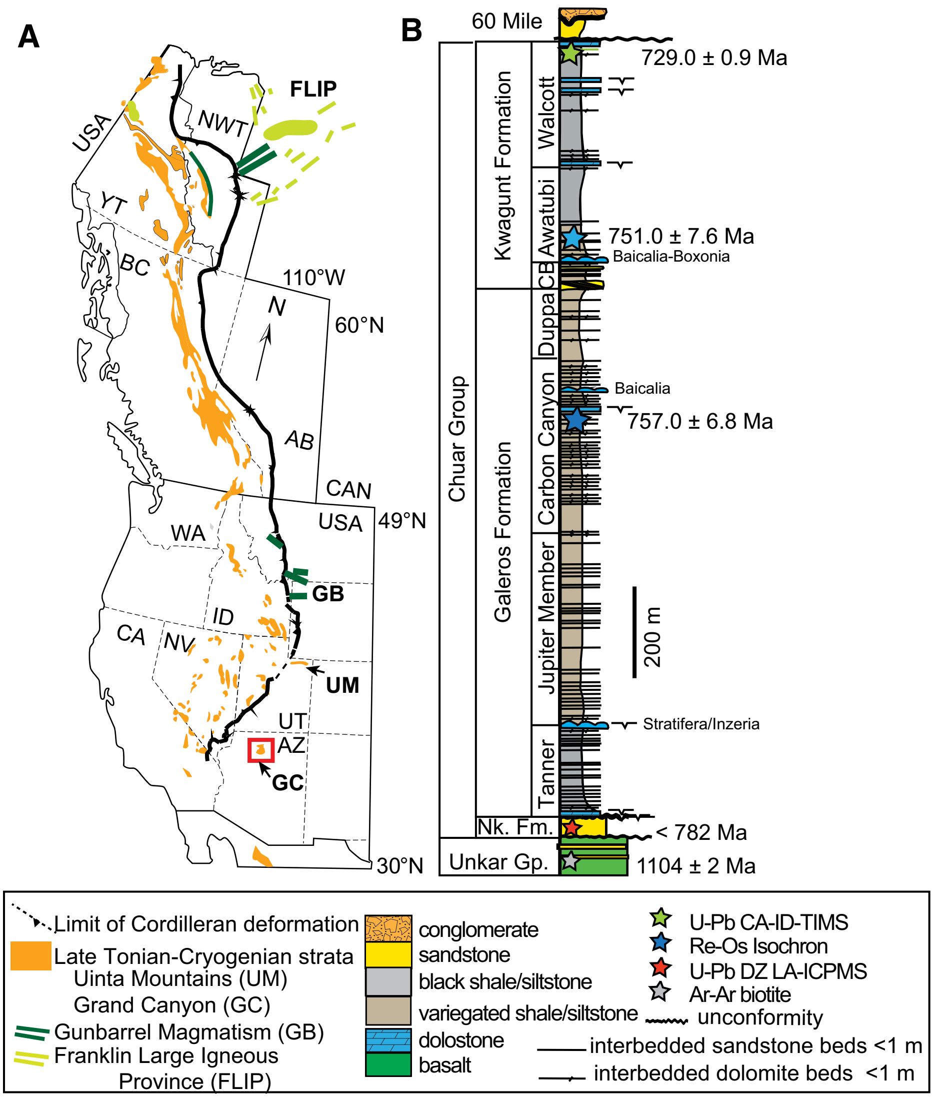

Figure 1. (A) Map of western North America with Neoproterozoic inliers (after Lund et al., 2010) and locations of Uinta Mountains (UM), Gunbarrel magmatism (GB; Harlan et al., 2003; Milton et al., 2017), and Franklin large igneous province (FLIP; Buchan and Ernst, 2004; Buchan et al., 2010; Buchan and Ernst, 2013). Red box highlights location of the Grand Canyon (GC) and the Neoproterozoic Chuar group. (B) Composite stratigraphic column of the Grand Canyon stratigraphy along with updated age constraints from Rooney et al. (2017) and Dehler et al. (2017). Stratigraphic column is after Karlstrom et al. (2000) and Dehler et al. (2001). CB—Carbon Butte Member; Nk. Fm.—Nankoweap Formation. Stratifera/Inzeria/Baicalia/Boxonia refer to stromatolite morphologies. Canadian Provinces: NWT—Northwest Territories; BC—British Columbia; AB—Alberta. U.S. States: WA—Washington, ID—Idaho, CA—California, NV—Nevada, UT—Utah, AZ—Arizona. Dating techniques: CA-ID-TIMS—chemical abrasion–isotope dilution–thermal ionization mass spectrometry; DZ—detrital zircon; LA-ICP-MS—laser ablation–inductively coupled plasma–mass spectrometry.

(e.g., Fedo and Cooper, 2001). Thus, basal Windermere magmatism is too old to be tied to the thermal subsidence and development of the Paleozoic passive margin. This discrepancy in ages could suggest multiple rift events or protracted rifting (Prave, 1999; Colpron et al., 2002; Macdonald et al., 2013). Indeed, a third episode of late Ediacaran rift-related volcanism has also been identified in British Columbia (Colpron et al., 2002), Sonora Mountains of California, and the Wichita Mountains of Oklahoma (Bowring and Hoppe, 1982; Wright et al., 1996; Thomas et al., 2012; Hanson et al., 2013).

This recent evidence for an extended period of tectonic activity starting at 720 Ma and a final rift-drift transition not occurring until after 539 Ma is not reflected in global reconstructions that depict full separation of continents from the Laurentian margin by ca. 750 Ma (e.g., Li et al., 2008, 2013; Gernon et al., 2016; Merdith et al., 2017). Toward resolving this issue, recent Re-Os and detrital zircon U-Pb geochronology from the Chuar Group in the Grand Canyon constrained deposition from 782 to 729 Ma (Dehler et al., 2017; Rooney et al., 2017). These units provide an opportunity to test global reconstructions through this critical interval during which geological data suggest the core of Rodinia was just starting to break apart.

Currently, the 780–720 Ma Laurentian apparent polar wander path (APWP) includes magmatic poles from the ca. 775 Ma Gunbarrel event and ca. 720 Ma Franklin large igneous province, as well as sedimentary poles from the Uinta Mountain and Chuar groups (Harlan et al., 1997; Buchan et al., 2000; Denyszyn et al., 2009a; Weil et al., 2004, 2006). Due to a previous paucity of age constraints, it was uncertain how the sedimentary poles were temporally related to the magmatic poles. In addition to APWP calibration uncertainties, the Chuar Group poles are mean poles that average multiple members and several hundred meters of stratigraphy now known to span 20 m.y. (Weil et al., 2004; Rooney et al., 2017). When the Chuar Group results were reanalyzed, there was only one member for which bedding variability in the tilts permitted a fold test to be robustly conducted. Additionally, true polar wander (TPW) or large plate motions may have been averaged in the mean formation poles, as the virtual geomagnetic poles (VGPs) from the uppermost member (Walcott Member) were 30° away from the underlying VGPs (Weil et al., 2004). Alternatively, this difference could have been caused by the reported steep overprints (Weil et al., 2004). Thus, questions remain about stratigraphic variation of the paleomagnetic poles, potentially high rates of plate motion or TPW, and the nature of overprints. Resolving these issues is critical for accurate reconstruction of Neoproterozoic paleogeography and is the subject of this paper.

Here, we present new Laurentian paleomagnetic data from the Chuar Group and refine the Laurentian APWP from 780 to 720 Ma. We then compare the Laurentian poles with those from other cratons to evaluate paleogeographic models for the makeup and breakup of Rodinia.

Geologic Overview

The Grand Canyon Supergroup consists of the Mesoproterozoic Unkar Group (1255–1100 Ma) and the Neoproterozoic Chuar Group (782–729 Ma; Dehler et al., 2017; Rooney et al., 2017). Along with the Uinta Mountains Group in Utah, the Chuar Group displays rare preservation of Neoproterozoic strata within the craton, compared with other strata distributed within the Cordilleran fold-and-thrust belt (Fig. 1A; Karlstrom et al., 2000). Sitting above a basal unconformity, the Chuar Group is divided into the Nankoweap, Galeros, and Kwagunt formations (Fig. 1B). The Nankoweap Formation is 100–150 m thick and consists of two informal members. The lower red member is dominated by hematite-cemented sandstone and mudstone, while the upper white member is composed of siltstone and thin-bedded, fine-grained sandstone (Van Gundy, 1951). Due to unconformities both above and below, the stratigraphic position of the Nankoweap Formation was previously uncertain (Timmons et al., 2012). However, new laser ablation–inductively coupled plasma–mass spectrometry (LA-ICP-MS) U-Pb detrital zircon data giving an age of ca. 782 Ma ($n = 14$) provide a maximum depositional age constraint and, along with similar detrital zircon populations in overlying strata, lead to the inclusion of the Nankoweap Formation within the Chuar Group (Dehler et al., 2017). The overlying Galeros and Kwagunt formations consist of 1600 m of shale with interbedded meter-scale sandstone and dolomite marker beds (Dehler et al., 2001). Lying unconformably above the Kwagunt Formation, there are sandstone and conglomerate of the Sixtymile Formation. Although the Sixtymile Formation was previously thought to be Neoproterozoic in age, recent detrital zircon data now indicate a Cambrian age (U-Pb zircon $<527 \pm 0.7$ Ma; Karlstrom et al., 2018).

The Galeros Formation is divided into the Tanner, Jupiter, Carbon Canyon, and Duppa members (Ford and Breed, 1973). Both the Tanner and Jupiter Members are dominated by fine-grained siliciclastic rocks and have unique dolomite marker beds at the base: the Tanner dolomite and the *Stratifera/Inzeria* stromatolites, respectively (Ford and Breed, 1973). The overlying Carbon Canyon Member is characterized by alternations of varicolored mudstone with mudcracks, orange dolostone, pale carbonate stromatolite beds, and thin sandstone beds (Dehler et al., 2001). The upper member of the Galeros Formation is the Duppa Member, which is dominated by recessive sandstone and siltstone. The Kwagunt Formation conformably overlies the Galeros Formation and includes the sandstone-dominated Carbon Butte Member, variegated shale and *Boxonia* stromatolites of the Awatubi Member, and dolostone and black shale of the Walcott Member (Dehler et al., 2001).

Deposition of the Chuar Group occurred during movement on the south-striking Butte normal fault (Fig. 2A). Intraformational faults throughout the Chuar Group strata, including the Tanner Member and middle Carbon Canyon and Carbon Butte members, suggest continuing syndepositional extensional faulting. West of the Butte fault, the Chuar syncline is interpreted as a growth fold that developed during Chuar Group deposition (Fig. 3A). Here, the stratigraphy thickens toward the Chuar syncline axis, and the tightness of the fold appears to decrease up section. Taken together, these indicate that activity related to the Chuar syncline and Butte fault was syndepositional with the Chuar Group (Timmons et al., 2001). Samples were collected in two areas west of the Butte fault (Fig. 2A). The stratigraphic positions of samples are shown in Figure 2B.

There are several key marker beds within the Carbon Butte and Awatubi members: particularly the basal red sandstone marker bed of the Carbon Butte Member, the white sandstone marker bed at the top of the Carbon Butte Member, and the *Boxonia* stromatolite marker bed at the base of the Awatubi Member (Fig. 3B). These distinctive marker beds permit exact correlations for comparisons of strata across the Chuar syncline. The basal red sandstone marker bed (Figs. 3C and 3D), a 4–11-m-thick, resistant, ridge-forming quartz arenite to subarkosic sandstone, marks the base of the Carbon Butte Member (Dehler et al., 2001). A thick white sandstone (Figs. 3E and 3F) at the top of the Carbon Butte Member is 1–2 m thick with 3–10-cm-thick beds of mature quartz arenite with prominent ripples (Dehler et al., 2001). The basal *Boxonia* stromatolites (Figs. 3G and 3H) mark the base of the Awatubi Member. Along with the *Boxonia* stromatolites, this member laterally displays stratiform to domal microbial buildups with centimeter-scale laminae.

METHODS

Paleomagnetic block samples were collected with orientations measured by a combination

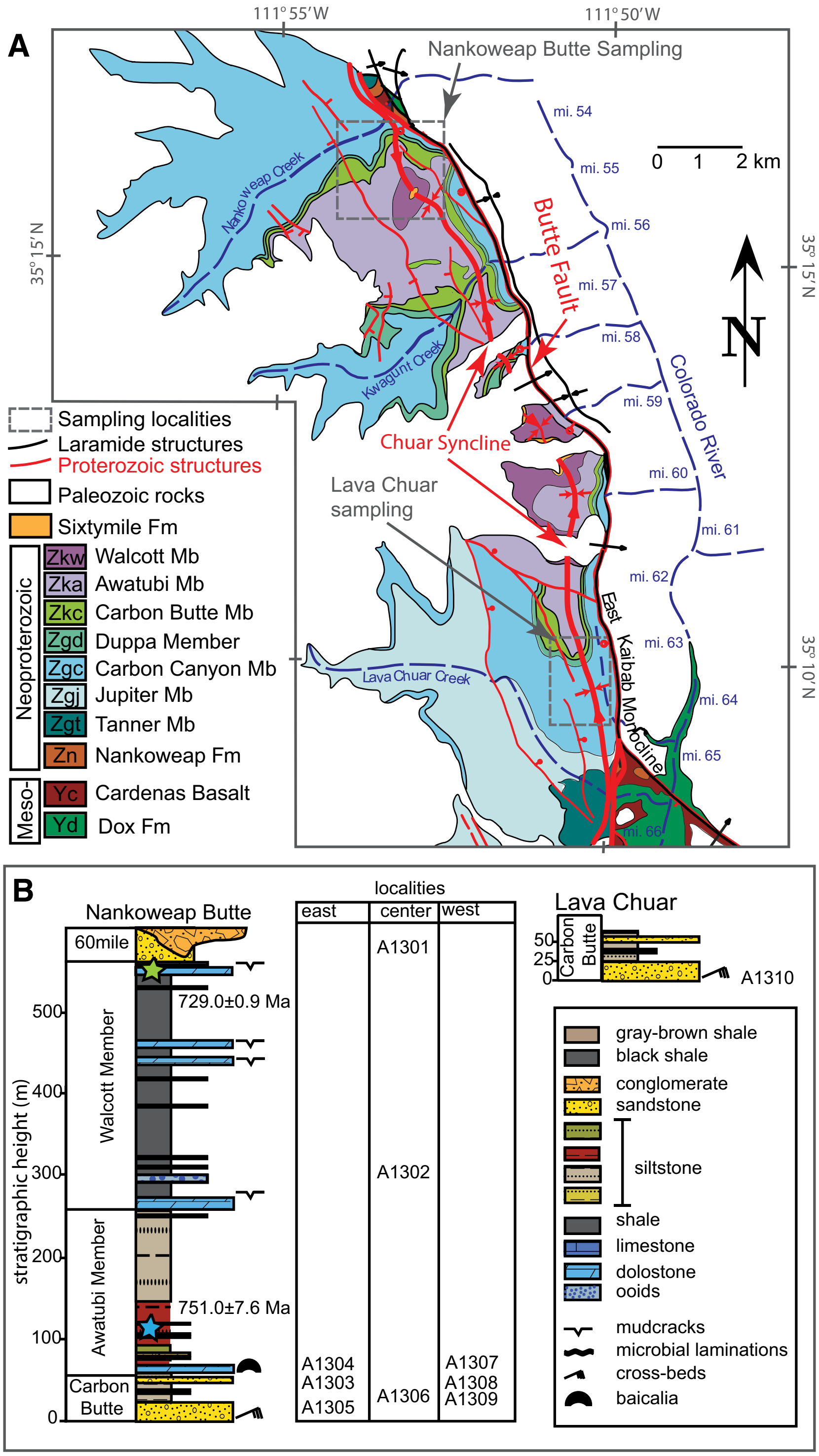

Figure 2. (A) Map of the Chuar Valley (after Karlstrom et al., 2000). Boxes highlight the sampling locations of Nankoweap Butte and Carbon Canyon. (B) Stratigraphic sampling localities.

of Brunton and sun compasses to identify any locations that may have experienced strong remagnetization due to lightning strikes. The orientation of bedding was measured to correct for tilting. Sampling was concentrated at two main areas: Nankoweap Butte and Lava Chuar Canyon (Fig. 2A; Table DR1[1]). At Nankoweap Butte, sampling on both limbs of the Chuar syncline focused on the Awatubi and Carbon Butte members of the Kwagunt Formation. Samples were also collected from the Walcott Member of the Kwagunt Formation and the overlying Cambrian Sixtymile Formation. The Walcott Member is composed of slope-forming shale with interbedded dolomite. It was difficult to collect paleomagnetic samples from the poorly lithified shale dominating the Walcott Member, and as a result, only one locality was sampled. At Lava Chuar, sampling focused on the Carbon Butte. In total, 28 oriented large block samples encompassing multiple horizons were collected from 10 localities (each spanning up to 4.5 m). After field work, a diamond drill press was used to drill one to three individually oriented cores from distinct beds within the blocks. Then, one specimen was prepared from each core.

Magnetization measurements were made with a 2G Enterprises 755 superconducting rock magnetometer (SRM) in the Massachusetts Institute of Technology Paleomagnetism Laboratory using an automated sample handling system (Kirschvink et al., 2008). This instrument has a sensitivity of 10^{-12} Am^2 (Wang et al., 2017) and is located in a magnetically shielded room (direct current [DC] field <150 nT). After first measuring their natural remanent magnetism (NRM), the specimens were immersed in a liquid nitrogen bath to preferentially remove the magnetization carried by multidomain magnetite grains via cycling through the Verwey transition (Dunlop and Argyle, 1991). This procedure was followed by alternating field (AF) demagnetization up to 15 mT. Finally, all the specimens were thermally demagnetized in air using an ASC Scientific thermal demagnetizer (with peak DC fields inside <10 nT). Specimens were thermally demagnetized in steps of 2.5–50 °C until completely demagnetized.

Magnetic components were determined using principal component analysis with linear fits for samples that displayed linear origin-trending demagnetization, and great circle fits anchored to the origin for samples where mid-temperature (MT) and high-temperature (HT)

[1]GSA Data Repository item 2019239, supplemental text, data tables, and figures, is available at http://www.geosociety.org/datarepository/2019 or by request to editing@geosociety.org.

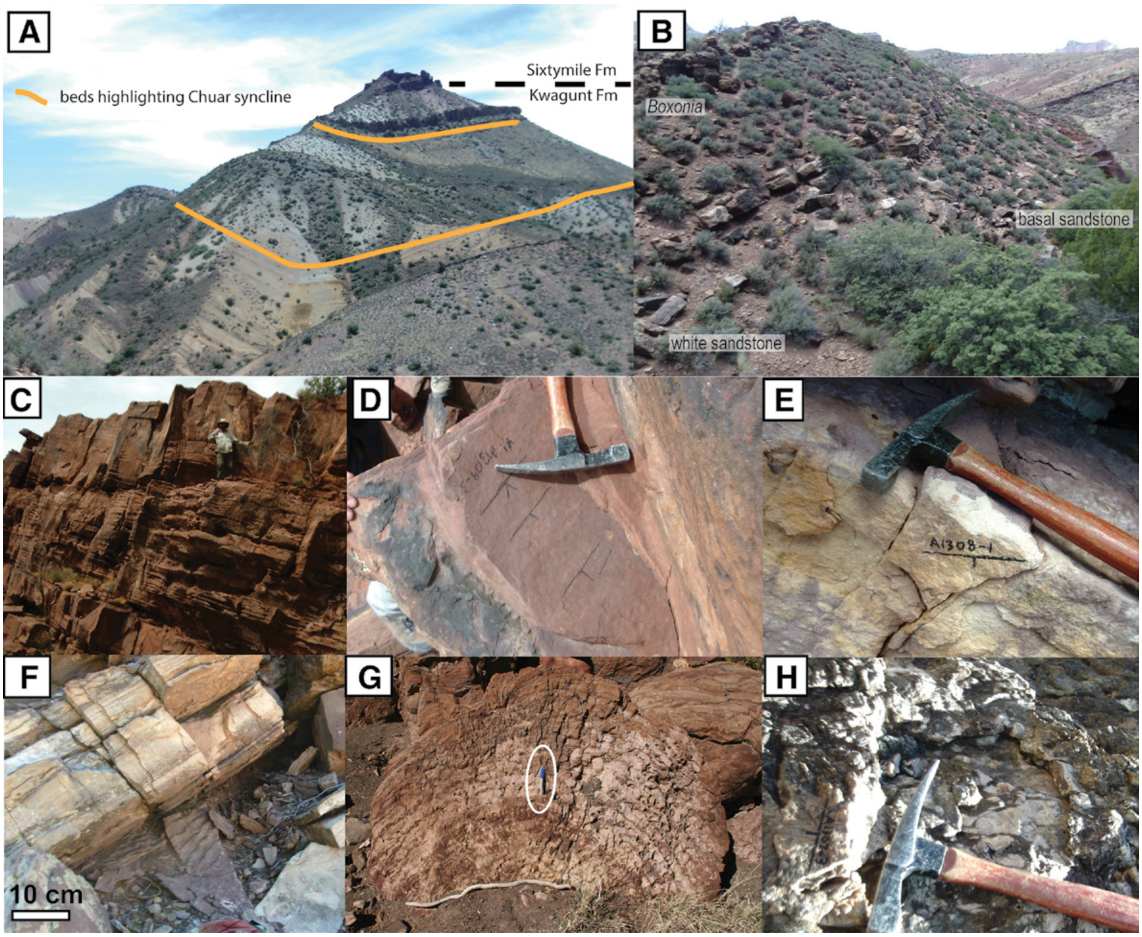

Figure 3. Field photos. (A) Nankoweap Butte with Chuar syncline. (B) Stratigraphy of Carbon Butte and basal Awatubi members. (C–D) Carbon Butte basal sandstone. (E–F) Carbon Butte white sandstone. (G–H) Basal Awatubi *Boxonia*.

components overlapped (Kirschvink, 1980; see also Table DR2 [footnote 1]). Following Butler (1992), we only accepted components for which the maximum angle of deviation (*MAD*) was ≤15°, although in many cases, the *MAD* was <10°. Specimen analysis was completed using the PaleoMag OS X program (Jones, 2002). Fisher statistics were used to calculate mean directions and plotting and analysis were done using the PmagPy software package (Tauxe et al., 2016). Paleomagnetic data sets for this paper are posted in the Magnetics Information Consortium (MagIC) database (https://www2.earthref.org/MagIC/).

RESULTS

Magnetization components were identified based on unblocking temperatures and directionality. Localities with directionally unstable sample demagnetization did not yield any useful data (e.g., A1308). The magnetization components were classified as dispersed low-temperature (LT), coherent steep mid-temperature (MT), and both shallow and steep high-temperature (HT and HTs, respectively) component directions (Figs. 4 and 5; Table DR2 [footnote 1]). The Tauxe and Watson (1994) fold test was applied, and uncertainty was quantified by utilizing bootstrapped data sets and repetition of the fold test for various percentages of unfolding.

The LT component was removed during alternating field demagnetization or very early thermal demagnetization. This component was highly scattered and will not be discussed further. The MT component direction was identified in seven localities (Figs. 4 and 5; Table DR2). This component was demagnetized during steps from the NRM to 560 °C. Although always lower in a single sample, this MT unblocking temperature range overlapped with HT component unblocking temperatures.

The HT directions were generally observed to fall into three locations, one with steep positive inclinations to the north (HTs), and two with shallow inclinations (HT). The steep direction (HTs) was oriented around 10° from the MT component direction, but with higher unblocking temperatures (up to 690 °C). The shallow inclination directions were either positive inclination to the west, or negative inclination toward the east (Figs. 4 and 5; Table DR4 [see footnote 1]). These shallow HT directions had demagnetization temperatures ranging from 100 °C to 680 °C, with peak unblocking temperatures consistent with both hematite and magnetite as the magnetic carriers. The samples that required great circle fits anchored to the origin (such as most of the samples from localities A1302 and A1307) were fully demagnetized well below 565 °C, with peak unblocking temperatures in some cases as low as 400 °C.

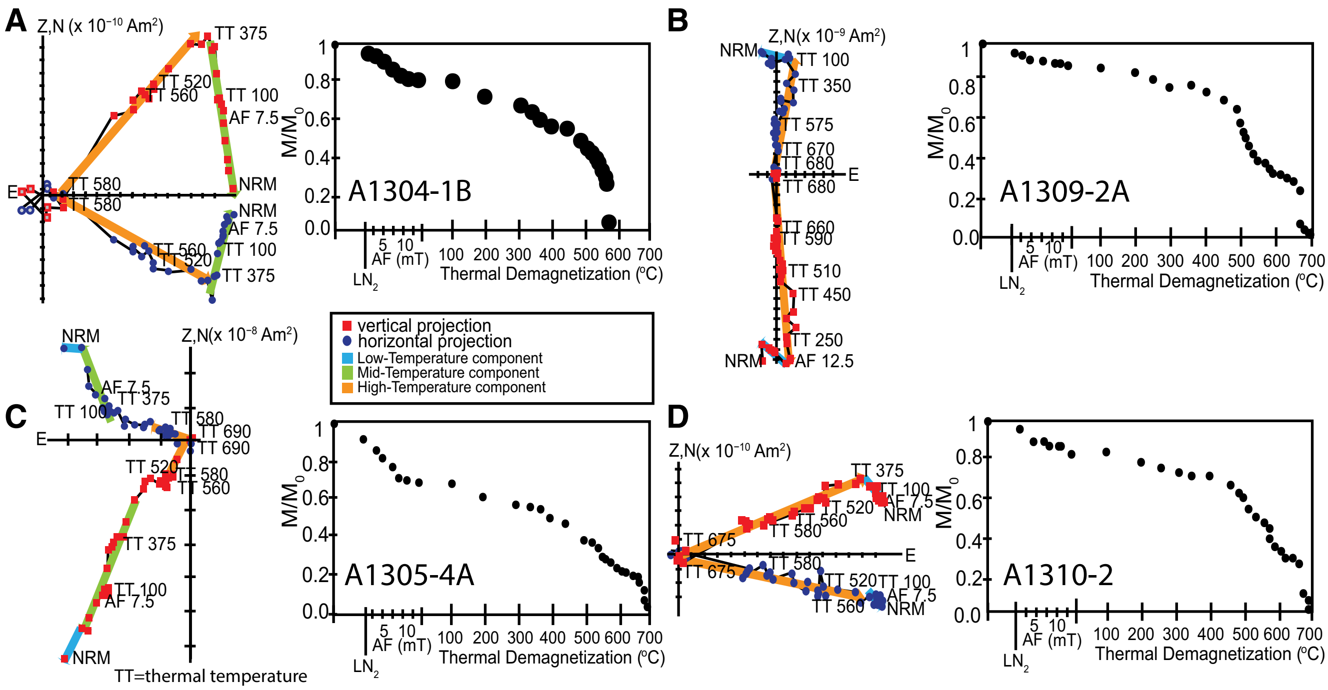

Figure 4. Representative examples of orthogonal projection diagrams showing demagnetization of natural remanent magnetization (NRM). (A) Sample A1304-1B, which carries a mid-temperature (MT) component and a shallow high-temperature (HT) component carried by low-unblocking-temperature hematite. (B) Sample A1309-2A, which carries a steep direction carried by hematite (HTs). (C) Sample A1305-4A, which carries a MT component as well as a shallow reversed HT component carried by hematite. (D) Sample A1310-2A, which carries a shallow HT component carried by hematite. Note both normal and reversed directions are carried by hematite. Red and blue symbols indicate projections of magnetization vector onto vertical-east (Z-E) and north-east (N-E) axes, respectively. Temperatures and peak fields of selected thermal and alternating field (AF) demagnetization steps are labeled in units of °C and mT, respectively. The representative orthogonal projections are shown using in situ (geographic) coordinates. The corresponding ratio of the moment to the original NRM (*M/M*$_0$) is shown to the right of each orthogonal projection.

Resolvable Directions

To better resolve the paleomagnetism that could correspond to the Re-Os age of 751.0 ± 7.6 Ma, particular focus was placed on the Carbon Butte Member and basal Awatubi Member. Resolvable HT component directions (stable directions with great circle or linear least squares fit with a *MAD* <15°) were obtained from the Carbon Butte Member (Fig. 5; Table DR4). These samples spanned the basal sandstone and the white sandstone. Of particular note, the top of the Carbon Butte basal red sandstone displayed a reversed shallow HT direction. For the lower Awatubi Member, samples displayed HT shallow directions to the east. These sites were from opposing limbs of the Chuar syncline. Demagnetization behavior included steep directions (MT or HTs), which were recovered from all samples with resolvable directions, followed by a linear or great circle decay toward the origin.

From the Walcott Member, HT directions were obtained from one locality (A1302; Table DR2), which displayed steep directions demagnetized around 450 °C, followed by great circle decay toward the east and negative inclinations.

From the Sixtymile Formation, resolvable directions were obtained from one basal matrix locality (A1301). Samples from A1301 that displayed HTs directions included demagnetization that spanned from NRM to 675 °C. All of the samples displayed trends toward shallow directions that were demagnetized during 450–705 °C, with peak unblocking temperatures of 650–705 °C. Great circle fits were required for two of the samples, while the rest could be fit with lines trending toward the origin. As the age of the Sixtymile Formation has been revised to be substantially younger, we do not discuss these results further.

Significance Tests and Corrections

For these resolvable directions, we applied the Tauxe and Watson (1994) fold test using the varying bed orientations resulting from the development of the Chuar syncline, which is constrained to be syndepositional based on stratigraphic data. This test was applied to the MT, HT, and HTs directions from all samples from the Carbon Butte and basal Awatubi members (Fig. 5).

Pervasive overprinting (in the form of the HTs and MT components) was identified throughout the Chuar Group, especially in the Carbon Butte Member. The MT direction was very similar in direction to the present-day field and failed the Tauxe and Watson (1994) fold test with 95% confidence bounds at –10% to 74% unfolding, thus likely indicating a postfolding direction. The HTs direction likely formed postfolding, as it also failed the fold test with the 95% confidence interval spanning –10% to 47% unfolding. The HTs direction was very similar to the MT, but it instead unblocked at higher temperatures. The MT direction was commonly followed by a higher-temperature component with a different direction. In certain cases, the prominent MT direction was dominantly followed by a great circle demagnetiza-

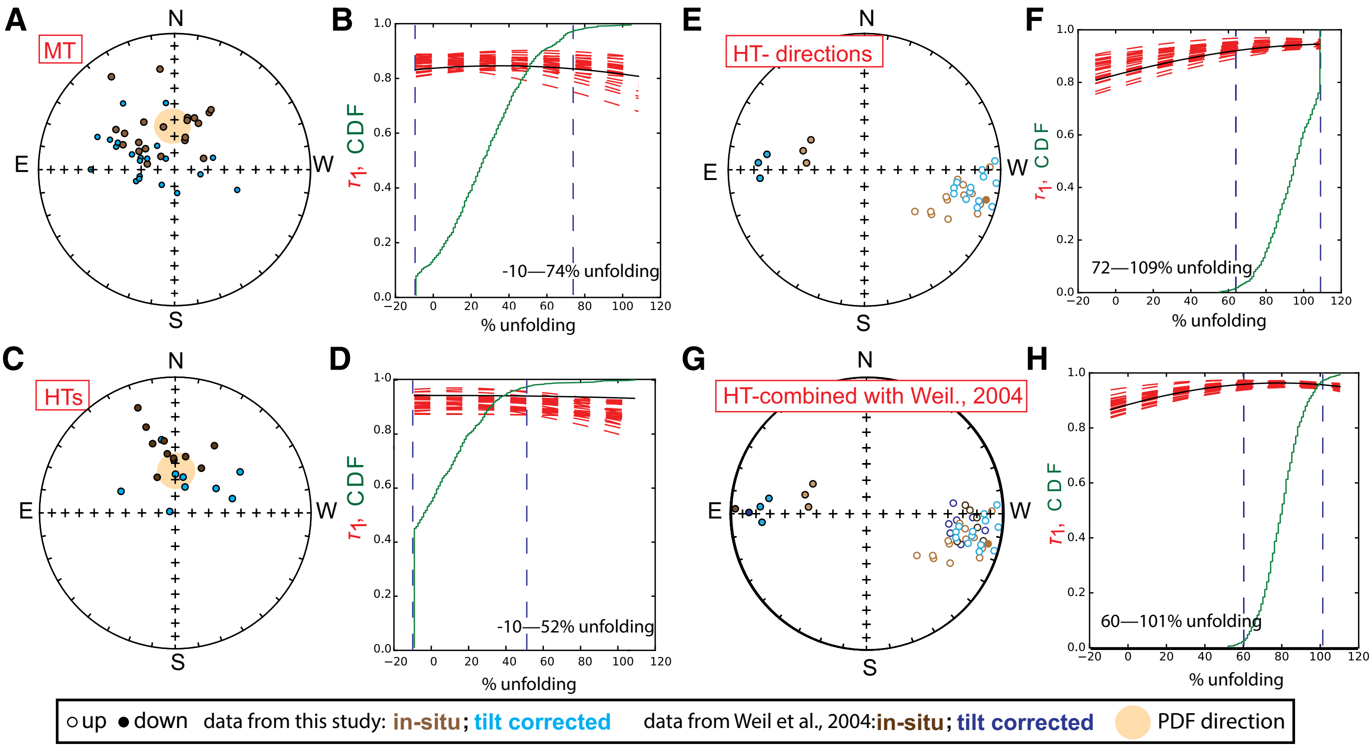

Figure 5. Equal-area component plots and results from the Tauxe and Watson (1994) fold test implemented using Tauxe et al. (2016). (A–B) Mid-temperature (MT) component directions from the Walcott Member, Awatubi Member, and Carbon Butte Member. (C–D) Steep high-temperature (HTs) component directions from the Carbon Butte and Awatubi members. (E–F) HT component origin-trending line-fit directions from samples from the Awatubi and Carbon Butte members. Note that locality A1305 has samples with high-stability HT directions of reverse polarity. (G–H) HT directions from Awatubi and Carbon Butte Member data from this study combined with that of Weil et al. (2004). For equal-area plots, negative directions are represented by open symbols, positive directions are represented by closed symbols, the geographic/in situ directions are plotted in brown, and the tilt-corrected directions are plotted in blue. The direction of the present-day field (PDF) is indicated in light orange. For the Tauxe and Watson (1994) fold tests, the solid black curves indicate maximum eigenvalue (τ_1) as a function of unfolding. The red dashed curves are a sampling of the first 25 bootstrapped results. The green solid line is the cumulative distribution function (CDF) of the percent unfolding required to maximize τ_1 for all the bootstrapped data sets. The blue dashed vertical lines are 95% confidence bounds on the % unfolding that yield the most clustered result (maximum τ_1). If the 95% confidence bounds include 0, then a prefold magnetization is indicated. If the 95% confidence bounds include 100, then a postfold magnetization is indicated. If the 95% confidence bounds exclude both 0 and 100, synfolding magnetization is possible.

tion trend to the origin. In such cases, if larger demagnetization step sizes had been applied instead, the origin-trending demagnetization could have been misidentified, and an apparently steeper origin-trending component could have been interpreted.

The Awatubi and Carbon Butte Member HT directions were combined for subsequent analysis to obtain a paleomagnetic direction close to the dated 751 Ma horizon. Combined, these directions passed the Tauxe and Watson (1994) fold test with 95% confidence bounds from 66% to 109% unfolding, suggesting that the magnetization was acquired prior to folding (Fig. 5). These samples were collected from individual horizons and may represent VGP spot readings of Earth's magnetic field—this makes them more applicable to paleosecular variation (PSV).

To better understand the significance of the reversed directions, we applied Watson's *V* test and the McFadden and McElhinny (1990) classification scheme. Watson's *V* test uses a test statistic, $V_{\text{Watson's}}$, that represents the difference between the mean directions of the data sets. If V_w is less than the critical value (V_{critical}) determined from a Monte Carlo simulation, then the null hypothesis that two data sets have a common mean direction cannot be rejected. In tilt-corrected coordinates, this reversal test passed the Watson's *V* test ($V_{\text{Watson's}} = 7.4 < V_{\text{critical}} = 7.6$). In addition, McFadden and McElhinny's (1990) reversal test classification scheme resulted in an observed angle of 10.3° between the mean normal direction and flipped reversed directions, while the calculated critical angle was 10.4°, for which the null hypothesis of a common mean direction for the two sets of observations would be rejected with 95% confidence. Thus, the directions passed this test with a "C" classification. Due to vector demagnetization revealing multiple components, the fold test, and the presence of reversals, we suggest that the shallow HT direction is a primary direction likely. It was isolated in both the Awatubi and Carbon Butte members.

Finally, sedimentary paleomagnetic data can suffer from inclination flattening. This effect involves initial depositional processes and later compaction causing the measured remanence to be shallower than expected from just the geomagnetic field. One way to identify and correct for this effect is using the Elongation-Inclination (E-I) (Tauxe and Kent, 2004; Kent and Tauxe, 2005; Tauxe, 2005; Tauxe et al., 2008). However, the small size of our data sets may hinder the reliability of our E-I flattening estimates (e.g., Tauxe et al., 2008). Using the PmagPy software package (Tauxe et al., 2016), series of assumed flattening factors were applied to the data. Then, a flattening factor was found with an elongation/inclination pair consistent with TK03 as well as bootstrap confidence bounds. For the Carbon Butte–Awatubi data, $f = 0.9$ was found to be the optimal flattening, with I_o = 19.3° and I_f = 20.8°, with bounds from 16.0° to 31.9° (Fig. DR3; see footnote 1). The elongation was found to be 2.4770, with bootstrap bounds from 2.1830 to 2.5956. Thus, we applied $f = 0.9$ as a correction to the Carbon Butte–Awatubi data sets. We included additional figure versions without the corrections for inclination flattening in the supplement (Fig. DR11; see footnote 1), although there were no substantial differences in the reconstructions, interpretations, and conclusions. We also explored the impact of any Colorado Plateau rotation on the Grand Canyon data (Hamilton, 1988), but we chose not to apply any corrections for large-scale tectonic block rotations (see supplement text and Fig. DR4; see footnote 1).

A major limitation of this study was in number of samples collected, in part due to time constraints in the study area. This could impact our results in two major respects, specifically in capturing within-site variation and secular variation. For the first, following the MagIC database, a site is defined as a "unit with common age and magnetization," i.e., a single sedimentary horizon. We were not able to sample each horizon laterally, characterize the intrasite variation, and obtain robust site means. To address how averaging might modify the reported directions, analysis of the data was also conducted two other ways (in addition to the approach detailed above, i.e., treating every sample as a site): first, by averaging samples within 15 cm of each other, and second by averaging all the samples at a given locality. In each case, a final mean of all the averages was calculated (Table DR2; see footnote 1). All three methods yielded similar results (Table 1; Table DR2). As our samples were focused on specific lithologies, we may not have fully characterized secular variation within the sections. Thus, in the discussion, we tried to overcome this issue by incorporating our new data into existing data sets (see discussion below).

Rock Magnetism Experiments

We characterized the bulk properties of magnetic carriers with rock magnetism experiments. The magnetic mineralogy of 11 different samples was analyzed with isothermal remanent magnetization (IRM) acquisition, IRM backfield experiments, and hysteresis experiments. To better characterize the magnetic minerals carrying HT, MT, and HTs components, we analyzed samples that displayed three different demagnetization patterns. Group A samples had random low- to mid-temperature components (no steep MT overprint) and HT components that trended to the origin. Group B samples had steep MT overprints removed to reveal HT components that trended to the origin. Group C samples had steep HTs components that trended to the origin.

Results from IRM Acquisition and Backfield IRM Experiments

We applied stepwise IRM acquisition to determine the coercivity spectra and saturation fields and to thereby resolve distinct populations of ferromagnetic minerals. Following the IRM acquisition, backfield IRM was applied in order to determine the coercivity of remanence (B_{cr}). Following Kruiver et al. (2001), we display the IRM acquisition data on the linear acquisition plot (LAP) and the gradient of acquisition plot (GAP; Figs. 6A, 6B, and 6C). In order to understand the carriers of magnetization, we decomposed the measured IRM data into cumulative log-Gaussian (CLG) curves, each characterized by saturation isothermal remanent magnetization (sIRM), mean coercivity ($B_{1/2}$), and dispersion (*dp*; Table DR3; see footnote 1). Magnetite and hematite are common remanence carriers in sedimentary rocks and typically have significantly different maximum coercivities

TABLE 1. PALEOMAGNETIC DIRECTIONS AND POLES FROM THE KWAGUNT AND GALEROS FORMATIONS

		In situ directions			Tilt-corrected directions			Fold test*	Paleomagnetic poles[†]			
Direction	N_{sites}	*D/I* (°)	*k*	α_{95} (°)	*D/I* (°)	*k*	α_{95} (°)	pass/fail/synfold: unfolding range	Latitude/ Longitude (°N/°E)	A_{95} (°)	*N*	*K*
MT Carbon Butte–Awatubi–Walcott	20	341.5/63.7	11.7	10.0	291.8/71.8	8.8	11.7	Fail: –10 to 74% unfolding	72.3/205.3[§]	13.7	20	6.7
HTs Carbon Butte–Awatubi	10	356.4/49.3	18.4	11.6	18.1/67.2	12.1	14.5	Fail: –10 to 47% unfolding	84.7/96.1[§]	12.6	10	15.7
HT Carbon Butte–Awatubi**	17	108.0/–31.2	16.3	9.1	98.1/–19.3	45.8	5.3	Pass: 66%–109% unfolding	12.5/161.6[#] 13.1/162.5**	4.0 4.1**	17 17**	82.3 76.7**
Combined HT Carbon Butte-Awatubi (combined with Weil et al., 2004[††])	23	104.6/–27.9	17.4	7.5	98.2/–21.8	43.4	4.6	Pass: 60%–101% unfolding	13.5/162.8[#] 14.2/163.8[§§]	3.3 3.5[§§]	23 23[§§]	82.3 75.8[§§]
HT Carbon Canyon (reanalyzed from Weil et al., 2004***)	14	265.1/5.3	7.0	16.1	264.9/6.1	17.9	9.7	Pass: 72%–109% unfolding	–2.1/163.7[#] –0.5/166.0[†††]	8.0 9.7[†††]	14 14[†††]	25.7 17.9[†††]

Note: N—number of sites, *D* and *I*—mean declination and inclination, *k*—Fisher's (1953) precision parameter, α_{95}—radius of confidence circle for the mean direction; MT—mid-temperature; HT—high-temperature. Elongation-Inclination (E-I) (e.g. Tauxe and Kent, 2004).

*Fold test—results from Tauxe and Watson (1994) fold test: pass, fail, synfolding, or indeterminate. The range indicates the 95% confidence bounds for % unfolding. Bootstrapped tests were run for 1000 iterations.

[†]Poles calculated as means from site mean poles (except for the mean virtual geomagnetic pole [VGP]) for site location 36.30°N, 248.10°E with HT directions from sites A1305 and AW-13-4 (both Carbon Butte) reversed.

[§]Pole calculated from the in situ direction.

[#]Pole calculated from the tilt-corrected direction.

**Pole corrected for inclination flattening. Mean of poles, each from individual tilt-corrected directions with I_f calculated using $f = 0.9$ obtained from the E-I method (Kent and Tauxe, 2005).

[††]Pole for only the tilt-corrected Carbon Butte–Awatubi sites of Weil et al. (2004): $Pole_{Longitude}$ = 166.2°E, $Pole_{Latitude}$ = 16.2°N, A_{95} = 6.8°, K = 98.8, N = 6.

[§§]Combined pole corrected for inclination flattening. Mean of poles, each from individual tilt-corrected directions with I_f calculated using $f = 0.9$ obtained from the E-I method.

***Pole when two Jupiter Member sites are included: $Pole_{Longitude}$ = 163.0°E, $Pole_{Latitude}$ = –1.9°N, A_{95} = 7.0°, K = 29, N = 16.

[†††]Pole corrected for inclination flattening. Mean of poles, each from individual tilt-corrected directions with I_f calculated using $f = 0.5$ obtained from the E-I method.

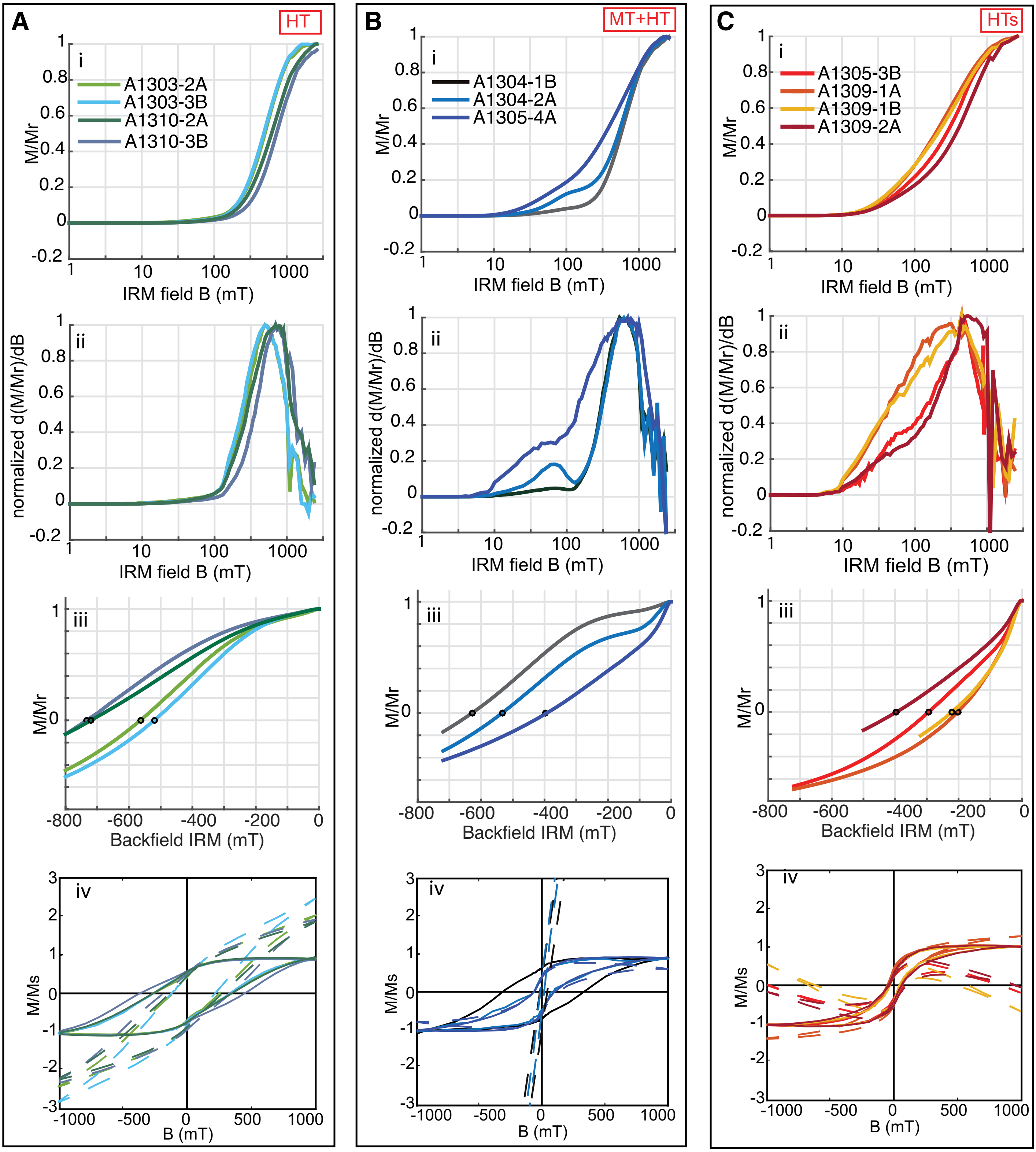

Figure 6. Comparison of rock magnetic results for representative samples including those shown above (Fig. 4) carrying (A) high-temperature (HT), (B) mid- and high-temperature (MT and HT), and (C) steep high-temperature (HTs) components: i—linear acquisition plots, ii—gradient curves of isothermal remanent magnetization (IRM) acquisition, iii—backfield IRM data, iv—hysteresis curves: dashed line—raw data, solid line—data corrected for paramagnetic slope.

(300 mT and >1000 mT, respectively) in addition to distinct unblocking temperatures (e.g., O'Reilly, 1984).

Our group A samples, those carrying origin-trending HT directions, were saturated when reaching around 1.6–2.6 T, consistent with a higher-coercivity mineral such as hematite (Figs. 6Ai and 6Aii). Furthermore, a single high-coercivity peak was displayed in the GAP plots, suggesting that the bulk of the magnetization was carried by a single significant high-coercivity ferromagnetic mineral (Fig. 6Aii). With CLG analysis, this magnetization displayed $B_{1/2}$ ranging from 485 to 708 mT with dispersions of dp = 0.26–0.32. Backfield experiments (Fig. 6Aiii) revealed B_{cr} = 520–734 mT.

Our group B samples with both steep MT and origin-trending shallow HT directions were also saturated when reaching around 2.2–2.6 T, again consistent with a higher-coercivity mineral such as hematite (Figs. 6Bi and 6Bii). This was true even for samples such as A1304-1B, which displayed nearly complete demagnetization at a temperature of 580 °C. In contrast to group A, these samples displayed two peaks on the GAP plots (Fig. 6Bii). For these samples, a lower-coercivity peak with $B_{1/2}$ = 50–63 mT and dp = 0.27–0.42 was revealed. However, despite this lower-coercivity component, the bulk (79%–94%) of the magnetization was still carried by a high-coercivity mineral, with $B_{1/2}$ = 617–631 mT and dp = 0.26–0.41. Backfield IRM of group B samples resulted in B_{cr} = 393–629 mT.

For group C, samples with the HTs component, 99.5% of the sIRM was also reached between 2.4 and 2.6 T (Figs. 6Ci and 6Cii), again suggesting that a high-coercivity mineral such as hematite carried the magnetization. In contrast to group A, these samples displayed either two peaks on the GAP plots, or one peak on the GAP plots that was best fit using two populations of magnetic carriers that slightly overlapped in coercivity (Figs. 6Cii). This was surprising as many of the samples carrying HTs only displayed one prominent component with *MAD* <15°. Despite this single-component demagnetization behavior, the samples all contained a lower-coercivity component ($B_{1/2}$ = 63–141 mT, dp = 0.40–0.55) carrying at least 25% of the sIRM. The rest of the sIRM was carried by higher coercivity components ($B_{1/2}$ = 398–588 mT, dp = 0.22–0.40). These calculated coercivities were all lower than those of the group B high-coercivity components. This influential contribution of the lower-coercivity mineralogy was manifest in the backfield IRM experiments, which indicated values of B_{cr} = 203–396 mT (Fig. 6Ciii), broadly lower than those of samples carrying HT.

Results from Hysteresis Experiments

We conducted hysteresis experiments with maximum fields of 1 T using the vibrating sample magnetometer (VSM) in the Massachusetts Institute of Technology laboratory of C. Ross. The uncorrected hysteresis data were processed by closing the ascending and descending loops when needed, subtracting the high field slope, and adjusting the data such that the *y*-intercepts were equal (analysis and plots from the PmagPy software package; Tauxe et al., 2016). As most samples carrying HT and HTs were not fully saturated by the maximum field allowed by the VSM, minor hysteresis loops were obtained. Based on the corrected hysteresis loop shape, magnetic carriers were classified.

The uncorrected data for samples carrying HT (groups A and B) displayed dominantly paramagnetic behavior (Fig. 6Aiv, 6Biv). The group A corrected hysteresis curves were all single domain, characterized by wide square loops (Fig. 6Aiv). Corrected group B loops revealed either single-domain (A1304-1B) or wide wasp-waisted behavior (A1304-2A, A1305-4A) behaviors (Fig. 6Biv). These wasp-waisted loops were only slightly constricted, with bulk coercive fields from 70 to 80 mT, B_{cr}/B_c ranging from 0.5 to 0.7, and squareness (Mr/Ms) around 0.5 (Table DR4; see footnote 1). All samples carrying HT (groups A and B) were characterized by wide hysteresis loops indicative of higher coercivities (Figs. 6Aiv and 6Biv).

The uncorrected data from group C samples exhibited strong diamagnetic behavior except for A1309-1A, which was slightly paramagnetic (Fig. 6Civ). The corrected hysteresis curves all involved loops that appeared wasp-waisted with constricted waists (Fig. 6Civ). Wasp-waisted curves occur when there are multiple fractions of magnetic minerals with strongly contrasting coercivities, consistent with results observed in the IRM experiments. These wasp-waisted loops were very narrow, with low bulk coercive fields of 35–60 mT, and lower squareness of 0.3–0.4 (Table DR4). Some of these hysteresis loops exhibited a more prominent constriction than others. In particular, A1305-3B did not have a dramatic waist. This degree of wasp-waistedness and constriction may depend on the relative contribution of the coercivity populations (Roberts et al., 1995).

Summary

Although hematite is the magnetic carrier for both the higher-temperature components, we suggest that there are some key differences between the samples displaying HT and HTs. Furthermore, these differences are proposed to reflect a detrital remanent magnetization (DRM) origin for the HT component versus chemical remanent magnetization (CRM) origin for the HTs component. Samples carrying the HT component are dominated by mineralogy with very high coercivity. In contrast, the magnetic mineralogy of samples carrying HTs includes two different populations that both contribute to the magnetization. Specifically, regarding the high-coercivity mineral carrying HT (proposed DRM) and HTs (proposed CRM), it appears that the HT component generally had higher coercivities than the HTs component. This might reflect variations in grain size of the hematite magnetic carriers. Finer grain sizes of hematite have lower coercivities than do grains in the tens of micrometer size range (Özdemir and Dunlop, 2014). Thus, the lower coercivities observed for the HTs samples could correspond to an authigenic population of fine-grained hematite that could be carrying a secondary CRM.

DISCUSSION

Comparison with Previous Work

In addition to our new paleomagnetic data, we also incorporated previously published Chuar Group demagnetization and sample data from a study by Weil et al. (2004) that focused on the Kwagunt and Galeros formations (Table DR5; see footnote 1). The Galeros pole included two sites from the upper Jupiter Member combined with sites from the Carbon Canyon Member, and the combined site mean directions passed a fold test (Weil et al., 2004). The Kwagunt pole relied on a combination of sites spanning almost 500 m of stratigraphy, and the associated parametric bootstrap fold test resulted in a maximum clustering at 80% unfolding and was interpreted to support a primary magnetization acquired at the time of, or soon after, deposition (Weil et al., 2004). The parametric bootstrap fold test can be applied in all cases: prefolding, synfolding and postfolding magnetization (Tauxe and Watson, 1994). However, many samples also displayed a north-directed, moderate to steep positive inclination magnetization overprint with unblocking temperatures also up to 680 °C, similar to the HTs we observed in our data (Weil et al., 2004).

In our reanalysis of the Weil et al. (2004) data set, instead of applying fold tests at the formation level and combining strata now known to span over 20 m.y. (Rooney et al., 2017), we applied fold tests to data from the Carbon Butte and Awatubi members close to the 751 Ma horizon, as well as to data from the individual members. When this was done, we found that a fold test could not be robustly conducted on any of the individual members within the Kwagunt Formation, or alternatively, to the Awatubi and Carbon Butte members combined (Table DR5).

The Carbon Butte Member sites come from locations with minimal bedding variation. As a result, the fold test is indeterminate, with a bootstrap fold test showing that 100% untilting is just as concentrated as 0% untilting. This was also the case when the single Awatubi site was combined with the Carbon Butte sites (Table DR5). These indeterminate fold tests are also mirrored by the negligible difference between the geographic and tilt-corrected site mean circles of 95% confidence (Table DR5).

In our new study, the directions from the combined Carbon Butte and basal Awatubi sites are similar to the previous results from the Carbon Butte and Awatubi members, yet they now pass the bootstrapped fold test (Weil et al., 2004). However, the combined Carbon Butte and basal Awatubi directions appear distinct from the published overlying Walcott directions. Unfortunately, none of our Walcott samples displayed linear decay to the origin; instead, the demagnetization data highlighted planes bridging the steep positive MT directions and low-inclination directions toward the west. The previously published positive-polarity Walcott directions may lie on similar planes to the results from this study (Fig. 7A). As only two Walcott site mean directions were obtained by Weil et al. (2004), and they were both on the same limb of the Chuar syncline, a fold test could not be conducted.

Although we were not able to reproduce the Walcott data, we offer three possible explanations why the Walcott directions of Weil et al. (2004) were distinct from those of the underlying units. Bearing in mind that the HTs and MT directions were pervasive among the upper section of the Kwagunt Formation, it is possible that overlapping thermal unblocking spectra between the two components may have prevented isolation of the primary HT direction. We suggest that the steep overprint directions may bias the Walcott samples, either by (1) allowing incomplete isolation of the primary HT direction, or (2) mixing of HT and HTs directions within a site (Figs. 7B and 7C).

First, the anomalous Walcott directions may be due to sample-level incomplete isolation of the HT direction (Fig. 7B). This was demonstrated by reanalyzing demagnetization data for sample A1301-3B, which specifically includes a HTs steep magnetization until 660 °C, followed by a shallow HT demagnetization until 700 °C. Depending on the chosen demagnetization temperature steps, the apparent origin-trending direction can range along a great circle between the primary direction (HT) and the overprint direction (HTs; Fig. 7B; Table DR6; see footnote 1). Thus, very high-resolution demagnetization steps are required to obtain a line fit that reflects the actual origin-trending direction.

Alternatively, at the site level, strong HTs overprints could be interpreted as primary, resulting in mixing of HT and HTs directions. This may explain the large within-site scatter (α_{95} = 18°) reported for one of the Walcott sites. Artificially Fisher distributed data sets were generated by increasing the percentage of HTs directions mixed with primary HT directions (Table DR6; Fig. 7C). For each case, site means were calculated. When 50%–75% of the samples had HTs directions instead of HT directions, the generated site mean directions overlapped with the Walcott directions, with similar α_{95}, but with smaller k than the reported Walcott directions.

Finally, the Walcott paleomagnetic directions may indeed be primary and distinct from those preserved in the underlying members. In order to better compare these potential explanations, as well to obtain a robust paleomagnetic pole for the Walcott Member, more sample-level data from the Walcott Member are required, the focus of future work. Whatever the case, the existing Walcott data were not combined with the Carbon Butte and Awatubi data into a single paleomagnetic pole. This is supported by the lack of sufficient data to conduct a Walcott Member fold test and by the position of the Walcott data stratigraphically far above the targeted 751 Ma horizon. This final point is especially appropriate as the new geochronology shows that the Carbon Butte and basal Awatubi members are as much as 20 m.y. older than the upper Walcott Member (Rooney et al., 2017).

Interpretation of MT and HTs Poles

For the HTs and MT directions, the poles are interpreted as CRM overprints with unblocking temperatures consistent with hematite as the main magnetic carrier. As the poles are very similar to the present-day field direction, they may reflect recent overprints and could be related to the Laramide orogeny or to Neogene volcanism associated with the Uinkaret volcanic field (e.g., Crow et al., 2008, 2015).

Proposed Primary Paleomagnetic Poles

The HT poles are interpreted as primary. We present two different options for the HT Carbon Butte–Awatubi (CB-A) pole that are very similar in location; one is from our VGPs calculated from samples that displayed HT components with linear decay to the origin, and the other combines our new results with the published Carbon Butte and Awatubi results from Weil et al. (2004). Importantly, this combined pole is based on a greater number of samples than the pole from just our study. When the Tauxe and Watson (1994) fold test was applied to the combined pole, it resulted in designation of prefolding, with 95% uncertainty range of 60%–101% unfolding (Figs. 5G and 5H). An inclination flattening correction of f = 0.9 was applied to the combined directions. These inclination flattening–corrected combined directions also passed the Watson's V reversal test. The Watson's V test was passed with a value of 6.3, which is less than the critical value of 6.9. The McFadden and McElhinny (1990) classification for this test is "B," with an angle between data set means of 7.6° and a critical angle of 8.0°. Finally, we applied the bootstrapped reversal test (Tauxe et al., 2016) to these directions and found that they are consistent with being antipodal at the 95% confidence level. When the inclination flattening–uncorrected directions were analyzed, all reversal tests were also passed. Despite the passage of the reversal tests, the limited number of reversed direction sites may bias the tests.

Several lines of evidence suggest that the Carbon Butte–Awatubi directions (HT CB-A) are primary. The HT direction has been documented at six localities (this study: 17 sites and 17 samples with α_{95} = 5.6° < 16°, and k = 41.3 > 10; or combined directions: 23 sites and 62 samples with α_{95} = 4.9° < 16°, and k = 39.1 > 10), is carried by hematite, and passes a fold test. In addition, the presence of reversed directions adds weight to the conclusion that HT is primary. However, the paleomagnetic poles do resemble younger paleomagnetic poles. While the pole from just this study passed five of the seven Van der Voo (1990) reliability criteria (Q1, Q3, Q4, Q5, Q6; this study), when combined with reanalysis of previously published results, the pole passed six of the seven (Q1, Q2, Q3, Q4, Q5, Q6). This HT Carbon Butte and Awatubi (CB-A) pole was assigned a 751 Ma age, since it passed the fold test, and it is from just below where Rooney et al. (2017) obtained the Re-Os age of 751.0 ± 7.6 Ma from the Awatubi Member. The proposed primary paleomagnetic poles were plotted (Fig. 8A) along with the Laurentian APWP from 510 Ma to the present (Torsvik et al., 2012). The combined Carbon Butte–Awatubi pole based on our new data and reanalysis of previously published data is the preferred ca. 751 Ma pole to incorporate into future Laurentian APWPs and reconstructions.

Paleosecular Variation in Carbon Butte–Awatubi Data

The origin and nature of magnetization carried by hematite in sediments are still being understood. The magnetization can be DRM, CRM, or a mixture of both. DRM typically preserves magnetization acquired during or shortly

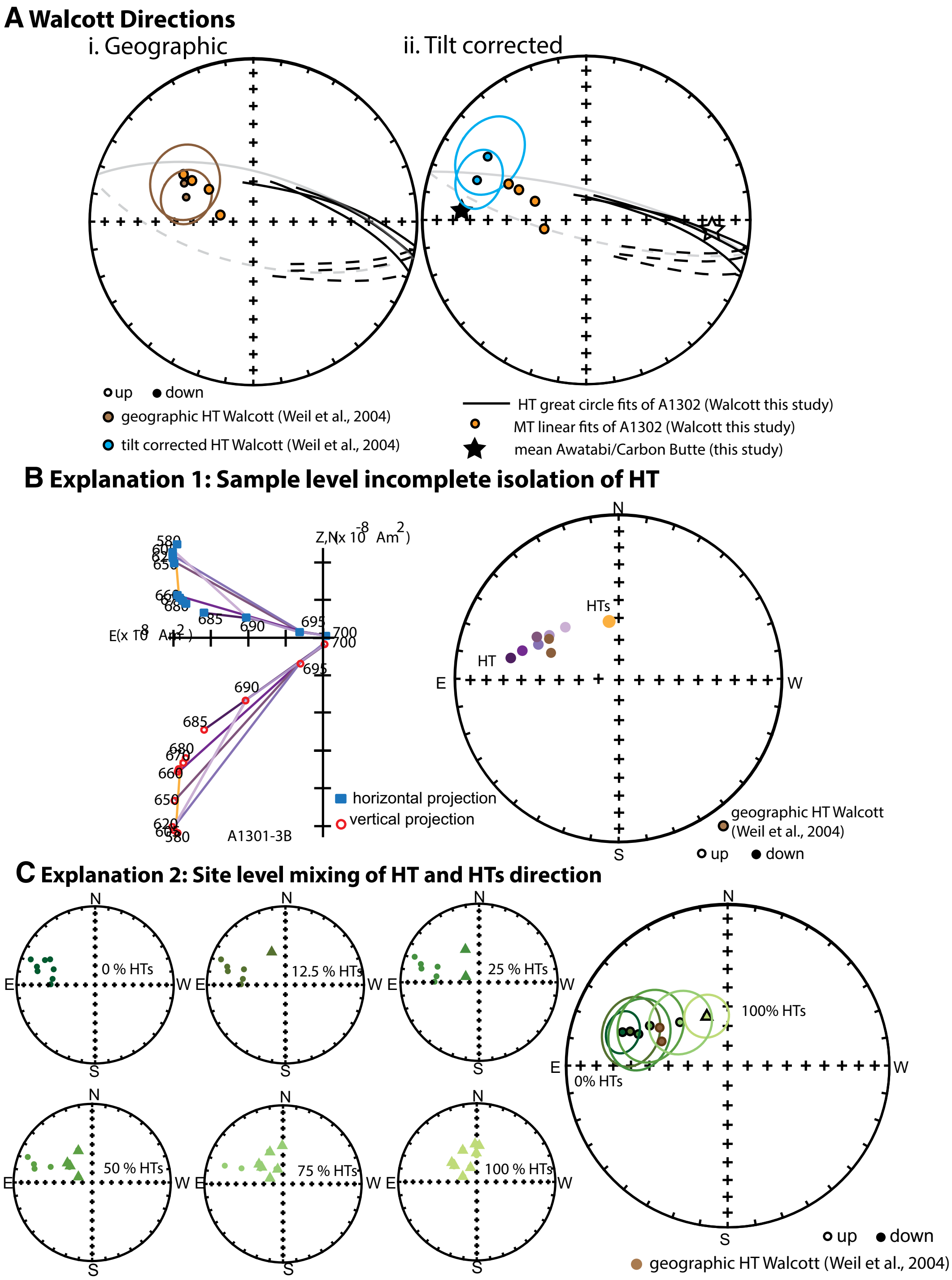

Figure 7. Walcott directions along with two possible interpretations for their dramatic difference from Awatubi and Carbon Butte directions. (A) Geographic (i) and tilt-corrected (ii) equal-area stereographic projections of the Walcott sites. The geographic directions are plotted in brown, and the tilt-corrected directions are plotted in blue. The mid-temperature (MT) Walcott directions and high-temperature (HT) great circle directions from this study are also indicated. The direction of the present-day field (PDF) is indicated in light orange. The mean normal and reversed Awatubi and Carbon Butte directions are plotted with stars. (B) Explanation 1 for Walcott directions: sample level incomplete isolation of HT. Shown to the left is the orthogonal projection diagram of the demagnetization of sample A1301-3B as an example. The yellow lines and shades of purple connect demagnetization steps used to calculate the "primary" linear fit, which is shown on the equal-area plot to the right. For the orthogonal projection diagram, red and blue symbols indicate projections of magnetization vector onto vertical-east (Z-E) and north-east (N-E) axes, respectively. Temperatures of selected thermal demagnetization steps are labeled in units of °C. (C) Explanation 2 for Walcott directions: site level mixing of HT and steep HT (HTs) directions. Here, on the left are equal-area plots showing Fisher distributed site level data sets of the HT and HTs directions (based on sample A1301-3B), with increasing number of directions consistent with HTs and fewer directions consistent with HT. To the right is an equal-area plot with the corresponding "site" mean directions.

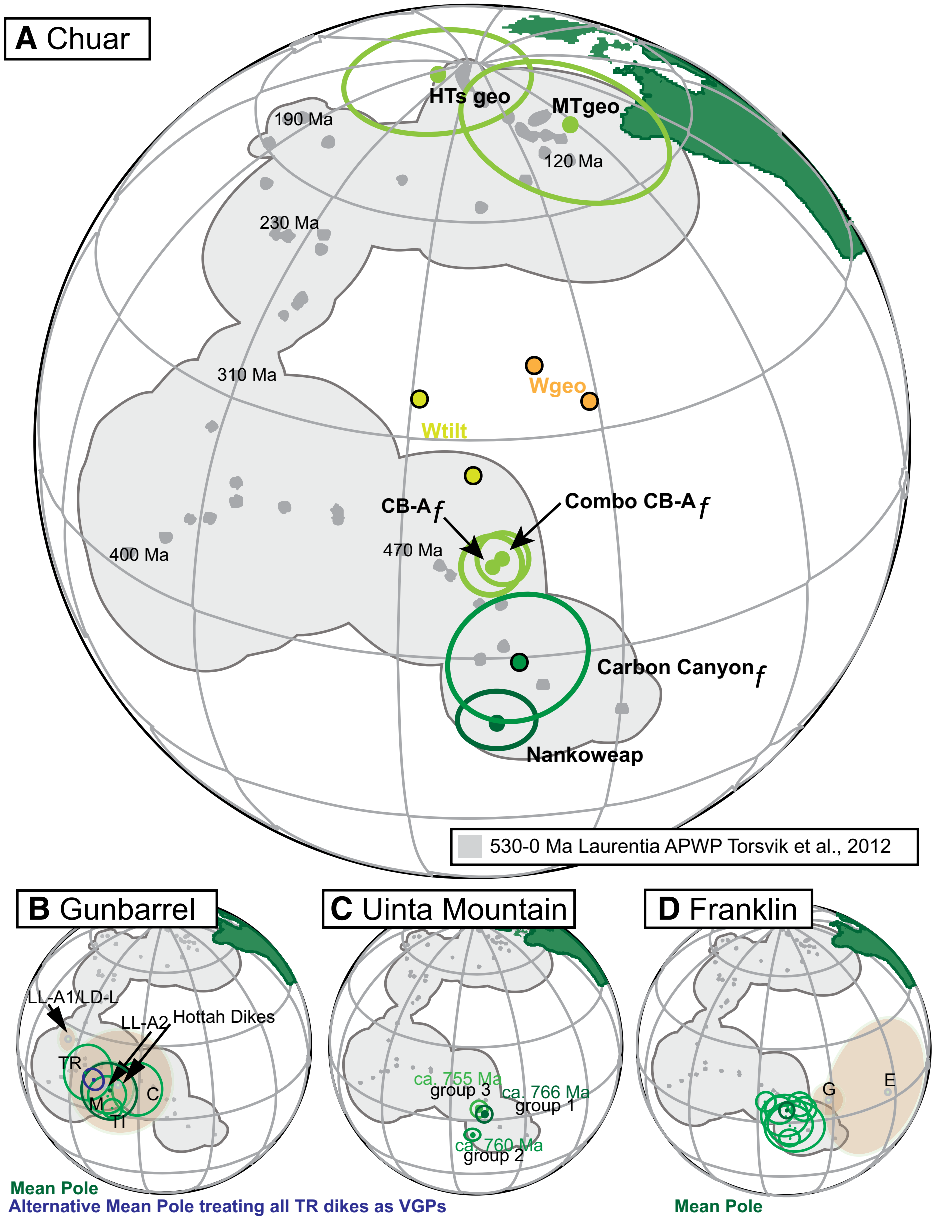

Figure 8. Laurentian paleomagnetic poles. (A) Paleomagnetic poles from the Chuar Group. HTsgeo—high-temperature steep direction in geographic coordinates; MTgeo—mid-temperature direction. Wgeo—Walcott virtual geomagnetic poles (VGPs) in geographic coordinates; Wtilt—VGPs in tilt-corrected coordinates (Weil et al., 2004). CB-A$_f$—Carbon Butte and Awatubi inclination flattening-corrected mean pole from this study only. Combo CB-A$_f$—pole from Awatubi and Carbon Butte inclination flattening-corrected directions combined from this study and Weil et al. (2004). Carbon Canyon$_f$—mean of inclination flattening-corrected Carbon Canyon directions from Weil et al. (2004), where the Nankoweap pole is from Weil et al. (2003). In gray is the 530–0 Ma Laurentian apparent polar wander path (APWP) from Torsvik et al. (2012). (B) Paleomagnetic poles from the Gunbarrel event. LD-L/LL-A1 and LL-A2 are Little Dal poles. Dark green—mean Gunbarrel pole calculated in this study. An alternative mean pole, calculated using all of the Tobacco Root B dikes (TR dikes) as individual VGPs, is shown in blue. (C) Uinta Mountain Group poles from Bressler (1981) and Weil et al. (2006). Reported and proposed sampling heights allowed separation of poles into three groupings that were used in subsequent analysis. (D) Paleomagnetic poles from the Franklin large igneous province. G—Greenland pole, E—Ellesmere pole. Dark green—mean Franklin pole calculated by Denyszyn et al. (2009).

after deposition and can reflect variations in the geomagnetic field (Steiner, 1983; Tauxe and Badgley, 1984). Alternatively, CRM can reflect magnetization acquired both over shorter time scales and record PSV (e.g., Molina-Garza et al., 1991), or very long time scales (~10 m.y.), averaging both PSV and plate motions (e.g., Larson et al., 1982). Depending on the magnetization and time scale over which the remanence was acquired, PSV may be averaged in a single sample of a sedimentary rock. Most studies assume that sediments with high-stability magnetization were likely acquired within 10^3 yr after deposition and reflect some averaging of PSV. In some cases, observed between-site dispersion supports acquisition of magnetization within 10^2 to 10^3 yr of deposition (Herrero-Bervera and Helsley, 1983; Shive et al., 1984). Furthermore, there are other sources of dispersion in paleomagnetic data sets such as ours.

To test our paleomagnetic data set for PSV, we followed Deenen et al. (2011), who suggested that the dispersion of VGPs in the Fisherian sets should be constant with latitude and that Fisher statistics should be applied to VGP directions, not to paleomagnetic directions. They also suggested that amended paleomagnetic criteria include an N-dependent A_{95} envelope, bounded by an upper limit $A_{95}max$, and a lower limit $A_{95}min$, to ascertain whether or not a distribution has sufficiently well-sampled PSV and therefore geomagnetic field behavior. Our mean pole from the inclination flattening–corrected VGPs has an A_{95} of 4.1° and thus falls just within the error bounds for N_{17} = 3.86°–13.76°. Thus, results obtained from using the A_{95} envelope of Deenen et al. (2011) suggest that our sample data set could be consistent with sufficiently sampled PSV. The combined inclination flattening–corrected pole has an A_{95} of 3.5° and also just falls inside the error bounds for N_{23} = 3.42°–11.37°. Thus, the A_{95} envelope of Deenen et al. (2011) suggests that the combined data set may contain the full variation of geomagnetic field behavior.

Reevaluation of the Tonian Laurentian APWP

We next integrated these results with previous data sets into a robust stratigraphic context with recent geochronology results to better calibrate the Laurentian APWP in space and time. The other poles constraining the Laurentian APWP are those from the ca. 775 Ma Gunbarrel event (Fig. 8B), the <775 Ma Nankoweap Formation (Fig. 8A), the ca. 757 Ma Carbon Canyon Member of the Chuar Group (Fig. 8A), the ca. 750 Ma Uinta Mountain Group (Fig. 8C), and the ca. 720 Ma Franklin large igneous province (Fig. 8D). We compiled these into a ca. 780–720 Ma APWP for Laurentia (Figs. 8 and 9), and in the following sections, we discuss each pole.

Gunbarrel Event

The Gunbarrel event (Table 2; Fig. 8B) is marked by ca. 775 Ma mafic dikes and sills in three widely separated areas of Cordilleran North America (the Wyoming Province, the Mackenzie Mountains in the northern Cordillera, and the Canadian Shield; e.g., Harlan et al., 2003). The magmatism has been attributed to mantle-plume activity or upwelling asthenosphere leading to crustal extension accompanying initial breakup of the supercontinent Rodinia and development of the proto–Pacific Ocean or thermal weakening of the crust (e.g., Harlan et al., 2003; Milton et al., 2017). In the Mackenzie Mountains, the extrusive Little Dal Basalt has been geochemically linked to the Tsezotene intrusives (Dudás and Lustwerk, 1997) and was recently precisely dated with chemical abrasion–isotope dilution–thermal ionization mass spectrometry (CA-ID-TIMS) U-Pb dating on zircon to 774.93 ± 0.54 Ma (Milton et al., 2017). This date agrees with the range of 788–772 Ar-Ar dates from Tobacco Root dikes, the Mount Moran dike, and the Christmas Lake dike in the Northwest United States (Harlan et al., 2008), as well as U-Pb dates from Northwest Canada intrusive units (Jefferson and Parrish, 1989; Harlan et al., 2003).

These ca. 780 Ma intrusive rocks have been the focus of paleomagnetic studies and have yielded paleomagnetic data that are relatively clustered (Park, 1981a; Park et al, 1989, 1995a; Park and Jefferson, 1991; Morris and Aitken, 1982; Harlan et al., 1997, 2008). In Montana, the Tobacco Root B dikes were grouped by major- and trace-element geochemistry (Wooden et al. 1978) before paleomagnetic and geochronologic analysis. There were 11 dikes from which resolvable directions were published. Results of the baked contact test were not straightforward to interpret, but the authors suggested that the baked contact test should be considered to be positive (Harlan et al., 2008).

Although clustering near the Wyoming intrusion poles, the commonly used mean pole for the Tsezotene intrusions (e.g., Li et al., 2008) combines 17 sites from 10 different intrusions from the Mackenzie Mountains all the way to the Yukon-Alaska border (Park et al., 1989). Unfortunately, these intrusions do not all correspond to geochronologically dated units and may potentially correspond to different events (e.g., Goodfellow et al., 1995; Martel et al., 2011). In addition, some of the published demagnetization data do not display a clear decay to the origin (e.g., figs. 3 and 4 of Park et al., 1989; fig. 4 of Park, 1981a). Finally, despite the broad sampling region, analysis resulted in an inconclusive fold test, and there were no other field tests. Because this commonly reported pole has these issues, we reanalyzed the previous studies of "Tsezotene intrusions" and only chose to use the paleomagnetic data interpreted as primary from the dated Tsezotene intrusion, the Concajou Canyon sill (A_R data from Park, 1981a; see Table DR7 for reanalyzed means; see footnote 1). As there was only minor tilting in this region, the fold test is inconclusive, but slightly smaller α_{95} values were calculated in tilt-corrected coordinates (Park, 1981a).

A paleomagnetic pole from the Hottah dikes with a large A_{95} value was originally regarded as preliminary (Park et al., 1995b). As there are no field tests to constrain the age of this magnetization (only a partial baked contact test), we experimented with the original Hottah dike data (Table DR8; see footnote 1) and calculated a Gunbarrel pole that included them, as well as one that did not (Gunbarrel Mean1 and Mean2 vs. Mean3 and Mean4; Table 2). We found that the inclusion of the Hottah dikes did not substantially change the overall Gunbarrel mean direction.

From the Little Dal Basalt, two directions that could be primary (LL-A1/LD-L and LL-A2) have been identified (Morris and Aitken, 1982; Park and Jefferson, 1991). As LL-A1 was more abundant in the lower, less-altered parts of the basalt sections, it was interpreted as primary. However, LL-A1 is ~20° away from the rest of the Gunbarrel poles, which may be due to vertical-axis block rotations within the Mackenzie Mountains (Park and Jefferson, 1991). The

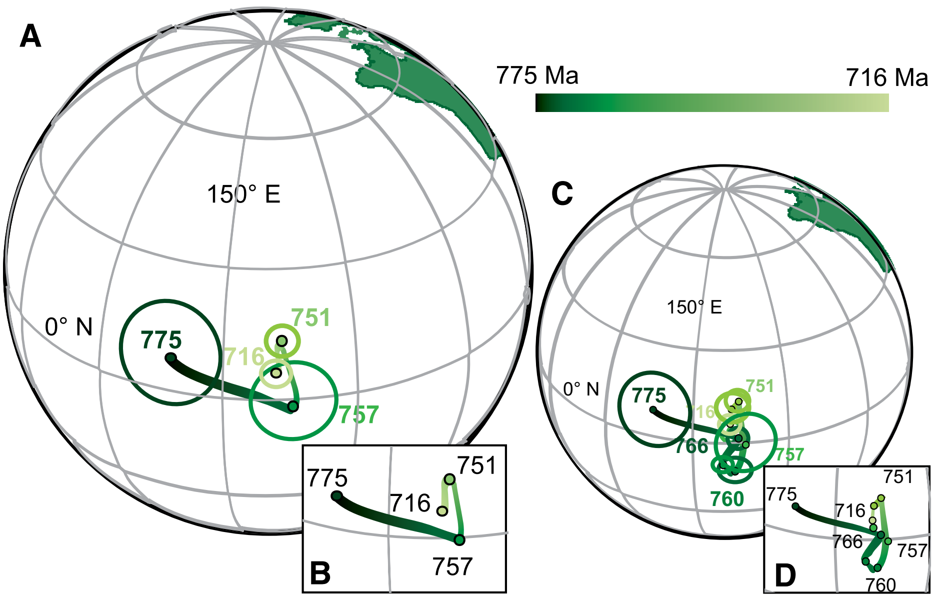

Figure 9. Late Tonian Laurentian apparent polar wander path (APWP) showing summary robust Laurentian APWP using poles with radiometric age constraints with circles of A_{95} uncertainty for each pole (A), and without the A_{95} errors plotted (B). In decreasing age are Gunbarrel pole (775 Ma), Carbon Canyon pole (757 Ma), the combined Carbon Butte–Awatubi mean pole (751 Ma), and the Franklin large igneous province pole (716 Ma). (C–D) Alternatively, we plotted the APWP using all the poles discussed. For this APWP, the poles are: Gunbarrel pole (775 Ma), Uinta Mountain Group 1 pole (ca. 766 Ma), Uinta Mountain Group 2 pole and Nankoweap pole (both ca. 760 Ma), Carbon Canyon pole (757 Ma), Uinta Mountain Group 3 pole (ca. 755 Ma), the combined Carbon Butte–Awatubi mean pole (751 Ma), and finally the Franklin large igneous province pole (716 Ma).

TABLE 2. 780–720 MA LAURENTIAN PALEOMAGNETIC POLES

Unit/Formation	Age (Ma)	Type of age and reference if different	Paleomagnetic pole Lat. (°N)	Long. (°E)	A_{95}* (°)	Paleomagnetic reference	Notes
Franklin individual studies							
Coronation sill–Baffin Int.	723 +4/–2	U-Pb badd. frac. upper intercept (Heaman et al., 1992)	8.0	167.0	5.0	Fahrig et al. (1971)	Composite age from 10. Badd. frac. from Coronation sill, Quadyuk Is./Bathhurst inlet, Cumberland dike
Coronation sills	723 +4/–2	See above (Heaman et al., 1992)	–1.0	163.0	9.0	Robertson and Baragar (1972)	N.A.§
Baffin dikes	N.D.†	N.A.§	6.3	168.2	4.8	Fahrig and Schwarz (1973)	N.A.§
Baffin dikes	716 +4/–5	U-Pb badd. frac. wt. average (Pehrsson and Buchan, 1999)	9.2	153.3	3.8	Christie and Fahrig (1983)	Age from one dike, 2 fractions
Miscellaneous dikes	N.D.†	N.A.§	3.0	161.3	9.2	Park (1974)	N.A.§
Victoria Is. Natkusiak lavas & sills	716.33 ± 0.54	U-Pb CA-ID-TIMS badd. (Macdonald et al., 2010)	–7.0	163.0	4.0	Palmer and Hayatsu (1975)	Additional sill ages: 718 ± 2 Ma upper intercept of 1 badd. and 3 zir. frac.(Heaman et al., 1992)
Victoria Is. Natkusiak upper lavas	N.D.†	No ages on extrusives, assumed correlative with sills	6.0	159.0	5.7	Palmer et al. (1983)	Additional ages (cont.) 723 +12/–2 from 5 badd. frac. (Heaman et al., 1992)
Brock Inlier sills	708 ± 4	Ar-Ar hbl (Ernst et al., 2004)	–2.0	165.0	12.0	Park (1981b)	Aka. Lasard River dikes
Greenland	712 ± 2, 721 ± 4	U-Pb ID-TIMS badd. frac. (Denyszyn et al., 2009a)	8.8	178.5	7.2	Denyszyn et al. (2009a)	Anomalous. Resolved by early Cenozoic block rotations around the Nares Strait
Ellesmere Island	721 ± 2	U-Pb ID-TIMS badd. frac. (Denyszyn et al., 2009a)	4.0	206.8	30.2	Denyszyn et al. (2009a)	Supports ~20° rotation of Devon-Ellesmere microplate Anomalous SW directions from secular variation sampling bias or pyrrhotite characteristic remanent magnetization (Denyszyn et al., 2009a, 2009b)
Devon Island	N.D.†	N.A.§	6.3	184.0	11.0	Denyszyn et al. (2009a)	Supports ~20° rotation of Devon-Ellesmere microplate
Franklin mean poles							
Victoria/Baffin	N.D.†	N.A.§	5.0	163.0	5.0	Park (1994)	N.A.§
Mainland/Baffin	N.D.†	N.A.§	5.8	165.8	3.8	Fahrig and Schwarz (1973)	N.A.§
Victoria/Baffin	N.D.†	N.A.§	8.0	163	4.0	Buchan et al. (2000)	N.A.§
Victoria/Baffin/Mainland**	716.33 ± 0.54	U-Pb CA-ID-TIMS badd. (Macdonald et al., 2010)	6.7	162.1	3.0	Denyszyn et al. (2009a)	Site-filtered by Denyszyn et al. (2009a) from previous studies
Victoria/Baffin/Mainland, Greenland/Ellesmere	N.D.†	N.A.§	8.4	163.8	2.8	Denyszyn et al. (2009a)	Site-filtered from previous studies combined with variably rotated data from Greenland and Ellesmere
Kwagunt							
Combined Carbon Butte+Awatubi**	751.0 ± 7.6	Re-Os(Rooney et al., 2017)	14.2	163.8	3.5	This study	This study combined with Weil et al. (2004). Corrected for inclination flattening $f = 0.9$ (E-I method from this study)
Carbon Butte+Awatubi	751.0 ± 7.6	Re-Os (Rooney et al., 2017)	13.1	161.6	4.1	This study	Corrected for inclination flattening $f = 0.9$ (E-I method)
Kwagunt	Ca. 750–736	Assumed correlation	18	166.0	7.0	Weil et al. (2004)	Pole was used with 740 Ma age
Galeros							
Carbon Canyon**	757.0 ± 6.8	Re-Os (Rooney et al., 2017)	–0.5	166.0	9.7	Data reanalyzed this study	Weil et al. (2004) data from Carbon Canyon Mb corrected for inclination flattening $f = 0.5$ (E-I method)
Galeros	Ca. 800	Assumed correlation	–1.9	163.0	7.0	Weil et al. (2004)	N.A.§
Uinta Mtn Group (UMG)							
Group 3††	Ca. 755	Correlative with mid-upper Kwagunt?	4.9	160.6	3.2	Data reanalyzed this study	Reanalyzed from Weil et al. (2006) and Bressler (1981); N = 46 sites; k = 43.82
UMG Group 2††	Ca. 760	Assumed correlation < UMG Group 1	–5.8	158.7	2.7	Data reanalyzed this study	Reanalyzed from Weil et al. (2006) and Bressler (1981); N = 21 sites; k = 140.58
UMG Group 1††	Ca. 766 <766 ± 4	U-Pb LA-ICP-MS det. zir. (Dehler et al., 2010)	3.0	163.5	3.2	Data reanalyzed this study	Reanalyzed from Weil et al. (2006) and Bressler (1981); N = 22 sites; k = 95.73
Nankoweap							
Nankoweap††	<782 Ma, <UMG group 1	U-Pb LA-ICP-MS det. zir. (Dehler et al., 2017)	–10	163	4.9	Weil et al. (2003)	Pole was used previously used with a with 900 Ma age. Inclination flattening could not be determined via E-I method

(*Continued*)

TABLE 2. 780–720 MA LAURENTIAN PALEOMAGNETIC POLES (*Continued*)

Unit/Formation	Age (Ma)	Type of age and reference if different	Paleomagnetic pole Lat. (°N)	Long. (°E)	A_{95}* (°)	Paleomagnetic reference	Notes
Gunbarrel event							
Mean Tobacco Root-B dikes	775 ± 3	Ar-Ar hbl.	14.6	127.0	11.6	Harlan et al. (2008)	Mean of the sampled dikes
Tobacco Root-B dike 1	*Ca. 775*	Geochemical correlation with dated dikes	18.8	118.8	15.1	Harlan et al. (2008)	N.A.§
Tobacco Root-B dike 2	772 ± 3, 781 ± 4	Ar-Ar bt. (TR50), Ar-Ar hbl. (TR6)	13.8	134.2	6.4	Harlan et al. (2008)	N.A.§
Tobacco Root-B dike 3	*Ca. 775*	Geochemical correlation with dated dikes	18.8	128.6	4.9	Harlan et al. (2008)	N.A.§
Tobacco Root-B dike 4	*Ca. 775*	Geochemical correlation with dated dikes	11.3	132.3	11.6	Harlan et al. (2008)	N.A.§
Tobacco Root-B dike 5	Ca. 775	Geochemical correlation with dated dikes	10.6	129.7	7.3	Harlan et al. (2008)	N.A.§
Tobacco Root-B dike 6	*Ca. 775*	Geochemical correlation with dated dikes	18.8	124.7	5.8	Harlan et al. (2008)	N.A.§
Tobacco Root-B dike 7	777 ± 4, 788 ± 4	Ar-Ar hbl. (TR19b), Ar-Ar hbl. (TR21b)	15.8	126.6	4.4	Harlan et al. (2008)	N.A.§
Tobacco Root-B dike 8	*Ca. 775*	Geochemical correlation with dated dikes	8.3	131.7	9.0	Harlan et al. (2008)	N.A.§
Tobacco Root-B dike 9	*Ca. 775*	Geochemical correlation with dated dikes	18.0	122.7	8.3	Harlan et al. (2008)	N.A.§
Tobacco Root-B dike 10	790 ± 2	Ar-Ar hbl. (TR62)	9.3	132.9	7.1	Harlan et al. (2008)	N.A.§
Tobacco Root-B dike 11	*Ca. 775*	Geochemical correlation with dated dikes	13.7	124.6	5.0	Harlan et al. (2008)	N.A.§
Christmas Lake dike	774 ± 4	Ar-Ar hbl.	7.4	137.0	8.3	Harlan et al. (1997)	N.A.§
Mount Moran dike	775 ± 10	discordant Ar-Ar on hbl.-px.	11.6	148.9	10.2	Harlan et al. (1997)	N.A.§
Tsezotene sills	777.7 +2.5/–1.8	U-Pb upper intercept on zir. frac. from intrusion chemically similar to sills (Jefferson and Parrish, 1989)	1.6	137.8	5.0	Park et al. (1989)	From multiple intrusions assumed to be correlative
Concajou Canyon sill	779.5 ± 2.3	Pb-Pb badd. frac. Concajou Canyon (Harlan et al., 2003)	2.6	139.6	4.1	This study	A_R reanalyzed from Park (1981a)
Little Dal Basalt LLA1/LD-L	774.93 ± 0.54	U-Pb CA-ID-TIMS zir. (Milton et al., 2017)	24.0	115.0	7.0	Morris and Aitken (1982)	Local tectonic rotations? Paleozoic overprinting event?
Little Dal Basalt LLA2	774.93 ± 0.54	U-Pb CA-ID-TIMS zir. (Milton et al., 2017)	11.0	137.0	11.0	Park and Jefferson (1991)	No published demagnetization data
Hottah Sheets	780 ± 1	Pb-Pb badd. frac. wt. average (Harlan et al., 2003)	13.0	141.0	22.0	Park et al. (1995b)	Large A_{95}; age from Gunbarrel, Calder and Faber Lake gabbros (7 badd. fractions)
Hottah Sheets–Gunbarrel sheet	779.6 ± 1.4	Pb-Pb badd. frac. wt. average (Harlan et al., 2003)	5.9	142.4	N.D.†	Park et al. (1995b)	N.A.§
Hottah Sheets–Calder sheet site 4	779.5 ± 1.8	Pb-Pb badd. frac. wt. average (Harlan et al., 2003)	22.0	138.4	N.D.†	Park et al. (1995b)	N.A.§
Hottah Sheets–mean Margaret sheet	N.D.†	N.D.†	11.9	147.0	14.8	This study (N = 2, K = 288.5)	Reanalyzed data from Park et al. (1995b)
Hottah Sheets recalculated mean	780 ± 1	Pb-Pb badd. frac. wt. average (Harlan et al., 2003)	13.3	142.7	14.0	This study (N = 3, K = 78.8)	Reanalyzed data from Park et al. (1995b) with site 5 omitted
Gunbarrel mean 1**	774.93 ± 0.54	U-Pb CA-ID-TIMS zir. (Milton et al., 2017)	9.1	138.2	11.7	This study (N = 4, K = 62.57)	Tobacco Root B mean, Christmas Lake dike, Mount Moran dike, Concajou Canyon sill
Gunbarrel mean 2	774.93 ± 0.54	U-Pb CA-ID-TIMS zir. (Milton et al., 2017)	12.9	131.0	4.4	This study (N = 14, K = 81.58)	11 VGPs from Tobacco Root-B, Christmas Lake dike, Mount Moran dike, Concajou Canyon sill
Gunbarrel mean 3	774.93 ± 0.54	U-Pb CA-ID-TIMS zir. (Milton et al., 2017)	9.9	139.1	8.8	This study (N = 5, K = 72.44)	Tobacco Root B mean, Christmas Lake dike, Mount Moran dike, Concajou Canyon sill, recalculated Hottah mean
Gunbarrel mean 4	774.93 ± 0.54	U-Pb CA-ID-TIMS zir. (Milton et al., 2017)	13.0	133.0	4.3	This study (N = 17, K = 68.60)	11 VGPs from Tobacco Root-B, Christmas Lake dike, Mount Moran dike, Concajou Canyon sill, 3 VGPs from Hottah Sheets

Note: Type of age abbreviations: baddeleyite (badd.); zircon (zir.); biotite (bt.); hornblende (hbl.); pyroxene (px); detrital (det.); fraction (frac.); weighted average (wt. average); chemical abrasion (CA); isotope dilution–thermal ionization mass spectrometry (ID-TIMS); laser ablation–inductively coupled plasma–mass spectrometry (LA-ICP-MS). Elongation-Inclination (E-I) (e.g. Tauxe and Kent, 2004).

*A_{95}— radius of the circle of 95% confidence about the mean. If not available, $A_{95} \sim \sqrt{dp \times dm}$, where dp and dm are the semi-axes of the 95% ellipse of confidence about the mean (McElhinny and McFadden, 2000).

†N.D—not determined.

§N.A.—not applicable.

**Pole used in proposed robust apparent polar wander path (APWP) and reconstructions.

††Pole lacks robust age constraints but could be used in APWP and reconstructions.

other pole, LL-A2, bears similarity to the other Gunbarrel poles, but it lacks published demagnetization data. Due to these uncertainties, the paleomagnetic data from the Little Dal Basalt were not included in our calculated mean Gunbarrel pole.

Thus, for our APWP and reconstructions, we integrated the Concajou Canyon sill pole, interpreted to be a VGP, with those of the Wyoming dike VGPs. The mean pole was calculated in two different ways, first (Gunbarrel Mean1) by averaging the Christmas Lake dike VGP, the Mount Moran dike VGP, the Concajou Canyon sill VGP, and the Tobacco Root Mountain B dikes mean pole. Alternatively, we incorporated the 11 different VGPs from the Tobacco Root Mountain B dikes (Gunbarrel Mean2). The resultant mean Gunbarrel poles and associated A_{95} values are shown in Figure 8B (Table 2). The difference between the mean Gunbarrel poles is manifested only in a slight difference in the rotation orientation of Laurentia, but in our subsequent reconstructions, we took the Gunbarrel Mean1 as the best estimate for the 775 Ma pole for Laurentia, as it is possible that giving equal weight to all the Tobacco Root B dike poles (Gunbarrel Mean2) may be oversampling intrusions recording the same snapshot of the time-varying geomagnetic field.

Mackenzie Mountains Supergroup

There are also paleomagnetic data from sedimentary strata of the Mackenzie Mountains Supergroup in northwestern Canada (Park, 1984; Park and Aitken, 1986; Park and Jefferson, 1991; Fig. DR8; Table DR9; see footnote 1). However, several issues hamper these data sets and their incorporation into any APWP. Specifically, these sedimentary poles lack age constraints and field tests, involve coarse demagnetization steps (in some cases, lacking published demagnetization data), and, finally, may have been complicated by unrecognized or recognized block rotations associated with Cordilleran tectonics (Park, 1984; Park and Aitken, 1986; Park and Jefferson, 1991, and references therein). Thus, we chose not to include these paleomagnetic poles in our APWPs and reconstructions.

Nankoweap Formation

The paleomagnetism of sandstones of the Nankoweap Formation was investigated by Weil et al. (2003). The demagnetization data demonstrated that almost all samples displayed a single vector component with a minor secondary component. The in situ secondary component was subparallel to Earth's present-day field (PDF). This secondary component was normally demagnetized by 200 °C and was interpreted as a viscous overprint. Previously, the parametric bootstrap fold test was applied to the combined seven sites with resolvable directions and resulted in a 95% confidence interval that included 100% unfolding (Weil et al., 2003; see also Tables 2 and 3 here).

New detrital zircon data show that the age of the Nankoweap Formation is younger than 782 Ma (LA-ICP-MS; Dehler et al., 2017). Because of the difference in pole position, we further suggest that the Nankoweap Formation is younger than the Gunbarrel event and thus younger than 775 Ma. Finally, examination of, and comparison with the Uinta Mountain Group 1 may be compatible with the interpretation that the Nankoweap Formation is younger than 766 Ma (see discussion below). Thus, we assigned an age of ca. 760 Ma to the Nankoweap paleomagnetic pole. Inclination flattening could not be ascertained via the E-I method, as the Nankoweap data set produced a pathological result.

Carbon Canyon

To obtain an appropriate paleomagnetic pole to associate with the 757.0 ± 6.8 Ma Re-Os age from the middle of the Carbon Canyon Member (Rooney et al., 2017), data only from the Carbon Canyon Member were reanalyzed (Weil et al., 2004). Because of the stratigraphic separation between the Jupiter Member sites and the Carbon Canyon Member sites, this reported 757 Ma pole only included the Carbon Canyon data. However, a decision to include the Jupiter Member data would only shift the pole and the A_{95} each by <1°. These Carbon Canyon directions passed the fold test, with a 95% interval of 72%–109% unfolding (Table 1; Fig. DR5). Inclination flattening was determined using the E-I method (Kent and Tauxe, 2005) as implemented in the PmagPy software package (Tauxe et al., 2016). For this data set, $f = 0.5$ was found to be the optimal flattening correction, with I_o = 5.8° and I_f = 9.5° with bounds from 0.6 to 22.9° (Fig. DR5). The elongation was found to be 2.7372, with bootstrap bounds from 2.4404 to 2.9124. This Carbon Canyon Member pole was given a ca. 757 Ma age for the presented reconstructions (Table 1).

Uinta Mountain Group

From the Uinta Mountain Group of Utah, Bressler (1981) reported data within a stratigraphic framework from four sites in the western Uinta Mountains and three in the eastern Uinta Mountains (173 samples total; Fig. 8D; Fig. DR6; Table DR10; see footnote 1). One site (Bressler site 6-B6) displayed reversed directions slightly anomalous from the rest. This difference was initially suggested to indicate apparent polar wander during deposition (Bressler, 1981); however, it included samples with rather large demagnetization steps (see discussion in Weil et al., 2006). Later work by Weil et al. (2006) expanded the paleomagnetic data set from the Eastern Uinta Mountains (Home Mountain Canyon: N = 3; Bull Canyon: N = 10; Sparks-Talamantes Creek: N = 9 localities) as well as from the north-central Uintas (Sheep Creek Canyon: N = 23; Browne Lake: N = 1; Carter Creek: N = 5; Dowd Springs: N = 5; and Flaming Gorge Reservoir dam: N = 16). Sampling was focused on hematite-cemented medium- to fine-grained sandstone and siltstone. Samples commonly displayed a single component magnetization, either shallow directions to the east or west (50%), or steep positive directions (45%). Weil et al. (2006) isolated both normal and reversed polarity directions, but only one locality displayed mixed polarity (Dowd Springs; Table DR11; Fig. DR6).

We reevaluated the Uinta Mountain Group paleomagnetic data by incorporating new mapping (Sprinkel, 2006, 2007, 2015; Constenius, 2009) to assign stratigraphic information to the sampling localities of Weil et al. (2006) (Fig. 8D; Fig. DR6). Three paleomagnetic poles were calculated based on stratigraphic information and site pole locations from all sites with α_{95} <20°. Group 1 (stratigraphically lowest) was mixed polarity and included sites 1, 2, 3, and 4 from Bressler (1981), and sites from Sparks–Talamantes Creek, Home Mountain Canyon (Willow Creek), and Bull Canyon from Weil et al. (2006). Group 2 was single polarity to the west and included site 5 from Bressler (1981), and sites from Carter Creek and Flaming Gorge from Weil et al. (2006). Finally, Group 3 (stratigraphically highest) included site 6 from Bressler (1981), and sites from Browne Lake, Sheep Creek, and Dowd Springs as studied by Weil et al. (2006).

We incorporated correlations with the Chuar Group stratigraphy to help estimate ages of the less well-dated Uinta Mountain Group. The group 3 poles are from the upper Hades Pass Formation, which is broadly correlative with the upper Galeros Formation to the lower Kwagunt Formation in the Grand Canyon (Dehler et al., 2017). Given this correlation and the recent Re-Os age constraints on the Grand Canyon strata, we assigned a ca. 755 Ma age to the group 3 pole (potentially between 757 ± 6.8 Ma and 751.0 ± 7.6 Ma Re-Os; Rooney et al., 2017). This group 3 pole is not coincident with the Carbon Canyon pole, and thus may be younger. The underlying group 2 poles are above a horizon dated with U-Pb on detrital zircon at <766 ± 4 Ma (Dehler et al., 2010), and thus we assigned it an age of ca. 760 Ma. Interestingly, this pole

TABLE 3. 780–720 MA CRATON PALEOMAGNETIC POLES

Unit/Formation	Age (Ma)	Type of age and reference	Paleomagnetic pole Lat. (°N)	Long. (°E)	A_{95}* (°)	Paleomagnetic reference	Notes
Laurentia							
Franklin large igneous province Victoria/ Mainland/Baffin**	716.33 ± 0.54	U-Pb CA-ID-TIMS badd. (Macdonald et al., 2010)	6.7	162.1	3.0	Denyszyn et al. (2009a)	Site-filtered by Denyszyn et al. (2009a) from previous studies
Combo Carbon Butte–Awatubi**	751.0 ± 7.6	Re-Os from basal Awatubi Mb (Rooney et al., 2017)	14.2	163.8	3.5	This study	Data from this study combined with data from Weil et al. (2004). All corrected for inclination flattening f = 0.9 (E-I method from this study)
Carbon Canyon**	757.0 ± 6.8	Re-Os from middle Carbon Canyon Mb. (Rooney et al., 2017)	–0.5	166.0	9.7	Data reanalyzed this study	Weil et al. (2004) data from Carbon Canyon Mb corrected for inclination flattening f = 0.5 (E-I method)
Uinta Mtn Group (UMG) Group 3††	Ca. 755	Correlative with mid-upper Kwagunt?	4.9	160.6	3.2	Data reanalyzed this study	Reanalyzed from Weil et al. (2006) and Bressler (1981); N = 46 sites; k = 43.82
Nankoweap††	<782 <UMG group 1	U-Pb LA-ICP-MS det. zir (Dehler et al., 2017)	–10.0	163.0	4.9	Weil et al. (2003)	N.A.§
UMG Group 2††	Ca. 760	Assumed correlation < UMG Group 1	–5.8	158.7	2.7	Data reanalyzed this study	Reanalyzed from Weil et al. (2006) and Bressler (1981); N = 21 sites; k = 140.58
UMG Group 1††	Ca. 766 <766 ± 4	U-Pb LA-ICP-MS det. zir. (Dehler et al., 2010)	3.0	163.5	3.2	Data reanalyzed this study	Reanalyzed from Weil et al. (2006) and Bressler (1981); N = 22 sites; k = 95.73
Gunbarrel mean**	774.93 ± 0.54	U-Pb CA-ID-TIMS zir. (Milton et al., 2017)	9.1	138.2	11.7	This study (N = 4, K = 62.57)	Tobacco Root B mean, Christmas Lake dike, Mount Moran dike, Concajou Canyon sill
Southern Australia							
Mundine Well dykes**	755 ± 3	Pb-Pb SHRIMP zir. wt. average	45.3	135.4	4.1	Wingate and Giddings (2000)	N.A.§
Kanpa Fm	760–720	Chemo- and lithostratigraphic correlations	74.0	128.8	10.6	Pisarevsky et al. (2007)	Close to some Middle Devonian Australian poles; preliminary result
Hussar Fm††	800–760	Chemo- and lithostratigraphic correlations	62.2	85.8	10.3	Pisarevsky et al. (2007)	N.A.§
Browne Fm	830–800	Chemo- and lithostratigraphic correlations	44.5	141.7	6.7	Pisarevsky et al. (2007)	N.A.§
Northern Australia							
Bitter Springs Fm. Johnny's Creek Mb.††	Ca. 788	Chemo- and lithostratigraphic correlations	15.8	83.0	13.5	Swanson-Hysell et al. (2012)	See text of paper for discussion of age constraints
Yilgarn B dikes	Ca. 750–700	Original correlations	77.9	162.0	28.1	Giddings (1976)	Younger (possibly Mesozoic) overprint (Halls and Wingate, 2001)
S. China							
Liantuo sediments	748 ± 12	U-Pb SHRIMP det. zir. (Ma et al., 1984)	4.4	161.1	12.9	Evans et al. (2000)	Alternatively ca. 790–730. Basal reworked tuff U-Pb SHRIMP zir. 779 ± 12 Ma (Du et al., 2013)
Liantuo	780–714	U-Pb SIMS det. zir. (Lan et al 2015)	12.7	157.4	5.2	Jing et al. (2015)	N.A.§
Liantuo average**	780–714	U-Pb SIMS det. zir. (Lan et al., 2015)	13.2	155.2	5.27	Jing et al. (2015)	Average pole calculated by Jing et al. (2015). Due to existing spread of ages, mean pole used in ca. 750 Ma reconstruction
UWA site 1	N.D†	Basal unit of the upper Liantuo	11.7	159.0	10.7	Evans et al. (2000)	No reversals, N < 25 samples and no field test
N. China							
Huaibi Group	Ca. 700	Mean of several undated poles	–42.9	107.0	5.7	Zhang et al. (2006)	Mean of undated poles studied in the 1980s
Nanfen Formation	Ca. 800–780	Original correlations	–16.5	121	11.1	Zhang et al. (2006)	Unclear geologic context, ca. 925 Ma based on recent correlations (Fu et al., 2015). No demag data available

(*Continued*)

TABLE 3. 780–720 MA CRATON PALEOMAGNETIC POLES (*Continued*)

Unit/Formation	Age (Ma)	Type of age and reference	Paleomagnetic pole Lat. (°N)	Long. (°E)	A_{95}* (°)	Paleomagnetic reference	Notes
Tarim							
Upper Baiyisi (Baiyixi) volcanics**	725 ± 10	U-Pb SHRIMP zir. (Xu et al., 2009)	17.7	194.2	4.2	Huang et al. (2005)	Age may include inherited grains. Sampled volcanics overlie the Sturtian diamictites, also volcanics underlie diamictites
Qiaoenbrak Formation††	Ca. 717	Correlated with Sturtian diamictite	–6.3	17.5	9.1	Wen et al. (2013)	Ca. 717 Ma
India							
Malani igneous suite**	771 ± 5	U-Pb SIMS zir. (Gregory et al., 2009)	69.4	75.7	6.5	Meert et al. (2013)	LA-ICP-MS Pb-Pb discordant zir.: 752 ± 18 Ma (Meert et al., 2013)
Malani igneous suite	771 ± 5	U-Pb SIMS zir. (Gregory et al., 2009)	67.8	72.5	8.8	Gregory et al. (2009)	N.A.§
Malani igneous suite	771–751: 751 ± 3, 771 ± 2	U-Pb zir. unpublished	68.0	88.0	8.0	Torsvik et al. (2001a)	Age cited as personal communication from R.D. Tucker to T.H. Torsvik (2001)
Mahe dikes	750.2 ± 2.5	U-Pb ID-TIMS zir. Takamaka dolerite	80.0	79.0	11.0	Torsvik et al. (2001b)	From the Seychelles. Must be restored to India
Congo							
Mbozi gabbro**	748 ± 6	748 Ma: U-Pb zir. (Mbede et al., 2004),	46.0	325.0	9.0	Meert et al. (1995)	Mbede et al. age only published in conference proceedings
Luakela volcanics§§	765 ± 5	U-Pb SHRIMP zir. (Key et al., 2001)	40.0	302.0	14.0	Wingate et al. (2010)	N.A.§
Gagwe Lavas	795 ± 7	Ar-Ar cooling age (Deblond et al., 2001)	25.0	93.0	10.0	Meert et al. (1995)	May actually be an overprint (Wingate et al., 2010)
Siberia							
Kitoi (Sayan) dikes**	758 ± 4	Ar-Ar plag. (Sklyarov et al., 2003)	1.1	22.4	7.4	Pisarevsky et al. (2013)	Alternatively correlative with ca. 720 Ma Irkutsk-Franklin large igneous provinces (Ernst et al., 2016)
Svalbard							
lGFm††	ca. 811	Chemo- and lithostratigraphic correlations	19.6	211.3	3.0	Maloof et al. (2006)	Correlated with 811 Ma Yukon Fifteenmile Gp. (Macdonald et al., 2010)
uGfm††	ca. 800	Chemo- and lithostratigraphic correlations	2.6	71.9	2.0	Maloof et al. (2006)	N.A.§
S4mb††	ca 788	200 m above end of Bitter Springs Stage	25.9	226.8	5.8	Maloof et al. (2006)	See text of paper for further discussion of age constraints

Note: Type of age abbreviations: baddeleyite (badd.); zircon (zir.); plagioclase (plag.); detrital (det.); weighted average (wt. average); chemical abrasion (CA); isotope dilution–thermal ionization mass spectrometry (ID-TIMS); laser ablation–inductively coupled plasma–mass spectrometry (LA-ICP-MS); sensitive high-resolution ion microprobe (SHRIMP); secondary ion mass spectrometry (SIMS). Unit abbreviations: Fm—Formation; Mb—Member. Upper Grusdievbreen Fm. (uGfm); Lower Grusdievbreen Fm. (lGfm); Svanbergfjellet 4 Member (S4mb). Elongation-Inclination (E-I) (e.g. Tauxe and Kent, 2004). UWA—University of Western Australia.

*A_{95}—radius of the circle of 95% confidence about the mean. If not available, $A_{95} \sim \sqrt{dp \times dm}$, where dp and dm are semi-axes of the 95% ellipse of confidence about the mean (McElhinny and McFadden, 2000).

†N.D—Not determined.

§N.A.—Not applicable.

**Pole used in proposed robust apparent polar wander path (APWP) and reconstructions.

††Pole lacks radiometric age constraints but is displayed with Laurentian APWP and reconstructions.

§§Pole plotted with Laurentian APWP.

bears similarity to the Chuar Group Nankoweap pole. This correlation is not inconsistent with existing detrital zircon geochronological data that would suggest that most of the lower formations of the Uinta Mountain Group were deposited prior to the Chuar Group. The group 1 poles include the horizon dated with U-Pb on detrital zircon at <766 ± 4 Ma (Dehler et al., 2010), and we propose that it is older than the Nankoweap Formation, possibly as old as ca. 765 Ma. With these groupings, the Uinta Mountain data oscillate between ca. 765 and 755 Ma and broadly along the same great circle path defined by the Chuar poles (Fig. 8).

Franklin Large Igneous Province

Paleomagnetic data from the ca. 720 Ma Franklin large igneous province provide robust Neoproterozoic constraints for Laurentia and an important tie point for Neoproterozoic paleogeography (Table 2; Fig. 8C). The Franklin large igneous province includes sills, dikes, and volcanic rocks in northern and northwestern Canada and northwestern Greenland. U-Pb zircon and baddeleyite ages from the Franklin large igneous province rocks span from ca. 730 to 710 Ma (Heaman et al., 1992; Pehrsson and Buchan, 1999; Ernst et al., 2004; Denyszyn et al., 2009a; Macdonald et al., 2010). However, this large spread may be due in part to imprecise multigrain techniques. The upper intercept of multigrain fractions of zircon and baddeleyite results in ages of 723 +4/–2 Ma and 718 ± 2 Ma (Heaman et al., 1992), while single-grain CA-ID-TIMS on baddeleyite associated with the Franklin large igneous province yielded an age of 716.33 ± 0.54 Ma (Macdonald et al., 2010).

Paleomagnetic studies span six key regions: the Canadian mainland, Victoria Island, Baffin Island, Devon Island, Ellesmere Island, and northern Greenland (Fahrig et al., 1971; Robertson and Baragar, 1972; Fahrig and Schwarz, 1973; Park, 1974; Palmer and Hayatsu, 1975; Palmer et al., 1983; Park, 1981b; Denyszyn et al., 2009a, 2009b; Christie and Fahrig, 1983; Park, 1994; Buchan et al., 2000). These sites span enough time to average out secular variation, as both normal and reverse directions were found over a wide area. The mean paleomagnetic directions from mainland Canada, Victoria Island, and Baffin Island overlap at the 95% confidence level (Fig. 8C), but this is not the case for directions isolated from the Borden dikes on Baffin Island and certain intrusives on Ellesmere Island, Devon Island, and Greenland. Reevaluation of the Borden dikes by Pehrsson and Buchan (1999) suggested that their steep magnetizations resulted from the superposition of a Cretaceous–Tertiary–aged CRM on normal and reversed primary Franklin components. The anomalous directions from Ellesmere and Devon Island can be explained by rotation of an Ellesmere microplate, unintentionally concentrated sampling of secular variation, or pyrrhotite CRM during the Ellesmerian orogeny (Denyszyn et al., 2009a, 2009b). Finally, the anomalous poles from Greenland can be explained in part by closure of the Labrador Sea (e.g., Denyszyn et al., 2009a). Use of the adjusted/rotated mean pole of Denyszyn et al. (2009a), the mean pole from Canada of Denyszyn et al. (2009a), or the mean pole of Buchan et al. (2000) yields almost indistinguishable results. In construction of the Laurentian APWP, we used the mean pole from Canada of Denyszyn et al. (2009a) with an assigned age of 716 Ma.

Thus, we present two new 780–720 Ma Laurentian APWPs (Fig. 9). The first is a robust APWP only using paleomagnetic data with well-determined radiometric geochronologic ages that now include ca. 757 Ma and ca. 751 Ma poles (Figs. 9A and 9B). We also present a more complex APWP that also incorporates poles from the Uinta Mountain Group and Nankoweap Formation with only detrital and relative stratigraphic age constraints (Figs. 9C and 9D).

780–720 MA PALEOGEOGRAPHIC RECONSTRUCTIONS

Our new APWP allows more accurate comparison between the Laurentian data set and paleomagnetic and geochronologic data from other cratons (Table 3) and hence allows a refined understanding of Rodinian paleogeography. In particular, we focused on testing previously proposed models for the conjugate margin to western Laurentia. These proposed conjugates include Australia and East Antarctica (Southwest U.S.–East Antarctic [SWEAT] model; Moores, 1991; Hoffman, 1991), Australia (Australia–SouthWest United States [AUSWUS] model; Karlstrom et al., 1999), South China (missing link; Li et al., 2008), Tarim (modified missing link; Wen et al., 2017, 2018), Siberia (Sears and Price, 1978, 2003), and West Africa and Rio de la Plata, Brazil (North American Cordillera and BRAsiliano-Pharuside [COBRA] model; Evans, 2009; see Figure DR1 and supplement text [footnote 1]). First, we reviewed existing data for continental cratons, with a focus on published paleomagnetic poles in the 780–720 Ma interval. After compiling paleomagnetic and geochronologic data sets (Table 3 and supplement text), reconstructions were created for three time windows: ca. 775, 751 Ma, and 716 Ma, which correspond to dated poles from Laurentia (Fig. 10). Comparison of existing paleomagnetic data with the Laurentian APWP can eliminate some of the previous craton candidates as the conjugate margin.

Precambrian paleogeographic maps often do not reflect uncertainty in paleomagnetic data. This is particularly true when considering the continents that have well-dated robust poles for a particular time interval, and those that do not. Often, plotted poles can be 50 m.y. older or younger than the selected time step. As this uncertainty is not obvious when looking at the resultant paleogeographic map, it gives the false impression that the paleogeography is well constrained. To reflect these uncertainties in our paleogeographic reconstructions, we only displayed outlines and no labels for those continents that either (1) have poles with large age uncertainties or uncertainties that do not overlap with ages of the Laurentian poles or (2) lack robust paleomagnetic data dated within 10 m.y. of the time interval (Fig. 10). In contrast, continents displayed by color-filled polygons and letter labels do have robust paleomagnetic data with overlapping age constraints and small errors for the given time slice.

In addition, many reconstructions suggest that the A_{95} values of paleomagnetic poles do not adequately reflect the actual errors. Therefore, instead of reconstructing the paleomagnetic poles to the geographic north or south pole, paleopoles were placed within 30° of the geographic pole for the reconstructions. It is true that the A_{95} can underrepresent the actual errors in cases where the paleomagnetic data set has not provided the time averaging of PSV required for accurate determination of a paleomagnetic pole. However, one hopes that the use of field tests and PSV analyses may minimize these underrepresentations. Overall, the A_{95} value reflects the most likely possibility, given the data available. Thus, we have created our reconstructions by aligning the paleomagnetic pole with the geographic north/south poles. In certain cases, the pole of the examined craton had a well constrained age that was between the ages of two robust Laurentian poles. In this case, it was aligned between the two well constrained Laurentian poles, one of which was aligned with the north/south pole. We acknowledge that other paleogeographies are possible but suggest that they may be less probable given the data. In creating these reconstructions, we considered and compared both poles and APWPs. For this, we plotted the APWP of Laurentia, anchored at 751 Ma, as well as all the robust poles highlighted in Table 3 (Fig. 10D).

For the ca. 775 Ma reconstruction, we included the Malani igneous suite paleomagnetic pole for India. Although the earliest models of Rodinia suggested that East Gondwana

(India-Australia-Antarctica) remained intact (Hoffman, 1991), the paleomagnetic pole from the Malani igneous suite (U-Pb secondary ion mass spectrometry [SIMS] age of 771 ± 5 Ma on zircon; Gregory et al., 2009) showed that India was at intermediate latitudes and likely not part of East Gondwana or Rodinia (Torsvik et al., 2001a, 2001b; Meert et al., 2013).

For the ca. 751 Ma reconstruction, poles were included for Congo (Mbozi Complex and Luekala volcanics), Australia (Mundine Well dykes), South China (Liantuo Formation), and Siberia with the slightly older Kitoi-Sayan pole. For Congo, aligning the Mbozi gabbro pole (U-Pb zircon 748 ± 6 Ma; Meert et al., 1995; Mbede et al. 2004) with the Carbon Butte–Awatubi pole and the Luekala volcanics pole (sensitive high-resolution ion microprobe [SHRIMP] U-Pb zircon 765 ± 5 Ma; Wingate et al., 2010; Key et al., 2001) between the 775 and 757 Ma Laurentian poles required a reconstruction of Congo either in the Southern Hemisphere outboard of Rodinia, or in the Northern Hemisphere near Australia (Fig. DR8). These reconstructions fulfilled the constraint of fitting the two Congo poles with the Laurentian APWP. Alternatively, if all constraints from Luekala pole are ignored, and Congo is placed on the western margin of Laurentia using just the ca. 751 Ma Mbozi Complex pole aligned with the combined Carbon Butte–Awatubi pole, there is ~400 km of craton overlap between Laurentia and Congo. However, these reconstructions represent stringent interpretations. Refinement of the ages and positions of the Luekala and Mbozi poles could favor the Congo craton as the conju-

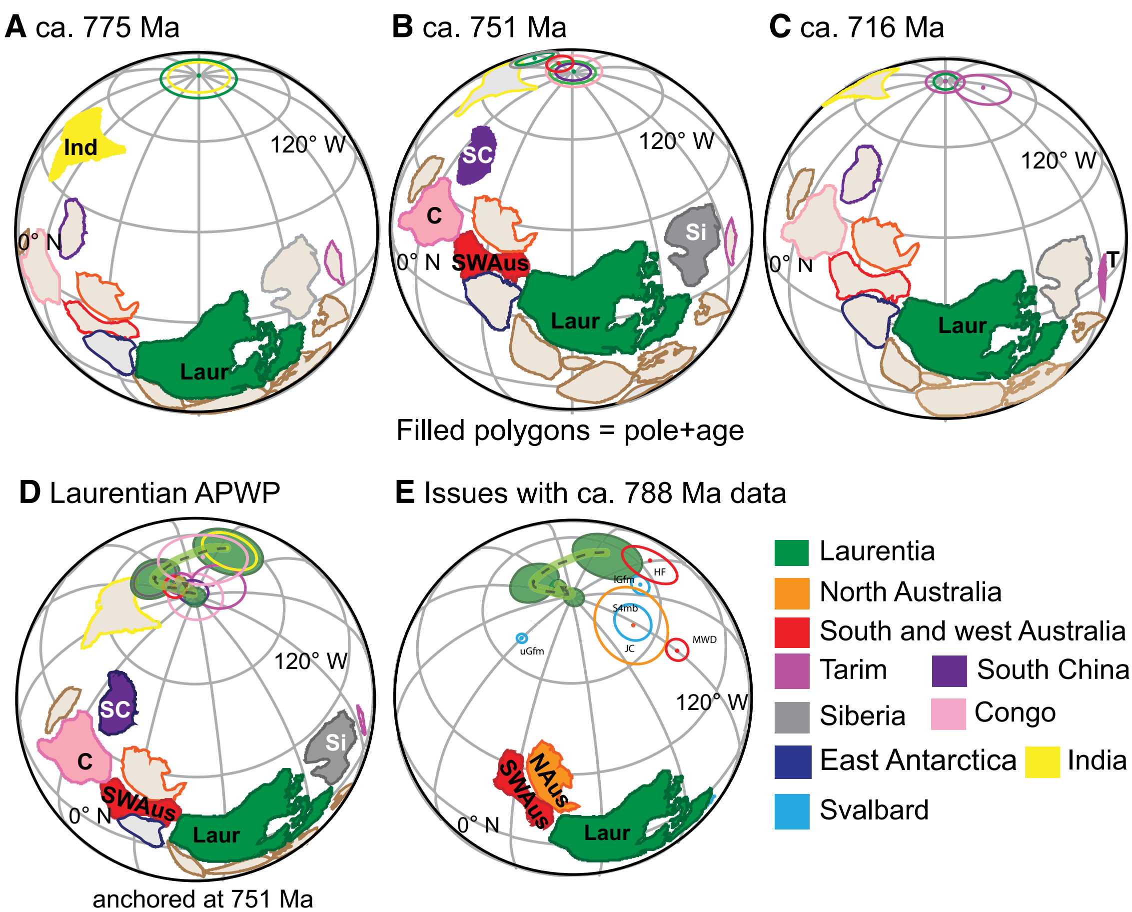

Figure 10. Paleogeographic reconstructions. Uncertainties are highlighted by having only colored outlines for continents that lack paleomagnetic data dated within 10 m.y. or with paleomagnetic data but with age errors that do not overlap with ages of the Laurentian path. Continents with color-filled polygons and letter labels have robust paleomagnetic data with overlapping age constraints for the given short time interval. (A) 775 Ma. (B) 751 Ma. Note that the 755 Ma Mundine Well dykes pole is placed coincident on the Laurentian apparent polar wander path (APWP) between the 757 and 751 Ma poles. (C) 716 Ma. Note that reconstruction was made with the Baiyisi pole for Tarim, but the Qiaoenbrak pole is also included, and it falls slightly off axis. (D) Laurentian APWP anchored at 751 Ma along with the other poles and continents reconstructed. (E) Ca. 788 Ma reconstruction using chemostratigraphic correlations and published restoration of Svalbard to Laurentia (Maloof et al., 2006). Note different pole positions of the ca. 788 Ma Hussar Formation (HF) and Johnny's Creek Member (JC) poles. With this restoration, the Mundine Well dykes pole (MWD) does not overlap with the 755 Ma portion of the Laurentian APWP as expected. Upper Grusdievbreen Fm. (uGfm); Lower Grusdievbreen Fm. (lGfm); Svanbergfjellet 4 Member (S4mb).

gate to the western Laurentian margin, although suggested differences in magmatic and tectonic histories would need to be reconciled (e.g., Li et al., 2008, and references therein).

For Australia, the 755 Ma Mundine Well dykes pole (755 ± 3 Ma; Pb-Pb zircon SHRIMP weighted mean; Wingate and Giddings, 2000) was plotted between the ca. 751 Ma Carbon Butte–Awatubi pole and the ca. 757 Ma Carbon Canyon pole. Laurentia was positioned using the 751 Ma pole, while Australia was positioned using the 755 Ma Mundine Well dykes pole placed coincident on the Laurentian APWP between the 757 and 751 Ma poles. These reconstructions place Australia in a position similar to the Australia-Mexico (AUSMEX) configuration, not as the conjugate margin for western Laurentia.

For South China, two important paleomagnetic studies have focused on the Liantuo Formation (Evans et al., 2000; Jing et al., 2015). Despite geochronologic data obtained from the both the lower and upper Liantuo Formation, the age of the paleomagnetic pole is still being refined (Du et al., 2013; Lan et al., 2015). Sampling of a reworked tuff in the lower Liantuo Formation that was dated with U-Pb SHRIMP zircon to 779 ± 12 Ma led authors to suggest the Liantuo Formation was deposited between 790 and 730 Ma (Du et al., 2013). More recently, this was refined to 780–714 Ma, due to SIMS U-Pb zircon data (Lan et al., 2015). As this is a sedimentary unit spanning a range of detrital ages, we chose to assign the Liantuo paleomagnetic pole to constrain South China ca. 751 Ma. However, given continuing integrative paleomagnetism and geochronology investigations, we expect that this reconstruction may be refined. However, even with the age uncertainties, this pole suggests that South China was at latitudes of 35°–55° in the late Tonian by ca. 720 Ma rifting, i.e., much higher than the 10°–20° latitude of the western margin of Laurentia, and thus it is an unlikely candidate for the conjugate margin.

The Siberian craton contains paleomagnetic data from dikes proposed to be ca. 760 Ma (e.g., Pisarevsky et al., 2013; Sharyzhalgai massif Nersa Complex of Gladkochub et al., 2010; Sayan dikes of Ernst et al., 2016). Current age constraints on these Siberian dikes are ca. 751 Ma (Ar-Ar plagioclase age 758 ± 4 Ma—Sklyarov et al., 2003; nearby dikes in the Biryusa massif, Ar-Ar plagioclase 741 ± 4 Ma—Gladkochub et al., 2006). Alternatively, the orientations of these dikes led others to provisionally consider them as part of the younger ca. 720 Ma Irkutsk large igneous province (see Ernst et al., 2016; 724 ± 3 Ma, ID-TIMS U-Pb baddeleyite). The Siberian Irkutsk large igneous province is correlated with the Franklin large igneous province in Laurentia (Ernst et al., 2016; Evans et al., 2016). Given the geochronology constraints on the units with paleomagnetic data, we have depicted Siberia in the ca. 751 panel (Fig. 9B) placed to the north of Laurentia with the Kitoi pole coincident with the ca. 757 Ma Carbon Canyon pole in a configuration similar to those previously suggested in Pisarevsky et al. (2013) and Ernst et al. (2016). Alternatively, if the Kitoi dikes are instead Franklin large igneous province correlatives, then the paleomagnetic reconstruction requires a larger seaway between Siberia and northern Laurentia in order to prevent unrealistic latitudinal overlap of the Siberian craton with the Greenland portion of Laurentia. Reconstructions placing Siberia on the western margin of Laurentia (e.g., Sears and Price, 2003) are unlikely, given that the paleomagnetic data would then require the proposed Siberian margin to lie at an angle to the Laurentian margin, as well as requiring substantial overlap of the Siberian craton with western Laurentia.

Finally, for the ca. 716 Ma reconstruction, Tarim displays paleomagnetic poles within the selected time window. The Baiyisi volcanics and Qiaoenbrak Formation poles are both from units that are likely Cryogenian correlatives. The Baiyisi Formation includes a sequence of siliciclastic rocks, diamictite, and lower and upper volcanic units (Huang et al., 2005; Xu et al., 2005, 2009; Wen et al., 2015). SHRIMP U-Pb zircon dates from the lower volcanics yielded a weighted mean age of 740 ± 7 Ma (Xu et al., 2009). SHRIMP U-Pb zircon dates from the upper volcanics resulted in a weighted mean age of 725 ± 10 Ma (Xu et al., 2009). These analyses display a wide spread of dates, suggesting that they include inherited grains that bias the weighted mean to an older age. A paleomagnetic study on the upper volcanics yielded a pole that we chose to incorporate into the 716 Ma reconstruction of Tarim. Given the possible inheritance in their age and the fact that they overlie the Sturtian Baiyisi diamictites, these upper volcanics are likely Sturtian in age (younger than 717 Ma; Huang et al., 2005). The Baiyisi volcanics pole bears similarity to the undated Sturtian-correlative Qiaoenbrak Formation pole, which is interpreted as an early postdepositional remanent magnetization due to a negative soft-sediment fold test but a positive conglomerate test (Wen et al., 2013). Although the Qiaoenbrak Formation pole does not exactly coincide with the Baiyisi pole, it is also plotted in the 716 Ma reconstruction of Tarim.

For Tarim, when reconstructions were attempted using either polarity of the Baiyisi pole, Tarim and Laurentia were located at similar latitudes, resulting in overlap (Fig. DR9A; see footnote 1). Additionally, Tarim was restored almost perpendicularly to the Laurentian margin, an odd orientation for a conjugate margin. Alternatively, reconstruction using the Franklin pole (Laurentia) and the Qiaoenbrak pole (Tarim) would allow Tarim to be located off the Laurentian margin within the A_{95} uncertainties. However, the A_{95} uncertainties do not allow for southern Tarim to lie parallel to the Laurentian margin, as a proposed conjugate margin.

As there is uncertainty in the age constraints of the Baiyisi volcanics and Qiaoenbrak Formation paleomagnetic poles, the proposed Tarim juxtaposition could be correct (Wen et al., 2017, 2018). However, this reconstruction is currently less tenable given the existing constraints and comparison with the ca. 716 Ma paleomagnetic data, which suggests that the potential conjugate margins of Tarim and Laurentia were, in fact, perpendicular. Thus, we suggest that Tarim should be instead placed near Siberia, consistent with geochronological constraints on the basement of these cratons and cratonic fragments (e.g., Bold et al., 2016).

Finally, it could be important to consider chemostratigraphic correlations for paleomagnetic data sets. Advances in Neoproterozoic chemostratigraphy have provided ties between basins otherwise lacking geochronologic constraints. In particular, the Bitter Springs Stage (named after its identification in the Love's Creek Member of the Bitter Springs Formation, Australia) is marked by global negative carbonate $\delta^{13}C$ values (Halverson, 2006; Swanson-Hysell et al., 2015). Integration of data from Ethiopia and northwestern Canada demonstrated that the Bitter Spring Stage was globally synchronous, starting after 811.51 ± 0.25 Ma (U-Pb CA-ID-TIMS zircon; Macdonald et al., 2010) and ending just before 788.72 ± 0.24 Ma (Swanson-Hysell et al., 2015).

Of the several published 800–760 Ma poles from Australia (Table 3 and supplement), the poles from the Hussar Formation and Johnny's Creek Formation of the Bitter Springs Group could be primary and similar in time to our Laurentian APWP. The main drawback for both Australian poles is the lack of direct geochronological constraints. However, chemostratigraphic correlations paired with geochronologic data from other localities can allow us to develop more robust age models.

The top 200 m section of the Hussar Formation from the Lancer 1 drill hole in the central Officer Basin, Australia was the focus of a paleomagnetic study by Pisarevsky et al. (2007). The samples were oriented in the core using acoustic scanner images with associated errors in azimuthal orientation on the order of 10° and errors in vertical orientation of <5°. Despite lacking field tests, the Hussar Formation displayed normal and reversed directions, suggesting it was not likely an overprint direction. The Hussar pole was modified slightly by Schmidt (2014) through the application of a flattening correction of $f = 0.35$ to the direction carried in the Hussar mudstone samples. To the north, the paleomagnetism of the Bitter Springs Formation was investigated by Swanson-Hysell et al. (2012). A high-temperature component carried by hematite was isolated from the basal ~150 m of the Johnny's Creek Formation of the Bitter Springs Group (previously referred to as Johnny's Creek Member, upper Love's Creek Member, or unit 3 of the Love's Creek Member). This component direction passed a regional fold test, suggesting that the magnetization was acquired prior to Paleozoic folding and that it was a near-primary early diagenetic magnetization (Swanson-Hysell et al., 2012).

In the Lancer drill hole, chemostratigraphic data were measured (Hill, 2005), with $\delta^{13}C$ values in the Browne Formation (underlying the Hussar Formation) swinging from approximately +6‰ to –5‰. This was thought to represent the Bitter Springs Stage in the western Officer Basin (Hill, 2005; Grey et al., 2005, 2011). However, a pronounced swing to negative $\delta^{13}C_{carb}$ values between –3‰ and –1‰ was also identified in the middle of the Hussar Formation (just below the strata studied paleomagnetically), but only in the Lancer 1 drill hole (Hill, 2005). Alternatively, these values can be correlated with the Bitter Springs Stage.

With this interpretation, the upper Hussar Formation is correlative with the Johnny's Creek Member. Accordingly, the paleomagnetic poles from the Johnny's Creek Member and top of the Hussar Formation might both be from strata overlying the termination of the Bitter Springs Stage, at approximately the same age, and constrained to be younger than 788 Ma. Unfortunately, if the Hussar and Johnny's Creek strata are the same age, the associated poles should be similar, but this is not the case, even when relative rotations (Li and Evans, 2011) are accounted for (see Table 3; Fig. 10). Thus, we suggest that the Johnny's Creek Member pole is a more robust paleomagnetic pole, and that the Hussar Formation pole might be biased due to fewer samples and unresolved tilt corrections.

Using this interpretation, the Johnny's Creek Member pole (ca. 788 Ma) is potentially 13 m.y. older than the Gunbarrel pole of Laurentia, and comparing them for paleogeographic reconstructions might overlook substantial plate motions. Instead, the pole might be compared with other paleomagnetic poles directly associated with the Bitter Springs Stage. In the Laurentian Mackenzie Mountains Supergroup, the Bitter Springs event has been identified in the mid-lower section of the upper carbonate of the Little Dal Group (Macdonald et al., 2012; Fig. DR7; see footnote 1). The closest stratigraphic paleomagnetic pole is from the underlying Rusty Shale unit (Park and Jefferson, 1991), which, based on correlations with strata in the Coal Creek inlier in Yukon, is unfortunately older than 811 Ma (Macdonald et al., 2012). As the Laurentian pole is then at least 20 m.y. older than the paleomagnetic pole from the Australian Johnny's Creek Member, we thus suggest that, beyond any of the problematic issues with Mackenzie Mountains Supergroup paleomagnetic data discussed above, these poles should not be compared in reconstructions.

An alternative is to incorporate data from Svalbard (e.g., Maloof et al., 2006). In Svalbard, the Svanbergfjellet 4 Member (S4mb) stratigraphically overlies the end of the Bitter Spring Stage (ca. 788 Ma). A paleomagnetic study of the S4mb limestones ~200 m above the termination of the Bitter Springs Stage was conducted by Maloof et al. (2006) (see Table 3 herein). They found a primary magnetic component, carried by magnetite and hematite, that passed the synsedimentary fold test at the 99% confidence level and was interpreted as an early primary magnetization. We restored Svalbard and the S4mb pole relative to Laurentia given the Euler pole rotation parameters of Maloof et al. (2006), and North Australia and the Johnny's Creek pole were rotated relative to South and West Australia following Li and Evans (2011). Although Australia can be restored similarly to the Australia-Mexico (AUSMEX) configuration, the resultant location of the Mundine Well dykes pole is no longer close to the well-constrained 757–751 Ma portion of the Laurentian APWP (Carbon Canyon and Carbon Butte–Awatubi poles). This large difference in pole location demonstrates the problems caused by using Svalbard data to constrain Laurentia's position. As the exact restoration of small continental fragments to larger cratons is often unclear, using them to create global reconstructions can bring additional issues and uncertainties.

Despite the promise of chemostratigraphic correlations, the current geochronologic, paleomagnetic, and chemostratigraphic data sets do not allow us to distinguish between SWEAT, AUSWUS, or AUSMEX-like reconstructions immediately prior to 750 Ma. The uncertainty in the position of Laurentia permits the possibility that Australia remained in AUSMEX-like configuration throughout the Tonian, or it could have been in a different configuration prior to 750 Ma, such as SWEAT, followed by strike-slip tectonics to an AUSMEX-like configuration by 750 Ma. In either case, Australia was likely in an AUSMEX-like configuration by 750 Ma, making it an unlikely conjugate margin to Laurentia for Ediacaran rift-drift tectonics.

The paleomagnetic reconstructions presented here suggest that Congo, India, Australia, South China, Siberia, and Tarim are currently unlikely candidates for the conjugate margin for western Laurentia. In addition, the AUSMEX-like configuration is consistent with global paleomagnetic data from ca. 790 to 720 Ma. In fact, paleomagnetic evidence for long-lived AUSMEX-like connections exists (see supplement Fig. DR10; Wingate et al., 2002). This AUSMEX configuration could be consistent with a different craton as the conjugate margin alongside the western margin of Laurentia.

One complication for this AUSMEX-like model is that juvenile crust was accreting to the eastern and southern margins (present-day coordinates) of Laurentia until ca. 1.3 Ga. Thus, this model would require that our AUSMEX-like configuration formed after 1.3 Ga, in order to allow for the long-lived collisional and accretionary history on the Laurentian margin. It is possible that with an AUSMEX-like reconstruction, the Grenville orogeny could potentially have been a longer linear orogenic belt, if traced south (present-day coordinates) through Australia as the Albany-Frasier belt (as previously suggested by Wingate et al., 2002). The second complication is the existence of the linear and long-lived rift margin along western Laurentia. However, this issue is a limitation of all previously published models. Even missing links such as Tarim are not large enough to be a conjugate for the entire length of the western Laurentian margin (Wen et al., 2018). It is possible that there were several continental fragments in combination along the margin. In some cases, these fragments could have continued to disintegrate and subsequently accreted to various cratons. As discussed below, the long-lived rifting likely reflected a much more complex history than a simple rift that initiated ca. 720 Ma and continued until the Cambrian.

Regarding the conjugate craton to western Laurentia, geologic tie points suggest that Antarctica was likely attached to Australia within the Mawson continent in pre- or early Rodinia times (Goodge and Fanning, 2016) and thus could not have been the conjugate for the western margin of Laurentia at ca. 750 Ma (Fitzsimons, 2003a, 2003b; Cawood and Buchan, 2007; Cawood and Korsch, 2008; White et al., 1999). Similarly, geological tie points for Baltica and Amazonia, Kalahari, and Rio de la Plata have been used to suggest they were on or near the eastern margin of Laurentia and thus unlikely to be conjugates for the western margin (Bogdanova et al., 2008; Loewy et al., 2003; Davidson, 2008; Li et al., 2008). Finally, North China is not a good candidate for the conjugate margin because it lacks Cryogenian–Ediacaran basins that could act as tie points to the western margin of Laurentia (Xiao et al., 2014). Instead, Mesoproterozoic data support North China positioned near Siberia (Fu et al., 2015). Furthermore, based on tectonic and geologic relationships, it is proposed that the Tarim and North China cratons were linked along with other cratons in the Neoproterozoic as a single continental strip (Zuza and Yin, 2017). With these points in mind, we tenuously placed North China close to Tarim and Siberia, but this reconstruction lacks robust paleomagnetic constraints. Thus, we suggest that the conjugate craton for western Laurentia is also not one of the cratons discussed above. Further work refining paleomagnetic, geochronologic, and geologic rift histories would help to clarify if the conjugate margin is a craton with previously suggested connections to Laurentia such as Congo or Tarim, or a craton lacking paleomagnetic data like West Africa, or, instead, a combination of continental fragments.

Although Rodinia was first conceived based on Grenville orogenic tie points and rift basins fringing Laurentia, those conjugate margins have not yet been definitively identified. Most Proterozoic paleogeographic models assume the existence of a long-lived supercontinent with a roughly stable configuration from amalgamation to initial rifting. However, Rodinia's geometry could have undergone dramatic changes during the ~400 m.y. supercontinent tenure. For example, it has been proposed that the western margin of Laurentia experienced 780–720 Ma transcurrent faulting (Strauss et al., 2014; Smith et al., 2016; Eyster et al., 2017; Macdonald et al., 2017). Translations along margins could allow for changing configurations of Rodinia, and potentially the formation of separate continental masses before the proposed late Neoproterozoic rifting. We may need to redefine the paleogeographic configuration(s) that we refer to as Rodinia, as there could be dramatic changes between the 1.1 Ga orogenesis and the final 539 Ma passive-margin development. The paleomagnetic database coupled with refined chemostratigraphic correlations, geochronological constraints, orogenic histories, sedimentary provenance, and development of rifted passive margins can be used to further test the Rodinia hypothesis. The improved polar wander path derived in this paper from the stable Laurentian craton provides a template for future reconstructions of Neoproterozoic paleogeography.

CONCLUSIONS

A new paleomagnetic pole preserved in hematite from the Awatubi and Carbon Butte members of the Kwagunt Formation, northern Arizona, is interpreted as primary and passes five of the seven Van der Voo (1990) reliability criteria (Q1, Q3, Q4, Q5, Q6). Pervasive steep overprints were identified, both a mid-temperature component direction demagnetized between 200 °C and 560 °C and a high-temperature component direction demagnetized up to 680 °C. These overprints are found in the Carbon Butte, the Awatubi, and the Walcott members of the Kwagunt Formation. Previously reported directions from the Walcott Member might be biased by the pervasive overprint and should be studied further. The biggest limitation of this study is in the small number of samples. We thus tried to augment our data set with a reanalysis of previously published samples within the updated geochronologic context. Thus, the results of this study are combined with those reported in Weil et al. (2004), resulting in a combined mean pole from the Awatubi and Carbon Butte members (Q1, Q2, Q3, Q4, Q5, Q6).

Existing paleomagnetic data and recent geochronological data were integrated into a new revised ca. 780–720 Ma Laurentian APWP. Having examined the 780–720 Ma database of other cratons, we discussed reconstructions for 775, 751, and 716 Ma and concluded that there is evidence for an AUSMEX-like configuration at 750 Ma. Given our new reconstructions, the identity of the conjugate margin for western Laurentia remains unknown, but current paleomagnetic data and the best age estimates do not support Australia or South China as the conjugate margin. Further work on the poles for Tarim and Congo and better constraints on their geologic rift histories are needed to clarify if one of them could be the conjugate margin. Alternatively, the conjugate may have been craton like West Africa, which lacks paleomagnetic data, or a combination of continental fragments. From a paleomagnetism viewpoint, the existing data do not yet lend themselves to robustly support a particular supercontinent configuration. Nonetheless, geological data sets support rifting and development of a thermally subsiding passive margin ca. 540 Ma.

To solve the Rodinia riddle, identify the missing margin, and test Rodinia's existence, a craton needs to be identified that follows the 780–720 Ma Laurentian APWP provided herein. In order to fully understand Neoproterozoic paleogeography and the putative supercontinent Rodinia, detailed polar wander paths that include precise well-dated poles need to be developed and integrated with geologic data, as well as focused geologic attention on the very long and puzzling time interval from 720 to 500 Ma. Clearly, a better understanding of both the history and mechanisms of western Laurentian rifting in the global context requires combined geologic and paleomagnetic scrutiny.

ACKNOWLEDGMENTS

We would like to thank Mark Holland, Barrett Salisbury, Brian Clarke, and Dylan Rose-Coss for assistance in collecting and carrying samples. Special thanks go to Jacob Kremers for his precise and focused work helping to collect, prepare, and measure paleomagnetic samples. Mark Timmons and Laurie Crossey provided valuable discussions while in the field. We thank Carol Dehler for suggestions on correlations of the Uinta Mountain Group and for sharing her thoughts on the most recent mapping of the eastern Uinta Mountain area. We thank Alan Rooney for helpful discussions on Chuar Group geochronology. Sample collection was made possible by a research and collecting permit from Grand Canyon National Park to K. Karlstrom. Eduardo Lima and Sonia Tikoo-Schantz were helpful at the Massachusetts Institute of Technology Paleomagnetism Laboratory. We thank the Massachusetts Institute of Technology Ross Laboratory for use of their vibrating sample magnetometer and Astera S. Tang for her assistance in measuring magnetic hysteresis curves. We thank Dave Evans, Nick Swanson-Hysell, and an anonymous reviewer for constructive feedback on this manuscript, as well as Science Editor Brad S. Singer and Associate Editor Zheng-Xiang Li for their comments. Financial support for this research was provided by National Science Foundation grant EAR-1215061. Macdonald thanks National Aeronautics and Space Administration (NASA) Astrobiology Institute (award NNA13AA90A) for support.

REFERENCES CITED

Armin, R.A., and Mayer, L., 1983, Subsidence analysis of the Cordilleran miogeocline: Implications for timing of late Proterozoic rifting and amount of extension: Geology, v. 11, no. 12, p. 702–705, https://doi.org/10.1130/0091-7613(1983)11<702:SAOTCM>2.0.CO;2.

Bogdanova, S.V., Bingen, B., Gorbatschev, R., Kheraskova, T.N., Kozlov, V.I., Puchkov, V.N., and Volozh, Y.A., 2008, The East European craton (Baltica) before and during the assembly of Rodinia: Precambrian Research, v. 160, no. 1, p. 23–45, https://doi.org/10.1016/j.precamres.2007.04.024.

Bold, U., Crowley, J.L., Smith, E.F., Sambuu, O., and Macdonald, F.A., 2016, Neoproterozoic to early Paleozoic tectonic evolution of the Zavkhan terrane of Mongolia: Implications for continental growth in the Central Asian orogenic belt: Lithosphere, v. 8, no. 6, p. 729–750, https://doi.org/10.1130/L549.1.

Bond, G.C., and Kominz, M.A., 1984, Construction of tectonic subsidence curves for the early Paleozoic miogeocline, southern Canadian Rocky Mountains: Implications for subsidence mechanisms, age of breakup, and crustal thinning: Geological Society of America Bulletin, v. 95, no. 2, p. 155–173, https://doi.org/10.1130/0016-7606(1984)95<155:COTSCF>2.0.CO;2.

Bond, G.C., Christie-Blick, N., Kominz, M.A., and Devlin, W.J., 1985, An early Cambrian rift to post-rift transition in the Cordillera of western North America: Nature, v. 315, no. 6022, p. 742–746, https://doi.org/10.1038/315742a0.

Bowring, S.A., and Hoppe, W.J., 1982, U-Pb zircon ages from Mount Sheridan Gabbro, Wichita Mountains, *in* Gilbert, M.C., and Donovan, R.N., eds., Geology of the Eastern Wichita Mountains, Southwestern Oklahoma: Oklahoma Geological Survey Guidebook 21, p. 54–59.

Bressler, S.L., 1981, Preliminary paleomagnetic poles and correlation of the Proterozoic Uinta Mountain Group, Utah and Colorado: Earth and Planetary

Science Letters, v. 55, no. 1, p. 53–64, https://doi.org/10.1016/0012-821X(81)90086-8.
Buchan, K.L., and Ernst, R.E., 2004, Diabase Dyke Swarms and Related Units in Canada and Adjacent Regions: Geological Survey of Canada Map 2022A, scale 1:5,000,000, with accompanying compilation, 39 p.
Buchan, K.L., and Ernst, R.E., 2013, Diabase Dyke Swarms of Nunavut, Northwest Territories and Yukon, Canada: Geological Survey of Canada Open-File 7464, no. 10.4095, p. 293149.
Buchan, K.L., Mertanen, S., Park, R.G., Pesonen, L.J., Elming, S.Å., Abrahamsen, N., and Bylund, G., 2000, Comparing the drift of Laurentia and Baltica in the Proterozoic: The importance of key palaeomagnetic poles: Tectonophysics, v. 319, no. 3, p. 167–198, https://doi.org/10.1016/S0040-1951(00)00032-9.
Buchan, K.L., Ernst, R.E., Bleeker, W., Davis, W.J., Villeneuve, M., van Breemen, O., Hamilton, M.A., and Söderlund, U., 2010, Proterozoic Magmatic Events of the Slave Craton, Wopmay Orogen and Environs: Geological Survey of Canada Open-File 5985, 25 p., https://doi.org/10.4095/285383.
Butler, R.F., 1992, Paleomagnetism: Magnetic Domains to Geologic Terranes: Boston, Massachusetts, Blackwell Scientific Publications, 238 p.
Cawood, P.A., 2005, Terra Australis orogen: Rodinia breakup and development of the Pacific and Iapetus margins of Gondwana during the Neoproterozoic and Paleozoic: Earth-Science Reviews, v. 69, no. 3, p. 249–279, https://doi.org/10.1016/j.earscirev.2004.09.001.
Cawood, P.A., and Buchan, C., 2007, Linking accretionary orogenesis with supercontinent assembly: Earth-Science Reviews, v. 82, no. 3, p. 217–256, https://doi.org/10.1016/j.earscirev.2007.03.003.
Cawood, P.A., and Korsch, R.J., 2008, Assembling Australia: Proterozoic building of a continent: Precambrian Research, v. 166, no. 1, p. 1–35, https://doi.org/10.1016/j.precamres.2008.08.006.
Christie, K.W., and Fahrig, W.F., 1983, Paleomagnetism of the Borden dykes of Baffin Island and its bearing on the Grenville Loop: Canadian Journal of Earth Sciences, v. 20, no. 2, p. 275–289, https://doi.org/10.1139/e83-025.
Colpron, M., Logan, J., and Mortensen, J., 2002, U-Pb zircon age constraint for late Neoproterozoic rifting and initiation of the lower Paleozoic passive margin of western Laurentia: Canadian Journal of Earth Sciences, v. 39, no. 2, p. 133–143, https://doi.org/10.1139/e01-069.
Condon, D., and Bowring, S.A., 2011, A user's guide to Neoproterozoic geochronology, *in* Arnaud, E., Shields, G., and Halverson, G., eds., The Geological Record of Neoproterozoic Glaciations: Geological Society [London] Memoir 36, p. 135–149.
Constenius, K.N., 2009, Interim Geologic Map of the Provo 30′ × 60′ Quadrangle, Utah, Wasatch, Salt Lake, and Duchesne Counties, Utah: Utah Geological Survey Open-File Report 586DM, 2 plates, scale 1:62,500.
Crow, R., Karlstrom, K.E., McIntosh, W., Peters, L., and Dunbar, N., 2008, History of Quaternary volcanism and lava dams in western Grand Canyon based on LiDAR analysis, $^{40}Ar/^{39}Ar$ dating, and field studies: Implications for flow stratigraphy, timing of volcanic events, and lava dams: Geosphere, v. 4, no. 1, p. 183–206, https://doi.org/10.1130/GES00133.1.
Crow, R.S., Karlstrom, K.E., McIntosh, W., Peters, L., Crossey, L., and Eyster, A., 2015, A new model for Quaternary lava dams in Grand Canyon based on $^{40}Ar/^{39}Ar$ dating, basalt geochemistry, and field mapping: Geosphere, v. 11, no. 5, p. 1305–1342, https://doi.org/10.1130/GES01128.1.
Dalziel, I.W., 1991, Pacific margins of Laurentia and East Antarctica–Australia as a conjugate rift pair: Evidence and implications for an Eocambrian supercontinent: Geology, v. 19, no. 6, p. 598–601, https://doi.org/10.1130/0091-7613(1991)019<0598:PMOLAE>2.3.CO;2.
Davidson, A., 2008, Late Paleoproterozoic to mid-Neoproterozoic history of northern Laurentia: An overview of central Rodinia: Precambrian Research, v. 160, no. 1, p. 5–22, https://doi.org/10.1016/j.precamres.2007.04.023.
Deblond, A., Punzalan, L.E., Boven, A., and Tack, L., 2001, The Malagarazi Supergroup of southeast Burundi and its correlative Bukoba Supergroup of northwest Tanzania: Neo- and Mesoproterozoic chronostratigraphic constraints from Ar-Ar ages on mafic intrusive rocks: Journal of African Earth Sciences, v. 32, no. 3, p. 435–449, https://doi.org/10.1016/S0899-5362(01)90107-1.
Deenen, M.H., Langereis, C.G., van Hinsbergen, D.J., and Biggin, A.J., 2011, Geomagnetic secular variation and the statistics of palaeomagnetic directions: Geophysical Journal International, v. 186, no. 2, p. 509–520, https://doi.org/10.1111/j.1365-246X.2011.05050.x.
Dehler, C.M., Elrick, M., Karlstrom, K.E., Smith, G.A., Crossey, L.J., and Timmons, J.M., 2001, Neoproterozoic Chuar Group (~800–742 Ma), Grand Canyon: A record of cyclic marine deposition during global cooling and supercontinent rifting: Sedimentary Geology, v. 141, p. 465–499, https://doi.org/10.1016/S0037-0738(01)00087-2.
Dehler, C.M., Fanning, C.M., Link, P.K., Kingsbury, E.M., and Rybczynski, D., 2010, Maximum depositional age and provenance of the Uinta Mountain Group and Big Cottonwood Formation, northern Utah: Paleogeography of rifting western Laurentia: Geological Society of America Bulletin, v. 122, no. 9-10, p. 1686–1699, https://doi.org/10.1130/B30094.1.
Dehler, C., Gehrels, G., Porter, S., Heizler, M., Karlstrom, K., Cox, G., Crossey, L., and Timmons, M., 2017, Synthesis of the 780–740 Ma Chuar, Uinta Mountain, and Pahrump (ChUMP) Groups, western USA: Implications for Laurentia-wide cratonic marine basins: Geological Society of America Bulletin, v. 129, p. 607–624, https://doi.org/10.1130/B31532.1.
Denyszyn, S.W., Halls, H.C., Davis, D.W., and Evans, D.A., 2009a, Paleomagnetism and U-Pb geochronology of Franklin dykes in High Arctic Canada and Greenland: A revised age and paleomagnetic pole constraining block rotations in the Nares Strait region: Canadian Journal of Earth Sciences, v. 46, no. 9, p. 689–705, https://doi.org/10.1139/E09-042.
Denyszyn, S.W., Davis, D.W., and Halls, H.C., 2009b, Paleomagnetism and U-Pb geochronology of the Clarence Head dykes, Arctic Canada: Orthogonal emplacement of mafic dykes in a large igneous province: Canadian Journal of Earth Sciences, v. 46, no. 3, p. 155–167, https://doi.org/10.1139/E09-011.
Du, Q., Wang, Z., Wang, J., Qiu, Y., Jiang, X., Deng, Q., and Yang, F., 2013, Geochronology and paleoenvironment of the pre-Sturtian glacial strata: Evidence from the Liantuo Formation in the Nanhua rift basin of the Yangtze block, South China: Precambrian Research, v. 233, p. 118–131, https://doi.org/10.1016/j.precamres.2013.04.012.
Dudás, F.Ö., and Lustwerk, R.L., 1997, Geochemistry of the Little Dal basalts: Continental tholeiites from the Mackenzie Mountains, Northwest Territories, Canada: Canadian Journal of Earth Sciences, v. 34, no. 1, p. 50–58, https://doi.org/10.1139/e17-004.
Dunlop, D.J., and Argyle, K.S., 1991, Separating multidomain and single domain–like remanences in pseudo-single-domain magnetites (215–540 nm) by low-temperature demagnetization: Journal of Geophysical Research, v. 96, p. 2007–2017, https://doi.org/10.1029/90JB02338.
Eisbacher, G.H., 1981, Sedimentary Tectonics and Glacial Record in the Windermere Supergroup, Mackenzie Mountains, Northwestern Canada: Geological Survey of Canada Paper 80–27, 40 p., https://doi.org/10.4095/119453.
Eisbacher, G.H., 1985, Late Proterozoic rifting, glacial sedimentation, and sedimentary cycles in the light of Windermere deposition, western Canada: Palaeogeography, Palaeoclimatology, Palaeoecology, v. 51, no. 1-4, p. 231–254, https://doi.org/10.1016/0031-0182(85)90087-2.
Ernst, R.E., Buchan, K.L., Harris, B.A., Hanes, J.A., Milner, M.W., and La Prairie, L.F., 2004, Ar^{40}-Ar^{39} dating of the Lasard River mafic dykes, and implications for the focus of the 0.72 Ga Franklin large igneous province of northern Canada: American Geophysical Union, Spring Meeting Abstracts, v. 1, abstract V43A-7.
Ernst, R.E., Hamilton, M.A., Söderlund, U., Hanes, J.A., Gladkochub, D.P., Okrugin, A.V., Kolotilina, T., Mekhonoshin, A.S., Bleeker, W., LeCheminant, A.N., Buchan, K.L., Chamberlain, K.R., and Didenko, A.N., 2016, Long-lived connection between southern Siberia and northern Laurentia in the Proterozoic: Nature Geoscience, v. 9, p. 464–469, https://doi.org/10.1038/ngeo2700.
Evans, D.A.D., 2009, The palaeomagnetically viable, long-lived and all-inclusive Rodinia supercontinent reconstruction, *in* Murphy, J.B., Keppie, J.D., and Hynes, A.J., eds., Ancient Orogens and Modern Analogues: Geological Society [London] Special Publication 327, p. 371–404, https://doi.org/10.1144/SP327.16.
Evans, D.A.D., 2013, Reconstructing pre-Pangean supercontinents: Geological Society of America Bulletin, v. 125, no. 11-12, p. 1735–1751, https://doi.org/10.1130/B30950.1.
Evans, D.A.D., Li, Z.X., Kirschvink, J.L., and Wingate, M.T., 2000, A high-quality mid-Neoproterozoic paleomagnetic pole from South China, with implications for ice ages and the breakup configuration of Rodinia: Precambrian Research, v. 100, no. 1-3, p. 313–334, https://doi.org/10.1016/S0301-9268(99)00079-0.
Evans, D.A.D., Veselovsky, R.V., Petrov, P.Y., Shatsillo, A.V., and Pavlov, V.E., 2016, Paleomagnetism of Mesoproterozoic margins of the Anabar Shield: A hypothesized billion-year partnership of Siberia and northern Laurentia: Precambrian Research, v. 281, p. 639–655, https://doi.org/10.1016/j.precamres.2016.06.017.
Eyster, A.E., Fu, R.F., Strauss, J.V., Weiss, B.P., Roots, C.F., Halverson, G.P., Evans, D.A.D., and Macdonald, F.A., 2017, Paleomagnetic evidence for a large rotation of the Yukon block relative to Laurentia: Implications for a low-latitude Sturtian glaciation and the break-up of Rodinia: Geological Society of America Bulletin, v. 129, p. 38–58, https://doi.org/10.1130/B31425.1.
Eyster, A., Ferri, F., Schmitz, M.D., and Macdonald, F.A., 2018, One diamictite and two rifts: Stratigraphy and geochronology of the Gataga Mountain of northern British Columbia: American Journal of Science, v. 318, no. 2, p. 167–207, https://doi.org/10.2475/02.2018.1.
Fahrig, W.F., and Schwarz, E.J., 1973, Additional paleomagnetic data on the Baffin diabase dikes and a revised Franklin pole: Canadian Journal of Earth Sciences, v. 10, no. 4, p. 576–581, https://doi.org/10.1139/e73-057.
Fahrig, W.F., Irving, E., and Jackson, G.D., 1971, Paleomagnetism of the Franklin diabases: Canadian Journal of Earth Sciences, v. 8, no. 4, p. 455–467, https://doi.org/10.1139/e71-047.
Fanning, C.M., and Link, P., 2004, U-Pb SHRIMP ages of Neoproterozoic (Sturtian) glaciogenic Pocatello Formation, southeastern Idaho: Geology, v. 32, no. 10, p. 881–884, https://doi.org/10.1130/G20609.1.
Fedo, C., and Cooper, J., 2001, Sedimentology and sequence stratigraphy of Neoproterozoic and Cambrian units across a craton-margin hinge zone, southeastern California, and implications for the early evolution of the Cordilleran margin: Sedimentary Geology, v. 141, p. 501–522, https://doi.org/10.1016/S0037-0738(01)00088-4.
Fisher, R.A., 1953, Dispersion on a sphere: Proceedings of the Royal Society of London. Series A, Mathematical and Physical Sciences, v. 217, no. 1130, p. 295–305, https://doi.org/10.1098/rspa.1953.0064.
Fitzsimons, I.C.W., 2003a, Does the late Neoproterozoic Darling fault zone of western Australia extend all the way to the Transantarctic Mountains?, *in* Specialist Group in Tectonics and Structural Geology Field Meeting: Kalbarri, Australia, Programs and Abstracts; Sydney, Australia: Geological Society of Australia, p. 130.
Fitzsimons, I.C.W., 2003b, Proterozoic basement provinces of southern and southwestern Australia, and their correlation with Antarctica, *in* Yoshida, M., Windley, B.F., and Dasgupta, S., eds., Proterozoic East Gondwana: Supercontinent Assembly and Break-Up: Geological Society [London] Special Publication 206, p. 93–130. https://doi.org/10.1144/GSL.SP.2003.206.01.07.
Ford, T.D., and Breed, W.J., 1973, Late Precambrian Chuar Group, Grand Canyon, Arizona: Geological Society of America Bulletin, v. 84, no. 4, p. 1243–1260, https://doi.org/10.1130/0016-7606(1973)84<1243:LPCGGC>2.0.CO;2.
Fu, X., Zhang, S., Li, H., Ding, J., Li, H., Yang, T., Wu, H., Yuan, H., and Lv, J., 2015, New paleomagnetic results from the Huaibei Group and Neoproterozoic mafic sills

in the North China craton and their paleogeographic implications: Precambrian Research, v. 269, p. 90–106, https://doi.org/10.1016/j.precamres.2015.08.013.

Gernon, T.M., Hincks, T.K., Tyrrell, T., Rohling, E.J. and Palmer, M.R., 2016, Snowball Earth ocean chemistry driven by extensive ridge volcanism during Rodinia breakup: Nature Geoscience, v. 9, no. 3, p. 242–248.

Giddings, J.W., 1976, Precambrian palaeomagnetism in Australia I: Basic dykes and volcanics from the Yilgarn block: Tectonophysics, v. 30, no. 1-2, p. 91–108, https://doi.org/10.1016/0040-1951(76)90138-4.

Gladkochub, D.P., Wingate, M.T.D., Pisarevsky, S.A., Donskaya, T.V., Mazukabzov, A.M., Ponomarchuk, V.A., and Stanevich, A.M., 2006, Mafic intrusions in southwestern Siberia and implications for a Neoproterozoic connection with Laurentia: Precambrian Research, v. 147, p. 260–278, https://doi.org/10.1016/j.precamres.2006.01.018.

Gladkochub, D.P., Pisarevsky, S.A., Donskaya, T.V., Ernst, R.E., Wingate, M.T., Söderlund, U., Mazukabzov, A.M., Sklyarov, E.V., Hamilton, M.A., and Hanes, J.A., 2010, Proterozoic mafic magmatism in Siberian craton: An overview and implications for paleocontinental reconstruction: Precambrian Research, v. 183, no. 3, p. 660–668, https://doi.org/10.1016/j.precamres.2010.02.023.

Goddéris, Y., Donnadieu, Y., Nédélec, A., Dupré, B., Dessert, C., Grard, A., Ramstein, G., and Francois, L.M., 2003, The Sturtian ‘snowball’ glaciation: Fire and ice: Earth and Planetary Science Letters, v. 211, no. 1, p. 1–12, https://doi.org/10.1016/S0012-821X(03)00197-3.

Goodfellow, W., Cecile, M., and Leybourne, M., 1995, Geochemistry, petrogenesis, and tectonic setting of Lower Paleozoic alkalic and potassic volcanic rocks, northern Canadian Cordilleran miogeocline: Canadian Journal of Earth Sciences, v. 32, no. 8, p. 1236–1254, https://doi.org/10.1139/e95-101.

Goodge, J.W., and Fanning, C.M., 2016, Mesoarchean and Paleoproterozoic history of the Nimrod Complex: Central Transantarctic Mountains, Antarctica: Stratigraphic revisions and relation to the Mawson continent in East Gondwana: Precambrian Research, v. 285, p. 242–271, https://doi.org/10.1016/j.precamres.2016.09.001.

Gregory, L.C., Meert, J.G., Bingen, B., Pandit, M.K., and Torsvik, T.H., 2009, Paleomagnetism and geochronology of the Malani igneous suite, Northwest India: Implications for the configuration of Rodinia and the assembly of Gondwana: Precambrian Research, v. 170, no. 1-2, p. 13–26, https://doi.org/10.1016/j.precamres.2008.11.004.

Grey, K., Hocking, R.M., Stevens, M.K., Bagas, L., Carlsen, G.M., Irimies, F., Pirajno, F., Haines, P.W., and Apak, S.N., 2005, Lithostratigraphic Nomenclature of the Officer Basin and Correlative Parts of the Paterson Orogen, Western Australia: Geological Survey of Western Australia Report 93, 89 p.

Grey, K., Hill, A.C., and Calver, C., 2011, Biostratigraphy and stratigraphic subdivision of Cryogenian successions of Australia in a global context, *in* Arnaud, E., Halverson, G.P., and Shields-Zhou, G., eds., The Geological Record of Neoproterozoic Glaciations: Geological Society [London] Memoir 36, p. 113–134, https://doi.org/10.1144/M36.8.

Halls, H.C., and Wingate, M.T.D., 2001, Paleomagnetic pole from the Yilgarn B (YB) dykes of Western Australia: No longer relevant to Rodinia reconstructions: Earth and Planetary Science Letters, v. 187, p. 39–53, https://doi.org/10.1016/S0012-821X(01)00279-5.

Halverson, G.P., 2006, A Neoproterozoic chronology, *in* Xiao, S., and Kaufman, A.J., eds., Neoproterozoic Geobiology and Paleobiology: Dordrecht, Netherlands, Springer, Topics in Geobiology 27, p. 231–271, https://doi.org/10.1007/1-4020-5202-2_8.

Hamilton, W., 1988, Laramide crustal shortening, *in* Schmidt, C.J., and Perry, W.J., Jr., eds., Interaction of the Rocky Mountain Foreland and the Cordilleran Thrust Belt: Geological Society of America Memoir 171, p. 27–39, https://doi.org/10.1130/MEM171-p27.

Hanson, R.E., Puckett, R.E., Jr., Keller, G.R., Brueseke, M.E., Bulen, C.L., Mertzman, S.A., Finegan, S.A., and McCleery, D.A., 2013, Intraplate magmatism related to opening of the southern Iapetus Ocean: Cambrian Wichita igneous province in the Southern Oklahoma rift zone: Lithos, v. 174, p. 57–70, https://doi.org/10.1016/j.lithos.2012.06.003.

Harlan, S.S., Geissman, J.W., and Snee, L.W., 1997, Paleomagnetic and $^{40}Ar/^{39}Ar$ geochronologic data from Late Proterozoic mafic dikes and sills: Montana and Wyoming: U.S. Geological Survey Special Paper, v. 1580, p. 1–16, https://doi.org/10.3133/pp1580.

Harlan, S.S., Heaman, L., LeCheminant, A.N., and Premo, W.R., 2003, Gunbarrel mafic magmatic event: A key 780 Ma time marker for Rodinia plate reconstructions: Geology, v. 31, no. 12, p. 1053–1056, https://doi.org/10.1130/G19944.1.

Harlan, S.S., Geissman, J.W., and Snee, L.W., 2008, Paleomagnetism of Proterozoic mafic dikes from the Tobacco Root Mountains, southwest Montana: Precambrian Research, v. 163, p. 239–264, https://doi.org/10.1016/j.precamres.2007.12.002.

Heaman, L., LeCheminant, A., and Rainbird, R., 1992, Nature and timing of Franklin igneous events, Canada: Implications for a late Proterozoic mantle plume and the break-up of Laurentia: Earth and Planetary Science Letters, v. 109, p. 117–131, https://doi.org/10.1016/0012-821X(92)90078-A.

Herrero-Bervera, E., and Helsley, C.E., 1983, Paleomagnetism of a polarity transition in the Lower(?) Triassic Chugwater Formation, Wyoming: Journal of Geophysical Research, v. 88, p. 3506–3522, https://doi.org/10.1029/JB088iB04p03506.

Hill, A.C., 2005, Stable isotope stratigraphy, GSWA Lancer 1, Officer Basin, western Australia, *in* Mory, A.J., and Haines, P.W., eds., GSWA Lancer Well Completion Report (Interpretive Papers), Officer and Gunbarrel Basins, Western Australia: Geological Survey of Western Australia Record 2005/4, p. 1–11.

Hoffman, P.F., 1991, Did the breakout of Laurentia turn Gondwanaland inside-out?: Science, v. 252, no. 5011, p. 1409–1412, https://doi.org/10.1126/science.252.5011.1409.

Huang, B., Xu, B., Zhang, C., Li, Y.A., and Zhu, R., 2005, Paleomagnetism of the Baiyisi volcanic rocks (ca. 740 Ma) of Tarim, northwest China: A continental fragment of Neoproterozoic Western Australia?: Precambrian Research, v. 142, no. 3-4, p. 83–92, https://doi.org/10.1016/j.precamres.2005.09.006.

Jefferson, C.W., and Parrish, R.R., 1989, Late Proterozoic stratigraphy, U-Pb zircon ages, and rift tectonics, Mackenzie Mountains, northwestern Canada: Canadian Journal of Earth Sciences, v. 26, no. 9, p. 1784–1801, https://doi.org/10.1139/e89-151.

Jing, X.Q., Yang, Z., Tong, Y., and Han, Z., 2015, A revised paleomagnetic pole from the mid-Neoproterozoic Liantuo Formation in the Yangtze block and its paleogeographic implications: Precambrian Research, v. 268, p. 194–211, https://doi.org/10.1016/j.precamres.2015.07.007.

Jones, C., 2002, User-driven integrated software lives: “PaleoMag” paleomagnetics analysis on the Macintosh: Computers & Geosciences, v. 28, no. 10, p. 1145–1151, https://doi.org/10.1016/S0098-3004(02)00032-8.

Karlstrom, K.E., Harlan, S.S., Williams, M.L., McLelland, J., Geissman, J.W., and Ahall, K.I., 1999, Refining Rodinia: Geologic evidence for the Australia–western US connection in the Proterozoic: GSA Today, v. 9, no. 10, p. 1–7.

Karlstrom, K.E., Bowring, S.A., Dehler, C.M., Knoll, A.H., Porter, S.M., Des Marais, D.J., Weil, A.B., Sharp, Z.D., Geissman, J.W., Elrick, M.B., and Timmons, J.M., 2000, Chuar Group of the Grand Canyon: Record of breakup of Rodinia, associated change in the global carbon cycle, and ecosystem expansion by 740 Ma: Geology, v. 28, p. 619–622, https://doi.org/10.1130/0091-7613(2000)28<619:CGOTGC>2.0.CO;2.

Karlstrom, K.E., Hagadorn, J., Gehrels, G., Matthews, W., Schmitz, M., Madronich, L., Mulder, J., Pecha, M., Giesler, D., and Crossey, L., 2018, Cambrian Sauk transgression in the Grand Canyon region redefined by detrital zircons: Nature Geoscience, v. 11, no. 6, p. 438–443, https://doi.org/10.1038/s41561-018-0131-7.

Keeley, J.A., Link, P.K., Fanning, C.M., and Schmitz, M.D., 2013, Pre- to synglacial rift-related volcanism in the Neoproterozoic (Cryogenian) Pocatello Formation, SE Idaho: New SHRIMP and CA-ID-TIMS constraints: Lithosphere, v. 5, p. 128–150, https://doi.org/10.1130/L226.1.

Kent, D.V., and Tauxe, L., 2005, Corrected Late Triassic latitudes for continents adjacent to the North Atlantic: Science, v. 307, no. 5707, p. 240–244, https://doi.org/10.1126/science.1105826.

Key, R.M., Liyungu, A.K., Njamu, F.M., Somwe, V., Banda, J., Mosley, P.N., and Armstrong, R.A., 2001, The western arm of the Lufilian arc in Zambia and its potential for copper mineralisation: Journal of African Earth Sciences, v. 33, p. 503–528, https://doi.org/10.1016/S0899-5362(01)00098-7.

Kirschvink, J.L., 1980, The least-squares line and plane and the analysis of paleomagnetic data: Geophysical Journal of the Royal Astronomical Society, v. 62, no. 3, p. 699–718, https://doi.org/10.1111/j.1365-246X.1980.tb02601.x.

Kirschvink, J.L., Kopp, R.E., Raub, T.D., Baumgartner, C.T., and Holt, J.W., 2008, Rapid, precise, and high-sensitivity acquisition of paleomagnetic and rock-magnetic data: Development of a low-noise automatic sample changing system for superconducting rock magnetometers: Geochemistry Geophysics Geosystems, v. 9, Q05Y01, https://doi.org/10.1029/2007GC001856.

Knoll, A.H., Hayes, J.M., Kaufman, A.J., Swett, K., and Lambert, I.B., 1986, Secular variation in carbon isotope ratios from Upper Proterozoic successions of Svalbard and East Greenland: Nature, v. 321, no. 6073, p. 832–838, https://doi.org/10.1038/321832a0.

Kruiver, P.P., Dekkers, M.J., and Heslop, D., 2001, Quantification of magnetic coercivity components by the analysis of acquisition curves of isothermal remanent magnetization: Earth and Planetary Science Letters, v. 189, no. 3-4, p. 269–276, https://doi.org/10.1016/S0012-821X(01)00367-3.

Lan, Z., Li, X.H., Zhu, M., Zhang, Q., and Li, Q.L., 2015, Revisiting the Liantuo Formation in Yangtze block, South China: SIMS U-Pb zircon age constraints and regional and global significance: Precambrian Research, v. 263, p. 123–141, https://doi.org/10.1016/j.precamres.2015.03.012.

Larson, E.E., Walker, T.R., Patterson, P.E., Hoblitt, R.P., and Rosenbaum, J.G., 1982, Paleomagnetism of the Moenkopi formation, Colorado Plateau: Basis for long-term model of acquisition of chemical remanent magnetism in red beds: Journal of Geophysical Research, v. 87, p. 1081–1106, https://doi.org/10.1029/JB087iB02p01081.

Li, Z.X., and Evans, D.A., 2011, Late Neoproterozoic intraplate rotation within Australia allows for a tighter-fitting and longer-lasting Rodinia: Geology, v. 39, no. 1, p. 39–42, https://doi.org/10.1130/G31461.1.

Li, Z.X., Evans, D.A.D., and Zhang, S., 2004, A spin on Rodinia: Possible causal links between the Neoproterozoic supercontinent, superplume, true polar wander and low-latitude glaciation: Earth and Planetary Science Letters, v. 220, no. 3, p. 409–421, https://doi.org/10.1016/S0012-821X(04)00064-0.

Li, Z.X., Bogdanova, S.V., Collins, A.S., Davidson, A., De Waele, B., Ernst, R.E., Fitzsimmons, I.C.W., Fuck, R.A., Gladkochub, D.P., Jacobs, J., Karlstrom, K.E., Lu, S., Natapov, L.M., Pease, V., Pisarevsky, S.A., Thrane, K., and Vernikovsky, V., 2008, Assembly, configuration, and break-up history of Rodinia: A synthesis: Precambrian Research, v. 160, no. 1-2, p. 179–210, https://doi.org/10.1016/j.precamres.2007.04.021.

Li, Z.X., Evans, D.A., and Halverson, G.P., 2013, Neoproterozoic glaciations in a revised global palaeogeography from the breakup of Rodinia to the assembly of Gondwanaland: Sedimentary Geology, v. 294, p. 219–232, https://doi.org/10.1016/j.sedgeo.2013.05.016.

Link, P., Christie-Blick, N., Devlin, W., Elston, D., Horodyski, R., Levy, M., Miller, J., Pearson, R., Prave, A., and Stewart, J., 1993, Middle and Late Proterozoic stratified rocks of the western U.S. Cordillera, Colorado Plateau, and Basin and Range Province, *in* Reed, J.C., Jr., et al., eds., Precambrian: Conterminous U.S.: Boulder, Colorado, The Geological Society of America, The Geology of North America, v. C-2, p. 463–595.

Linnemann, U., Ovtcharova, M., Schaltegger, U., Gärtner, A., Hautmann, M., Geyer, G., Vickers-Rich, P., Rich, T., Plessen, B., Hofmann, M., and Zieger, J., 2019, New high-resolution age data from the Ediacaran-Cambrian boundary indicate rapid, ecologically driven onset of the Cambrian explosion: Terra Nova, v. 31, p. 49–58, https://doi.org/10.1111/ter.12368.

Loewy, S.L., Connelly, J.N., Dalziel, I.W., and Gower, C.F., 2003, Eastern Laurentia in Rodinia: Constraints from whole-rock Pb and U/Pb geochronology: Tectonophysics, v. 375, no. 1, p. 169–197, https://doi.org/10.1016/S0040-1951(03)00338-X.

Lund, K., Aleinikoff, J., Evans, K., Dewitt, E., and Unruh, D., 2010, SHRIMP U-Pb dating of recurrent Cryogenian and Late Cambrian–Early Ordovician alkalic magmatism in central Idaho: Implications for Rodinian rift tectonics: Geological Society of America Bulletin, v. 122, p. 430–453, https://doi.org/10.1130/B26565.1.

Ma, G.G., Li, H.Q., and Zhang, Z.C., 1984, An investigation of the age limits of the Sinian System in South China: Bulletin of the Yichang Institute of Geology and Mineral Resources Chinese Academy of Geological Sciences, v. 8, p. 1–29 [in Chinese].

Macdonald, F.A., Schmitz, M.D., Crowley, J.L., Roots, C.F., Jones, D.S., Maloof, A.C., Strauss, J.V., Cohen, P.A., Johnston, D.T., and Schrag, D.P., 2010, Calibrating the Cryogenian: Science, v. 327, no. 5970, p. 1241–1243, https://doi.org/10.1126/science.1183325.

Macdonald, F.A., Halverson, G.P., Strauss, J.V., Smith, E.F., Cox, G.M., Sperling, E.A., and Roots, C.F., 2012, Early Neoproterozoic basin formation in Yukon, Canada: Implications for the make-up and break-up of Rodinia: Geoscience Canada, v. 39, p. 77–99.

Macdonald, F.A., Prave, A.R., Petterson, R., Smith, E.F., Pruss, S.B., Oates, K., Waechter, F., Trotzuk, D., and Fallick, A.E., 2013, The Laurentian record of Neoproterozoic glaciation, tectonism, and eukaryotic evolution in Death Valley, California: Geological Society of America Bulletin, v. 125, no. 7-8, p. 1203–1223, https://doi.org/10.1130/B30789.1.

Macdonald, F.A., Schmitz, M.D., Strauss, J.V., Halverson, G.P., Gibson, T.M., Eyster, A., Cox, G., Mamrol, P., and Crowley, J.L., 2017, Cryogenian of Yukon: Precambrian Research, v. 319, p. 114–143.

Maloof, A.C., Halverson, G.P., Kirschvink, J.L., Schrag, D.P., Weiss, B.P., and Hoffman, P.F., 2006, Combined paleomagnetic, isotopic, and stratigraphic evidence for true polar wander from the Neoproterozoic Akademikerbreen Group, Svalbard, Norway: Geological Society of America Bulletin, v. 118, no. 9-10, p. 1099–1124, https://doi.org/10.1130/B25892.1.

Martel, E., Turner, E.C., and Fischer, B.J., 2011, Geology of the Central Mackenzie Mountains of the Northern Canadian Cordillera, Sewki Mountain (105P), Mount Eduni (106A), and Northwestern Wrigley Lake (95M) Map-Areas, Northwest Territories: Yellowknife, Canada, Northwest Territories Geoscience Office, NWT Special Volume 1, 423 p.

Mbede, E.I., Kampunzu, A.B., and Armstrong, R.A., 2004, Neoproterozoic inheritance during Cainozoic rifting in the western and southwestern branches of the East African Rift system: Evidence from carbonatite and alkaline intrusions, *in* The East African Rift System: Development, Evolution and Resources, Abstracts: Addis Ababa, Ethiopia, 20–24 June 2004, *in* G. Yirgu, C. Ebinger, and G. Mulugeta, eds., Ethiopian Geosciences and Mineral Engineering Association.

McElhinny, M.W., and McFadden, P.L., 2000, Paleomagnetism: Continents and Oceans: San Diego, California, Academic Press, 386 p.

McFadden, P.L., and McElhinny, M.W., 1990, Classification of the reversal test in palaeomagnetism: Geophysical Journal International, v. 103, no. 3, p. 725–729, https://doi.org/10.1111/j.1365-246X.1990.tb05683.x.

Meert, J.G., and Torsvik, T.H., 2003, The making and unmaking of a supercontinent: Rodinia revisited: Tectonophysics, v. 375, no. 1, p. 261–288, https://doi.org/10.1016/S0040-1951(03)00342-1.

Meert, J.G., van der Voo, R., and Ayub, S., 1995, Paleomagnetic investigation of the Neoproterozoic Gagwe lavas and Mbozi complex, Tanzania, and the assembly of Gondwana: Precambrian Research, v. 74, no. 4, p. 225–244, https://doi.org/10.1016/0301-9268(95)00012-T.

Meert, J.G., Pandit, M., and Kamenov, G.D., 2013, Further geochronological and paleomagnetic constraints on Malani (and pre-Malani) magmatism in NW India: Tectonophysics, v. 608, p. 1254–1267, https://doi.org/10.1016/j.tecto.2013.06.019.

Merdith, A.S., Collins, A.S., Williams, S.E., Pisarevsky, S., Foden, J.F., Archibald, D., Blades, M.L., Alessio, B.L., Armistead, S., Plavsa, D., and Clark, C., 2017, A full-plate global reconstruction of the Neoproterozoic: Gondwana Research, v. 50, p. 84–134, https://doi.org/10.1016/j.gr.2017.04.001.

Miller, F.K., 1994, The Windermere Group and late Proterozoic tectonics in northeastern Washington and northern Idaho, *in* Lasmanis, R., and Cheney, E.S., conveners, Regional Geology of Washington: Washington Division of Geology and Earth Resources Bulletin 80, p. 1–19.

Miller, J.M.G., 1985, Glacial and syntectonic sedimentation: The Upper Proterozoic Kinston Peak Formation, southern Panamint Range, eastern California: Geological Society of America Bulletin, v. 96, p. 1537–1553, https://doi.org/10.1130/0016-7606(1985)96<1537:GASSTU>2.0.CO;2.

Milton, J.E., Hickey, K.A., Gleeson, S.A., and Friedman, R.M., 2017, New U-Pb constraints on the age of the Little Dal Basalts and Gunbarrel-related volcanism in Rodinia: Precambrian Research, v. 296, p. 168–180, https://doi.org/10.1016/j.precamres.2017.04.030.

Molina-Garza, R.S., Geissman, J.W., Van der Voo, R., Lucas, S.G., and Hayden, S.N., 1991, Paleomagnetism of the Moenkopi and Chinle Formations in central New Mexico: Implications for the North American apparent polar wander path and Triassic magnetostratigraphy: Journal of Geophysical Research–Solid Earth, v. 96, no. B9, p. 14,239–14,262, https://doi.org/10.1029/91JB00644.

Moores, E.M., 1991, Southwest US–East Antarctic (SWEAT) connection: A hypothesis: Geology, v. 19, no. 5, p. 425–428, https://doi.org/10.1130/0091-7613(1991)019<0425:SUSEAS>2.3.CO;2.

Morra, G., Seton, M., Quevedo, L., and Müller, R.D., 2013, Organization of the tectonic plates in the last 200 Myr: Earth and Planetary Science Letters, v. 373, p. 93–101, https://doi.org/10.1016/j.epsl.2013.04.020.

Morris, W.A., and Aitken, J.D., 1982, Paleomagnetism of the Little Dal lavas, Mackenzie Mountains, Northwest Territories, Canada: Canadian Journal of Earth Sciences, v. 19, no. 10, p. 2020–2027, https://doi.org/10.1139/e82-179.

Müller, R.D., Seton, M., Zahirovic, S., Williams, S.E., Matthews, K.J., Wright, N.M., Shephard, G.E., Maloney, K.T., Barnett-Moore, N., Hosseinpour, M., and Bower, D.J., 2016, Ocean basin evolution and global-scale plate reorganization events since Pangea breakup: Annual Review of Earth and Planetary Sciences, v. 44, p. 107–138, https://doi.org/10.1146/annurev-earth-060115-012211.

Murphy, J.B., Nance, R.D., and Cawood, P.A., 2009, Contrasting modes of supercontinent formation and the conundrum of Pangea: Gondwana Research, v. 15, no. 3, p. 408–420, https://doi.org/10.1016/j.gr.2008.09.005.

Nance, R.D., Murphy, J.B., and Santosh, M., 2014, The supercontinent cycle: A retrospective essay: Gondwana Research, v. 25, no. 1, p. 4–29, https://doi.org/10.1016/j.gr.2012.12.026.

O'Reilly, W., 1984, Rock and Mineral Magnetism: Glasgow, UK, Blackie and Son, Ltd., 230 p., https://doi.org/10.1007/978-1-4684-8468-7.

Özdemir, Ö., and Dunlop, D.J., 2014, Hysteresis and coercivity of hematite: Journal of Geophysical Research–Solid Earth, v. 119, p. 2582–2594, https://doi.org/10.1002/2013JB010739.

Palmer, H.C., and Hayatsu, A., 1975, Paleomagnetism and K-Ar dating of some Franklin lavas and diabases, Victoria Island: Canadian Journal of Earth Sciences, v. 12, no. 8, p. 1439–1447, https://doi.org/10.1139/e75-130.

Palmer, H.C., Baragar, W.R.A., Fortier, M., and Foster, J.H., 1983, Paleomagnetism of late Proterozoic rocks, Victoria Island, Northwest Territories, Canada: Canadian Journal of Earth Sciences, v. 20, no. 9, p. 1456–1469, https://doi.org/10.1139/e83-131.

Park, J.K., 1974, Paleomagnetism of miscellaneous Franklin and Mackenzie diabases of the Canadian Shield and their adjacent country rocks: Canadian Journal of Earth Sciences, v. 11, p. 1012–1017, https://doi.org/10.1139/e74-098.

Park, J.K., 1981a, Paleomagnetism of the late Proterozoic sills in the Tsezotene Formation, Mackenzie Mountains, Northwest Territories, Canada: Canadian Journal of Earth Sciences, v. 18, no. 10, p. 1572–1580, https://doi.org/10.1139/e81-145.

Park, J.K., 1981b, Paleomagnetism of basic intrusions from the Brock inlier, Northwest Territories, Canada: Canadian Journal of Earth Sciences, v. 18, no. 10, p. 1637–1641, https://doi.org/10.1139/e81-151.

Park, J.K., 1984, Paleomagnetism of the Mudcracked formation of the Precambrian Little Dal Group, Mackenzie Mountains, Northwest Territories, Canada: Canadian Journal of Earth Sciences, v. 21, p. 371–375, https://doi.org/10.1139/e84-039.

Park, J.K., 1994, Palaeomagnetic constraints on the position of Laurentia from middle Neoproterozoic to Early Cambrian times: Precambrian Research, v. 69, no. 1-4, p. 95–112, https://doi.org/10.1016/0301-9268(94)90081-7.

Park, J.K., and Aitken, J.D., 1986, Paleomagnetism of the Katherine Group in the Mackenzie Mountains: Implications for post-Grenville (Hadrynian) apparent polar wander: Canadian Journal of Earth Sciences, v. 23, no. 3, p. 308–323, https://doi.org/10.1139/e86-034.

Park, J.K., and Jefferson, C.W., 1991, Magnetic and tectonic history of the late Proterozoic Upper Little Dal and Coates Lake Groups of northwestern Canada: Precambrian Research, v. 52, p. 1–35, https://doi.org/10.1016/0301-9268(91)90011-X.

Park, J.K., Norris, D.K., and Larochelle, A., 1989, Paleomagnetism and the origin of the Mackenzie arc of northwestern Canada: Canadian Journal of Earth Sciences, v. 26, no. 11, p. 2194–2203, https://doi.org/10.1139/e89-186.

Park, J.K., Buchan, K.L., and Harlan, S.S., 1995a, A proposed giant radiating dyke swarm fragmented by the separation of Laurentia and Australia based on paleomagnetism of ca. 780 Ma mafic intrusions in western North America: Earth and Planetary Science Letters, v. 132, no. 1-4, p. 129–139, https://doi.org/10.1016/0012-821X(95)00059-L.

Park, K., Buchan, K.L., and Gandhi, S.S., 1995b, Paleomagnetism of 780 Ma Hottah Gabbro Sheets of the Wopmay Orogen, Northwest Territories, Canada: Current Research: Geological Survey of Canada Paper 1995C, p. 195–200.

Pehrsson, S.J., and Buchan, K.L., 1999, Borden dykes of Baffin Island, Northwest Territories: A Franklin U-Pb baddeleyite age and a paleomagnetic reinterpretation: Canadian Journal of Earth Sciences, v. 36, no. 1, p. 65–73, https://doi.org/10.1139/e98-091.

Pisarevsky, S.A., Wingate, M.T., Powell, C.M., Johnson, S., and Evans, D.A., 2003, Models of Rodinia assembly and fragmentation, *in* Yoshida, M., Windley, B.E., and Dasgupta, S., eds., Proterozoic East Gondwana: Supercontinent Assembly and Break-Up: Geological Society [London] Special Publication 206, p. 35–55, https://doi.org/10.1144/GSL.SP.2003.206.01.04.

Pisarevsky, S.A., Wingate, M.T.D., Stevens, M.K., and Haines, P.W., 2007, Palaeomagnetic results from the Lancer 1 stratigraphic drillhole, Officer Basin, Western Australia, and implications for Rodinia reconstructions: Australian Journal of Earth Sciences, v. 54, no. 4, p. 561–572, https://doi.org/10.1080/08120090701188962.

Pisarevsky, S.A., Gladkochub, D.P., Konstantinov, K.M., Mazukabzov, A.M., Stanevich, A.M., Murphy, J.B., Tait, J.A., Donskaya, T.V., and Konstantinov, I.K., 2013, Paleomagnetism of Cryogenian Kitoi mafic dykes in south Siberia: Implications for Neoproterozoic paleogeography: Precambrian Research, v. 231, p. 372–382, https://doi.org/10.1016/j.precamres.2013.04.007.

Prave, A.R., 1999, Two diamictites, two cap carbonates, two $\delta^{13}C$ excursions, two rifts: The Neoproterozoic Kingston Peak Formation, Death Valley, California: Geology, v. 27, no. 4, p. 339–342, https://doi.org/10.1130/0091-7613(1999)027<0339:TDTCCT>2.3.CO;2.

Roberts, A.P., Cui, Y., and Verosub, K.L., 1995, Wasp-waisted hysteresis loops: Mineral magnetic characteristics and discrimination of components in mixed magnetic systems: Journal of Geophysical Research–Solid Earth, v. 100, no. B9, p. 17,909–17,924, https://doi.org/10.1029/95JB00672.

Robertson, W.A., and Baragar, W.R.A., 1972, The petrology and paleomagnetism of the Coronation sills: Canadian Journal of Earth Sciences, v. 9, no. 2, p. 123–140, https://doi.org/10.1139/e72-011.

Rooney, A.D., Austermann, J., Smith, E.F., Li, Y., Selby, D., Dehler, C.M., Schmitz, M.D., Karlstrom, K.E., and Macdonald, F.A., 2017, Coupled Re-Os and U-Pb geochronology of the Tonian Chuar Group, Grand Canyon: Geological Society of America Bulletin, v. 130, no. 7-8, p. 1085–1098, https://doi.org/10.1130/B31768.1.

Ross, G.M., 1991, Tectonic setting of the Windermere Supergroup revisited: Geology, v. 19, no. 11, p. 1125–1128, https://doi.org/10.1130/0091-7613(1991)019<1125:TSOTWS>2.3.CO;2.

Schmidt, P.W., 2014, A review of Precambrian palaeomagnetism of Australia: Palaeogeography, supercontinents, glaciations and true polar wander: Gondwana Research, v. 25, no. 3, p. 1164–1185, https://doi.org/10.1016/j.gr.2013.12.007.

Sears, J.W., and Price, R.A., 1978, The Siberian connection: A case for Precambrian separation of the North American and Siberian cratons: Geology, v. 6, no. 5, p. 267–270, https://doi.org/10.1130/0091-7613(1978)6<267:TSCACF>2.0.CO;2.

Sears, J.W., and Price, R.A., 2003, Tightening the Siberian connection to western Laurentia: Geological Society of America Bulletin, v. 115, no. 8, p. 943–953, https://doi.org/10.1130/B25229.1.

Seton, M., Müller, R.D., Zahirovic, S., Gaina, C., Torsvik, T., Shephard, G., Talsma, A., Gurnis, M., Turner, M., Maus, S., and Chandler, M., 2012, Global continental and ocean basin reconstructions since 200 Ma: Earth-Science Reviews, v. 113, no. 3-4, p. 212–270, https://doi.org/10.1016/j.earscirev.2012.03.002.

Shields-Zhou, G.A., Hill, A.C., and Macgabhann, B.A., 2012, The Cryogenian Period, *in* Gradstein, F.M., Ogg, J.G., Schmitz, M., and Ogg, G., eds., The Geologic Time Scale 2012: New York, Elsevier, p. 393–411, https://doi.org/10.1016/B978-0-444-59425-9.00017-2.

Shive, P.N., Steiner, M.B., and Huycke, D.T., 1984, Magnetostratigraphy, paleomagnetism, and remanence acquisition in the Triassic Chugwater Formation of Wyoming: Journal of Geophysical Research, v. 89, p. 1801–1815, https://doi.org/10.1029/JB089iB03p01801.

Sklyarov, Eu.V., Gladkochub, D.P., Mazukabzov, A.M., Menshagin, Yu.V., Watanabe, T., and Pisarevsky, S.A., 2003, Neoproterozoic mafic dike swarms of the Sharyzhalgai metamorphic massif, southern Siberian craton: Precambrian Research, v. 122, no. 1, p. 359–376, https://doi.org/10.1016/S0301-9268(02)00219-X.

Smith, E.F., MacDonald, F.A., Crowley, J.L., Hodgin, E.B., and Schrag, D.P., 2016, Tectonostratigraphic evolution of the c. 780–730 Ma Beck Spring Dolomite: Basin Formation in the core of Rodinia, *in* Li, Z.X., Evans, D.A.D., and Murphy, J.B., eds., Supercontinent Cycles Through Earth History: Geological Society [London] Special Publication 424, p. 213–239, https://doi.org/10.1144/SP424.6.

Sprinkel, D.A., 2006, Interim Geologic Map of the Dutch John 30′ × 60′ Quadrangle, Daggett and Uintah Counties, Utah, Moffat County, Colorado, and Sweetwater County, Wyoming: Utah Geological Survey Open-File Report 491DM, compact disc, GID data, 3 plates, scale 1:100,000.

Sprinkel, D.A., 2007, Interim Geologic Map of the Vernal 30′ × 60′ Quadrangle, Uintah and Duchesne Counties, Utah, Moffat and Rio Blanco Counties, Colorado: Utah Geological Survey Open-File Report 506DM, compact disc, GID data, 3 plates, scale 1:100,000.

Sprinkel, D.A., 2015, Interim Geologic Map of the Eastern Part of the Duchesne 30′ × 60′ Quadrangle, Duchesne and Wasatch Counties, Utah (Year 3): Utah Geological Survey Open-File Report 647, 11 p., 1 plate, scale 1:62,500.

Steiner, M.B., 1983, Detrital remanent magnetization in hematite: Journal of Geophysical Research, v. 88, p. 6523–6539, https://doi.org/10.1029/JB088iB08p06523.

Stewart, J.N., 1972, Initial deposits of the Cordilleran geosyncline: Evidence for a late Precambrian (850 m.y.) continental separation: Geological Society of America Bulletin, v. 83, no. 5, p. 1345–1360, https://doi.org/10.1130/0016-7606(1972)83[1345:IDITCG]2.0.CO;2.

Strauss, J.V., Rooney, A.D., Macdonald, F.A., Brandon, A.D., and Knoll, A.H., 2014, 740 Ma vase-shaped microfossils from Yukon, Canada: Implications for Neoproterozoic chronology and biostratigraphy: Geology, v. 42, no. 8, p. 659–662, https://doi.org/10.1130/G35736.1.

Strauss, J.V., Macdonald, F.A., Halverson, G.P., Tosca, N.J., Schrag, D.P., and Knoll, A.H., 2015, Stratigraphic evolution of the Neoproterozoic Callison Lake Formation: Linking the break-up of Rodinia to the Islay carbon isotope excursion: American Journal of Science, v. 315, p. 881–944, https://doi.org/10.2475/10.2015.01.

Swanson-Hysell, N.L., Maloof, A.C., Kirschvink, J.L., Evans, D.A.D., Halverson, G.P., and Hurtgen, M.T., 2012, Constraints on Neoproterozoic paleogeography and Paleozoic orogenesis from paleomagnetic records of the Bitter Springs Formation, Amadeus Basin, central Australia: American Journal of Science, v. 312, p. 817–884, https://doi.org/10.2475/08.2012.01.

Swanson-Hysell, N.L., Maloof, A.C., Condon, D.J., Jenkin, G.R., Alene, M., Tremblay, M.M., Tesema, T., Rooney, A.D., and Haileab, B., 2015, Stratigraphy and geochronology of the Tambien Group, Ethiopia: Evidence for globally synchronous carbon isotope change in the Neoproterozoic: Geology, v. 43, no. 4, p. 323–326, https://doi.org/10.1130/G36347.1.

Tauxe, L., 2005, Inclination flattening and the geocentric axial dipole hypothesis: Earth and Planetary Science Letters, v. 233, no. 3-4, p. 247–261, https://doi.org/10.1016/j.epsl.2005.01.027.

Tauxe, L., and Badgley, C., 1984, Transition stratigraphy and the problem of remanence lock-in times in the Siwalik red beds: Geophysical Research Letters, v. 11, p. 611–613, https://doi.org/10.1029/GL011i006p00611.

Tauxe, L., and Kent, D.V., 2004, A simplified statistical model for the geomagnetic field and the detection of shallow bias in paleomagnetic inclinations: Was the ancient magnetic field dipolar? *in* Channell, J., Kent, D., Lowrie, W., and Meert, J., eds., Timescales of the Paleomagnetic Field: Washington, D.C., Geophysics Monograph American Geophysical Union, v. 145, p. 101–116, https://doi.org/10.1029/145GM08.

Tauxe, L., and Watson, G.S., 1994, The fold test: An eigen analysis approach: Earth and Planetary Science Letters, v. 122, no. 3, p. 331–341, https://doi.org/10.1016/0012-821X(94)90006-X.

Tauxe, L., Kodama, K.P., and Kent, D.V., 2008, Testing corrections for paleomagnetic inclination error in sedimentary rocks: A comparative approach: Physics of the Earth and Planetary Interiors, v. 169, no. 1, p. 152–165, https://doi.org/10.1016/j.pepi.2008.05.006.

Tauxe, L., Shaar, R., Jonestrask, L., Swanson-Hysell, N.L., Minnett, R., Koppers, A.A.P., Constable, C.G., Jarboe, N., Gaastra, K., and Fairchild, L., 2016, PmagPy: Software package for paleomagnetic data analysis and a bridge to the Magnetics Information Consortium (MagIC) database: Geochemistry Geophysics Geosystems, v. 17, p. 2450–2463, https://doi.org/10.1002/2016GC006307.

Thomas, W.A., Tucker, R.D., Astini, R.A., and Denison, R.E., 2012, Ages of pre-rift basement and synrift rocks along the conjugate rift and transform margins of the Argentine Precordillera and Laurentia: Geosphere, v. 8, no. 6, p. 1366–1383, https://doi.org/10.1130/GES00800.1.

Thorkelson, D., Abbott, J., Mortensen, J., Creaser, R., Villeneuve, M., McNicoll, V., and Layer, P., 2005, Early and Middle Proterozoic evolution of Yukon, Canada: Canadian Journal of Earth Sciences, v. 42, no. 6, p. 1045–1071, https://doi.org/10.1139/e04-075.

Timmons, J.M., Karlstrom, K.E., Dehler, C.M., Geissman, J.W., and Heizler, M.T., 2001, Proterozoic multistage (ca. 1.1 and 0.8 Ga) extension recorded in the Grand Canyon Supergroup and establishment of northwest- and north-trending tectonic grains in the southwestern United States: Geological Society of America Bulletin, v. 113, p. 163–181, https://doi.org/10.1130/0016-7606(2001)113<0163:PMCAGE>2.0.CO;2.

Timmons, J.M., Bloch, J., Fletcher, K., Karlstrom, K.E., Heizler, M., and Crossey, L., 2012, The Grand Canyon Unkar Group: Mesoproterozoic basin formation in the continental interior during supercontinent assembly, *in* Timmons, J.M., and Karlstrom, K.E., eds., Grand Canyon Geology: 2 Billion Years of Earth History: Geological Society of America Special Paper 489, p. 25–48, https://doi.org/10.1130/2012.2489(02).

Torsvik, T.H., Carter, L.M., Ashwal, L.D., Bhushan, S.K., Pandit, M.K., and Jamtveit, B., 2001a, Rodinia refined or obscured: Palaeomagnetism of the Malani igneous suite (NW India): Precambrian Research, v. 108, no. 3, p. 319–333, https://doi.org/10.1016/S0301-9268(01)00139-5.

Torsvik, T.H., Ashwal, L.D., Tucker, R.D., and Eide, E.A., 2001b, Neoproterozoic geochronology and palaeogeography of the Seychelles microcontinent: The India link: Precambrian Research, v. 110, no. 1, p. 47–59, https://doi.org/10.1016/S0301-9268(01)00180-2.

Torsvik, T.H., Van der Voo, R., Preeden, U., Mac Niocaill, C., Steinberger, B., Doubrovine, P., van Hinsbergen, D.J.J., Domeier, M., Gaina, C., Tohver, E., Meert, J.G., McCausland, P.J., and Cocks, L.R.M., 2012, Phanerozoic polar wander, palaeogeography and dynamics: Earth-Science Reviews, v. 114, no. 3, p. 325–368, https://doi.org/10.1016/j.earscirev.2012.06.007.

Van der Voo, R., 1990, The reliability of paleomagnetic data: Tectonophysics, v. 184, no. 1, p. 1–9, https://doi.org/10.1016/0040-1951(90)90116-P.

Van Gundy, C.E., 1951, Nankoweap group of the Grand Canyon Algonkian of Arizona: Geological Society of America Bulletin, v. 62, p. 953–959, https://doi.org/10.1130/0016–7606(1951)62[953:NGOTGC]2.0.CO;2.

Wang, H., Weiss, B.P., Bai, X.-N., Downey, B.G., Wang, J., Chen-Wiegart, Y.K., Wang, J., Suavet, C., Fu, R.R., and Zucolotto, M.E., 2017, Lifetime of the solar nebula constrained by meteorite paleomagnetism: Science, v. 355, p. 623–627, https://doi.org/10.1126/science.aaf5043.

Weil, A.B., Geissman, J.W., Heizler, M., and Van der Voo, R., 2003, Paleomagnetism of middle Proterozoic mafic intrusions and Upper Proterozoic (Nankoweap) red beds from the lower Grand Canyon Supergroup, Arizona: Tectonophysics, v. 375, no. 1-4, p. 199–220, https://doi.org/10.1016/S0040-1951(03)00339-1.

Weil, A.B., Geissman, J.W., and Van der Voo, R., 2004, Paleomagnetism of the Neoproterozoic Chuar Group, Grand Canyon Supergroup, Arizona: Implications for Laurentia's Neoproterozoic APWP and Rodinia break-up: Precambrian Research, v. 129, no. 1, p. 71–92, https://doi.org/10.1016/j.precamres.2003.09.016.

Weil, A.B., Geissman, J.W., and Ashby, J.M., 2006, A new paleomagnetic pole for the Neoproterozoic Uinta Mountain Supergroup, central Rocky Mountain states, USA: Precambrian Research, v. 147, no. 3, p. 234–259, https://doi.org/10.1016/j.precamres.2006.01.017.

Wen, B., Li, Y.X., and Zhu, W., 2013, Paleomagnetism of the Neoproterozoic diamictites of the Qiaoenbrak Formation in the Aksu area, NW China: Constraints on the paleogeographic position of the Tarim block: Precambrian Research, v. 226, p. 75–90, https://doi.org/10.1016/j.precamres.2012.10.018.

Wen, B., Evans, D.A., Li, Y.X., Wang, Z., and Liu, C., 2015, Newly discovered Neoproterozoic diamictite and cap carbonate (DCC) couplet in Tarim craton, NW China: Stratigraphy, geochemistry, and paleoenvironment: Precambrian Research, v. 271, p. 278–294, https://doi.org/10.1016/j.precamres.2015.10.006.

Wen, B., Evans, D.A., and Li, Y.X., 2017, Neoproterozoic paleogeography of the Tarim block: An extended or alternative "missing-link" model for Rodinia?: Earth and Planetary Science Letters, v. 458, p. 92–106, https://doi.org/10.1016/j.epsl.2016.10.030.

Wen, B., Evans, D.A., Wang, C., Li, Y.X., and Jing, X., 2018, A positive test for the Greater Tarim block at the heart of Rodinia: Mega-dextral suturing of supercontinent assembly: Geology, v. 46, no. 8, p. 687–690, https://doi.org/10.1130/G40254.1.

White, R.W., Clarke, G.L., and Nelson, D.R., 1999, SHRIMP U-Pb zircon dating of Grenville-age events in the western part of the Musgrave block, central Australia: Journal of Metamorphic Geology, v. 17, p. 465–482, https://doi.org/10.1046/j.1525-1314.1999.00211.x.

Wingate, M.T., and Giddings, J.W., 2000, Age and palaeomagnetism of the Mundine Well dykes swarm, Western Australia: Implications for an Australia-Laurentia connection at 755 Ma: Precambrian Research, v. 100, no. 1, p. 335–357, https://doi.org/10.1016/S0301-9268(99)00080-7.

Wingate, M.T., Pisarevsky, S.A., and Evans, D.A., 2002, Rodinia connections between Australia and Laurentia: No SWEAT, no AUSWUS?: Terra Nova, v. 14, no. 2, p. 121–128, https://doi.org/10.1046/j.1365-3121.2002.00401.x.

Wingate, M.T.D., Pisarevsky, S.A., and De Waele, B., 2010, Paleomagnetism of the 765 Ma Luakela volcanics in northwest Zambia and implications for Neoproterozoic positions of the Congo craton: American Journal of Science, v. 310, no. 10, p. 1333–1344, https://doi.org/10.2475/10.2010.05.

Wooden, J.L., Vitaliano, C.J., Koehler, S.W., and Ragland, P.C., 1978, The late Precambrian mafic dikes of the southern Tobacco Root Mountains, Montana: Geochemistry, Rb-Sr geochronology and relationship to Belt tectonics: Canadian Journal of Earth Sciences, v. 15, no. 4, p. 467–479, https://doi.org/10.1139/e78-055.

Wright, J.E., Hogan, J.P., and Gilbert, M.C., 1996, The Southern Oklahoma aulacogen: Not just another B.L.I.P.: Eos (Transactions, American Geophysical Union), v. 77, p. F845.

Xiao, S., Shen, B., Tang, Q., Kaufman, A.J., Yuan, X., Li, J., and Qian, M., 2014, Biostratigraphic and chemostratigraphic constraints on the age of early Neoproterozoic carbonate successions in North China: Precambrian Research, v. 246, p. 208–225, https://doi.org/10.1016/j.precamres.2014.03.004.

Xu, B., Jian, P., Zheng, H., Zou, H., Zhang, L., and Liu, D., 2005, U-Pb zircon geochronology and geochemistry of Neoproterozoic volcanic rocks in the Tarim block of northwest China: Implications for the breakup of Rodinia supercontinent and Neoproterozoic glaciations: Precambrian Research, v. 136, no. 2, p. 107–123, https://doi.org/10.1016/j.precamres.2004.09.007.

Xu, B., Xiao, S., Zou, H., Chen, Y., Li, Z.X., Song, B., Liu, D., Zhou, C., and Yuan, X., 2009, SHRIMP zircon U-Pb age constraints on Neoproterozoic Quruqtagh diamictites in NW China: Precambrian Research, v. 168, no. 3-4, p. 247–258, https://doi.org/10.1016/j.precamres.2008.10.008.

Zahirovic, S., Müller, R.D., Seton, M., and Flament, N., 2015, Tectonic speed limits from plate kinematic reconstructions: Earth and Planetary Science Letters, v. 418, p. 40–52, https://doi.org/10.1016/j.epsl.2015.02.037.

Zhang, S., Li, Z.X., and Wu, H., 2006, New Precambrian palaeomagnetic constraints on the position of the North China block in Rodinia: Precambrian Research, v. 144, no. 3-4, p. 213–238, https://doi.org/10.1016/j.precamres.2005.11.007.

Zhong, S., Zhang, N., Li, Z.X., and Roberts, J.H., 2007, Supercontinent cycles, true polar wander, and very long-wavelength mantle convection: Earth and Planetary Science Letters, v. 261, no. 3, p. 551–564, https://doi.org/10.1016/j.epsl.2007.07.049.

Zuza, A.V., and Yin, A., 2017, Balkatach hypothesis: A new model for the evolution of the Pacific, Tethyan, and Paleo-Asian oceanic domains: Geosphere, v. 13, no. 5, p. 1664–1712, https://doi.org/10.1130/GES01463.1.

Science Editor: Bradley S. Singer
Associate Editor: Zheng-Xiang Li

Manuscript Received 10 January 2018
Revised Manuscript Received 7 February 2019
Manuscript Accepted 11 April 2019

Printed in the USA